SUBSTITUTED PHTHALOCYANINES: DEVELOPMENT AND SELF-ASSEMBLED MONOLAYER SENSOR STUDIES

A thesis submitted in fulfillment of the
requirements for the degree of

MASTERS IN SCIENCE

of

RHODES UNIVERSITY

by

FUNGISAI MATEMADOMBO

January 2006

DEDICATION

AD MAJOREM DEI GLORIEM

ACKNOWLEDGMENT

John Quincy Adams, 1767-1848, 6th president of the United States

To furnish the means of acquiring knowledge is...the greatest benefit that can be conferred upon mankind. It prolongs life itself and enlarges the sphere of existence.

[*Report on the establishment of the Smithsonian Institution* c. 1846]

Thank-you Prof Nyokong for an extraordinary two years. The drive for science you inspire in me and all S22 certainly is remarkable. A particular thank-you Prof for Trip Belgium, which was incredible both academically and otherwise. Thank-you Dr Maree, Dr Ozoemena and Dr Westbroek for your invaluable supervision. Thank-you S22 and the Rhodes University Chemistry Department for your unique camaraderie.

St George's College (Zimbabwe) and my family instilled exceptional principles in me for which I am perpetually grateful.

Thank-you to my Lord, through whom *all* things are possible.

[QUOTE]

Joseph Addison, 1642-1719, English essayist

Education is a companion which no misfortune can depress, no crime can destroy, no enemy can alienate, no despotism can enslave. At home a friend, abroad an introduction, in solitude a solace, and in society an ornament. It chastens vice, it guides virtue, it gives at once, grace and government to genius. Without it, what is man? A splendid slave, a reasoning savage.

[*The Spectator* 1711]

ABSTRACT

Zinc, cobalt and iron phenylthio substituted phthalocyanines have been synthesized and characterized. Cyclic and square wave voltammetry in dimethylformamide containing tetrabutylammonium perchlorate revealed five and six redox processes respectively for the cobalt and iron phenylthio substituted phthalocyanines. These complexes are easier to reduce compared to the corresponding unsubstituted MPc and to butylthio substituted derivatives. Spectroelectrochemistry (in dimethylformamide containing tetrabutylammonium perchlorate) was employed to assign the cyclic voltammetry peaks, and gave spectra characteristic of Fe(I)Pc for reduction of iron phenylthio substituted phthalocyanine and Co(I)Pc for the reduction of cobalt phenylthio substituted phthalocyanine. The spectrum of the former is particularly of importance since such species have not received much attention in literature.

Cobalt and iron phenylthio substituted phthalocyanines have been deposited on Au electrode surfaces through the self assembled monolayer (SAM) technique. The so formed layers were studied using voltammetric techniques. These SAMs blocked a number of Faradic processes and electrocatalyzed the oxidation of L-cysteine.

Amine substituted cobalt phthalocyanine (CoTAPc) was deposited on gold surfaces by using an interconnecting SAM of mercaptopropionic acid or dithiobis(*N*-succinimidyl propionate) through the creation of an amide. Reductive and oxidative desorption of the SAMs limit the useful potential window. The SAM-CoTAPc layers show electrocatalytic activities towards oxygen reduction through the Co(I) central metal ion. Both SAMs were

highly stable and hence will be interesting tools for further research in surface modification and sensor development.

CONTENTS

Directory of Abbreviations

Ag|AgCl	Silver/silver chloride reference electrode
Au	Gold working electrode
C. M. E.	Chemically modified electrode
CoOBTPc	Octabutylthiophthalocyaninato cobalt (II)
CoOHETPc	Octa-(hydroxyethylthio) phthalocyaninato cobalt (II)
CoPc	Cobalt phthalocyanine
$CoPc(SCH_2Ph)_8$	Octaphenylthiophthalocyaninatocobalt
CoTAPc	Cobalt tetraamino phthalocyanine
C. E.	Counter electrode
CV	Cyclic voltammetry
CV	Cyclic voltammogram
DBU	1,8-diazabicyclo(5.4.0)undec-7-ene
DBN	1,5-diazabicyclo(4.3.0)non-5-ene
DMF	Dimethylformamide
DMSO	Dimethylsulfoxide
DTSP	Dthiobis(*N*-succinimidyl propionate)
EDC	1-Ethyl-3-(3-dimethylaminopropyl)-carbodiimide
FeOBTPc	Octabutylthiophthalocyaninato iron (II)
FeOHETPc	Octa-(hydroxyethylthio) phthalocyaninato iron (II)
FePc	Iron phthalocyanine
$FePc(SCH_2Ph)_8$	Octaphenylthiophthalocyaninatoiron
GCE	Glassy carbon electrode
HOMO	Highest unoccupied molecular orbital
^1H NMR	Proton nuclear magnetic resonance
$H_2Pc(SCH_2Ph)_8$	Unmetallated octaphenylthiophthalocyanine
$HS(CH_2)_2COOH$	Mercaptopropionic acid

IR	Infrared
$Li_2Pc(SCH_2Ph)_8$	Dilithium octaphenylthiophthalocyanine
LSWV	Linear square wave voltammogram
LUMO	Lowest unoccupied molecular orbital
$MPc(SCH_2Ph)_8$	Metallated octaphenylthiophthalocyanine
MPc	Metallophthalocyanine
MPc-SAM	Metallophthalocyanine-self assembled monolayer
OSWV	Osteryoung square wave voltammogram
OTTLE	Optically transparent thin layer electrode
Pc	Phthalocyanine
Ph	Phenyl group
R. E.	Reference electrode
RSH	L-cysteine
RSSR	Cystine
SAM	Self assembled monolayer
SWV	Square wave voltammogram
TBAP	Tetrabutylammonium perchlorate
THF	Tetrahydrofuran
UV-vis	Ultraviolet-visible
UPD	Underpotential deposition
W. E.	Working electrode
$ZnPc(SCH_2Ph)_8$	Octaphenylthiophthalocyaninatozinc

Directory of Symbols

α	Rate of electron transfer
ε	Extinction coefficient
Γ	Surface Coverage
Γ_{ibf}	Ion Barrier Factor
π	Pi-bonding
π^*	Anti pi-bonding
λ	Wavelength
A	Electrode Area
c	Analyte concentration
co	Initial analyte concentration
C	Capacitance
C_s	Interfacial Capacitance
D	Diffusion coefficient
E_{pa}	Anodic peak potential
E_{pc}	Cathodic peak potential
E	Potential
$E_{1/2}$	Half wave potential
ΔE	Anodic-to-cathodic peak potential separation
F	Faraday's constant
i_{ch}	Charging current
i_{pa}	Anodic peak current
i_{pc}	Cathodic peak current
n	Moles of electrons
η	Overpotential
$\varnothing$	Diameter

Q	Electrical charge
Q_{Bare}	Total charge under the peak of a bare gold electrode
Q_{SAM}	Total charge under the peak of a SAM modified gold electrode
R	Universal gas constant
v	Volume
ν	Scan rate
V	Volts

Directory of Figures

Directory of Schemes

Directory of Tables

CHAPTER 1: INTRODUCTION

1.1. Phthalocyanines

1.1.1. Synopsis

Phthalocyanines (Pcs, **1**) and their metal analogues metallophthalocyanines (MPcs, **2**), Figures 1.1 and 1.2, are macrocyclic 18 π-electron conjugated systems with a great diversity of technological applications.[1] The numbering system and substitution positions on a Pc (**1**) are given in Figure 1.1.

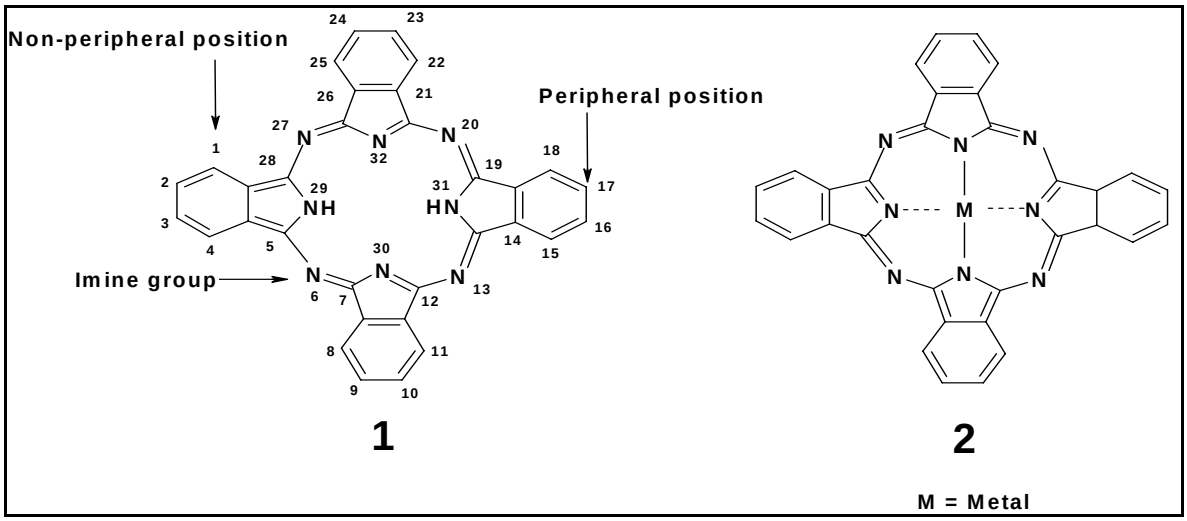

Figure 1.1 Molecular structures of metal free phthalocyanine (**1**) and a metallophthalocyanine (**2**).

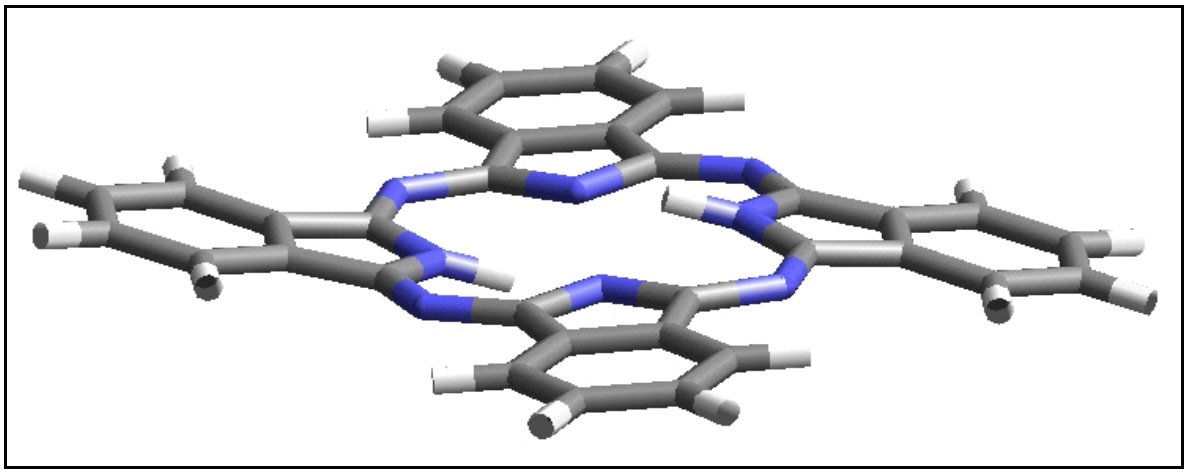

Figure 1.2 3-Dimensional configuration of **1** as determined by molecular modelling.

Pcs unique properties such as semiconductivity, electroconductivity, photoconductivity and non-linear optics have been widely studied for both fundamental science and application as opto-magnetically recording materials.[1] Pcs have been synthesised for use as possible Langmuir-Blodgett films.[2] Pcs, particularly their discotic liquid crystalline derivatives, have attracted attention for use in photovoltaic cells. Their extended π-conjugated electron systems make them very effective absorbers in the lower energy visible light region which is reflected in numerous applications in the field of opto-electronic devices.[1] Interest in the chemistry of Pcs as homogenous and heterogenous catalysts in a wide range of chemical reactions continues to grow. Pcs are found to be most useful in their soluble form and hence have been prepared in such a manner.[3] Pcs are used as sensors in conducting polymers,[1] batteries[1] and liquid crsytals.[4] Although the special nature of phthalocyanines and their metal complexes has been known for decades, their uses as commercial dyes, catalysts, optical and electrical materials are expanding enormously every year. Unsubstituted and substituted Pcs are widely used as agents in the photodynamic therapy of cancer.[1,5] The utility of the Pc species in these many applications arises primarily from their redox versatility, intense colour, overall chemical and thermal stability, and non-toxicity. For most of these applications, Pcs bearing ring substituents have been prepared in order to improve the above mentioned properties, and to enhance the solubility or to allow for coupling to other reagents like polymers.[6] The rich coordination chemistry of Pc complexes has encouraged researchers to 'tailor' specific products with certain properties which are required for high-technology applications. Inserting a great number of different metal ions into the Pc core combined

with the unlimited number and type of ring and axial substituents results in an infinite variety of novel products.

The aim of this study is to develop thiol octasubstituted and amide substituted metallophthalocyanines, coupled with cobalt and iron metals, for use as electrochemical sensors.

1.1.2. Methods of Synthesis

Pcs were first discovered accidentally in 1907.[7] This synthesis of phthalocyanine **1** involved the reaction of *o*-cyanobenzamide in refluxing ethanol from which **1** was recovered in low yield (Scheme 1.1, route a).[7] Linstead and co workers[8] reported that the yield could be improved if magnesium, antimony or magnesium salts such as its oxide and carbonate are mixed with *o*-cyanobenzamide and heated over 230 ^{o}C followed by demetallating the resultant metallophthalocyanine with cold concentrated H_2SO_4 (Scheme 1.1, route b). Use of substituted analogues of *o*-cyanobenzamide in order to synthesise substituted Pcs has been rare.

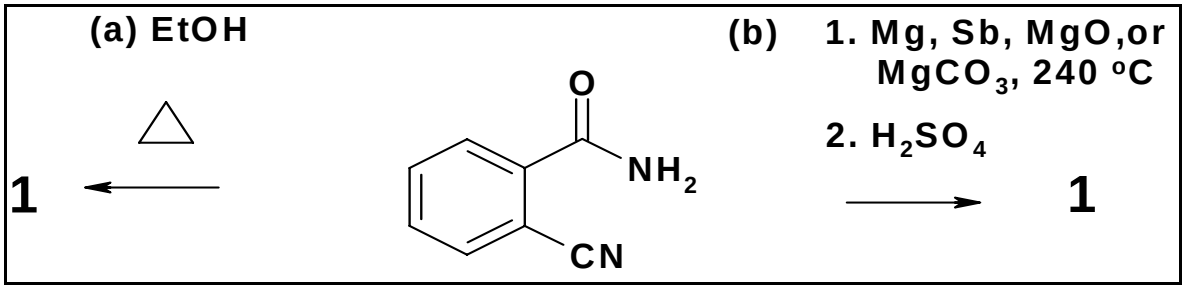

Scheme 1.1 Synthesis of metal free phthalocyanine (**1**).

Elvidge and Linstead[9] reported that 1,3-diminoisoindoline, on treatment with $NiCl_2$ in hot formamide, gave the nickel metallophthalocyanine in 96% yield. Heating 1,3-diminoisoindoline in the presence of a hydrogen donor such as succinonitrile or boiling

tetralin, produced **1** in average yields (Scheme 1.2, route a). **1** was moreover shown[10] to be produced from 1,3-diminoisoindoline in relatively high yields by refluxing the isoindoline in 2-N,N-dimethylaminoethanol (Scheme 1.2, route b).

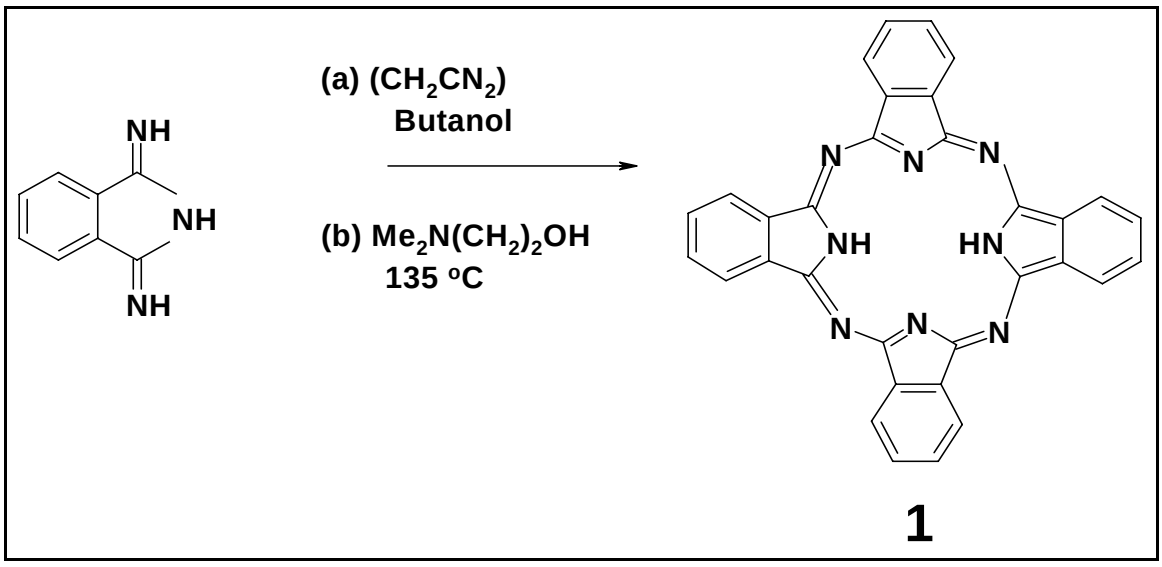

Scheme 1.2 Synthesis of metal free phthalocyanine (**1**).

Yields of identically and non-identically substituted Pcs have been found to vary over a wide range. Unfortunately, the synthesis of Pcs with dissimilar substituents at non-peripheral positions most likely results in a mixture of compounds that may not be separable by chromatography.

An essential part of the aim of this work sets to describe the synthesis and characterization of novel peripherally substituted octathiometallophthalocyanines, containing Co, Fe and Zn as central metals. Synthetic methods of octasubstituted and thiol substituted Pcs are presented below.

Pure substituted phthalocyanines and metallophthalocyanines have been prepared by cyclotrimerization of substituted 1,2-dicyanobenzenes or 1,3-diimino-*1H*-isoindoles.[11] 4,5-Disubstituted phthalonitriles as reactants lead to peripheral-identically substituted

phthalocyanines.[2] Non-peripheral octaalkoxy substituted Pcs were synthesised by alkylation of 2,3-dicyanohydroquinone with alcohols to 3,6-dialkoxy-1,2-dicyanobenzenes followed by their conversion to Pcs.[12]

Wöhrle *et al.*[2] have described a smart synthesis of 2,3,9,10,16,17,23,24-octasubstituted phthalocyanines (Scheme 1.3).[2] This procedure involves the reaction of 4,5-dichloro-1,2-dicyanobenzene with O- and S-nucleophiles to the corresponding 4,5-disubstituted-1,2-dicyanobenzenes which were then converted into octasubstituted Pcs.

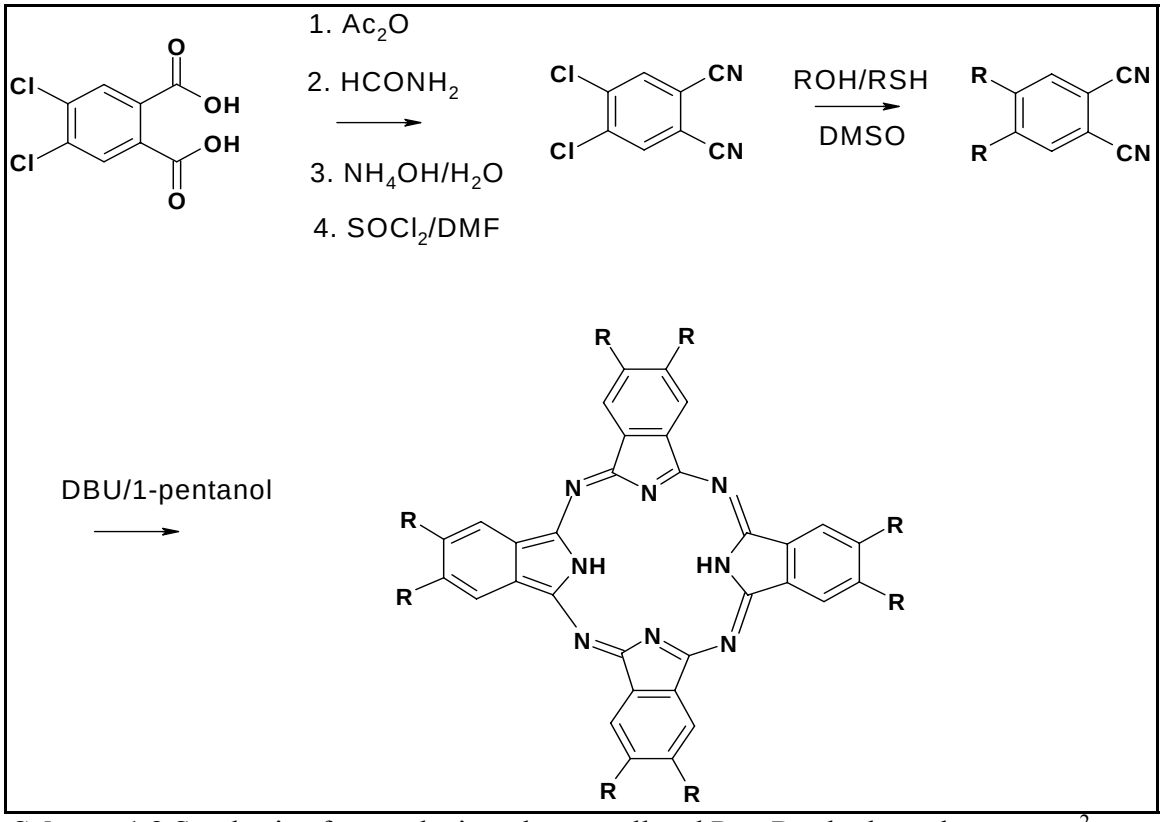

Scheme 1.3 Synthesis of octasubstituted unmetallated Pcs. R = hydrocarbon group.[2]

Wöhrle *et al.* also found that various substituted dinitriles reacting in the presence of strong non-nucleophilic bases such as 1,8-diazabicyclo(5.4.0)undec-7-ene (DBU) or 1,5-diazabicyclo(4.3.0)non-5-ene (DBN) in 1-pentanol results in high yields of Pc.[2] This

method was found to be relatively easy, occurring under mild conditions and yielding pure Pcs.

Few phthalocyanines with sulphur substituents have been reported.[13,14] Metal-free phthalocyanines and metal phthalocyaninates peripherally octasusbstituted with various alkylthio-groups have been synthesized.[15] Octabutylthiophthalocyanine complexes containing iron and zinc and their metal free analogue have been synthesised.[16-18] Novel liquid crystalline octakis(alkylthio)-substituted phthalocyanines, which may possibly be used for opto-electronic applications such as solar cells, have been synthesized and characterized.[19] A number of octakisalkylthiophthalocyanines and their copper complexes have been synthesized in order to study their mesomorphism and supramolecular structures.[20]

1.2. Electrochemical Basics

This section sets out to depict the electrochemical methods used to study phthalocyanines presented in this work.

1.2.1. Mass Transport

Electrochemistry may be broadly defined as the study of the chemical response of a system to an electrical stimulation. Electrochemistry may more specifically be defined as the study of chemical reactions to produce electric power or, on the other hand, the use of electricity to affect chemical processes or systems.[21]

The three mechanisms of mass transport are migration, convection and diffusion. In most electrochemical techniques, conditions are chosen so that transport of the electroactive

species is affected by a single mechanism, typically diffusion. A description of each mechanism is given below:[21]

- *Migration* is the movement of ions under the influence of an electric field. Migrational effects are removed by adding a large excess of an easily ionisable salt (the supporting electrolyte) e.g. KCl which dissociates to produce inert ions. These ions become the migration current carriers and also increase the conductivity of the solution;
- *Convection* is mass transport resulting from movements of the solution as a whole. In short experiments (as in this work), convection is not a factor in mass transport provided the solution is quiescent and the electrodes are stationary;
- *Diffusion* is mass transport driven by a gradient of chemical potential. Anytime that the concentration of a molecule or ions (charge is not considered here) is uneven throughout a solution, mass transport will occur to restore the homogeneity of the solution.

1.2.2. The Electrochemical Cell

The normal material for cell construction is Pyrex glass for reasons of both visibility and general chemical inertness. The size of the cell is variable and depends upon the volume of the sample being studied. Some electrochemical measurements can be run in cells under an atmosphere of air. Oxygen however is electrochemically active and its solubility in water is sufficiently high that oxygen reduction interference can be a problem. As a consequence, most measurements are carried out under an inert atmosphere of either nitrogen or argon.

A three-electrode electrochemical cell (Figure 1.3) is often used in electrochemical experiments. The electrochemical reaction takes place at the working (or indicator) electrode (labelled W.E. in Figure 1.3). This is the electrode at which the electrochemical phenomena being investigated takes place.[22] The working electrode should provide high signal-to-noise characteristics, including a reproducible response.[22] Hence working electrode selection depends on essentially two factors: the redox behaviour of the target analyte and the background current over the potential region required for the measurement. The reference electrode is labelled R. E. in Figure 1.3. This is the electrode whose potential is constant enough that it can be taken as the reference standard against which the potentials of the other electrodes present in the cell can be measured.[22] Reference electrodes with large surface areas are often employed in order to maintain low current densities and hence minimize polarization. The complete elimination of reference electrode polarization is only possible with modern potentiostatic instrumentation based on operational amplifiers. The potentiostat maintains a potential difference, ΔE, between the R. E. and W. E., and supplies the current (i) needed for affecting the changes occurring at the W. E.[23-25] An ideal R. E. is one whose potential does not shift from equilibrium (non-polarisable).

The counter (or auxiliary) electrode (labelled C. E. in Figure 1.3) completes the electrochemical circuit. This is the electrode which serves as a source or sink for electrons so that current can be passed from the external circuit through the cell. In general, neither its true potential nor current is ever measured or known.[22]

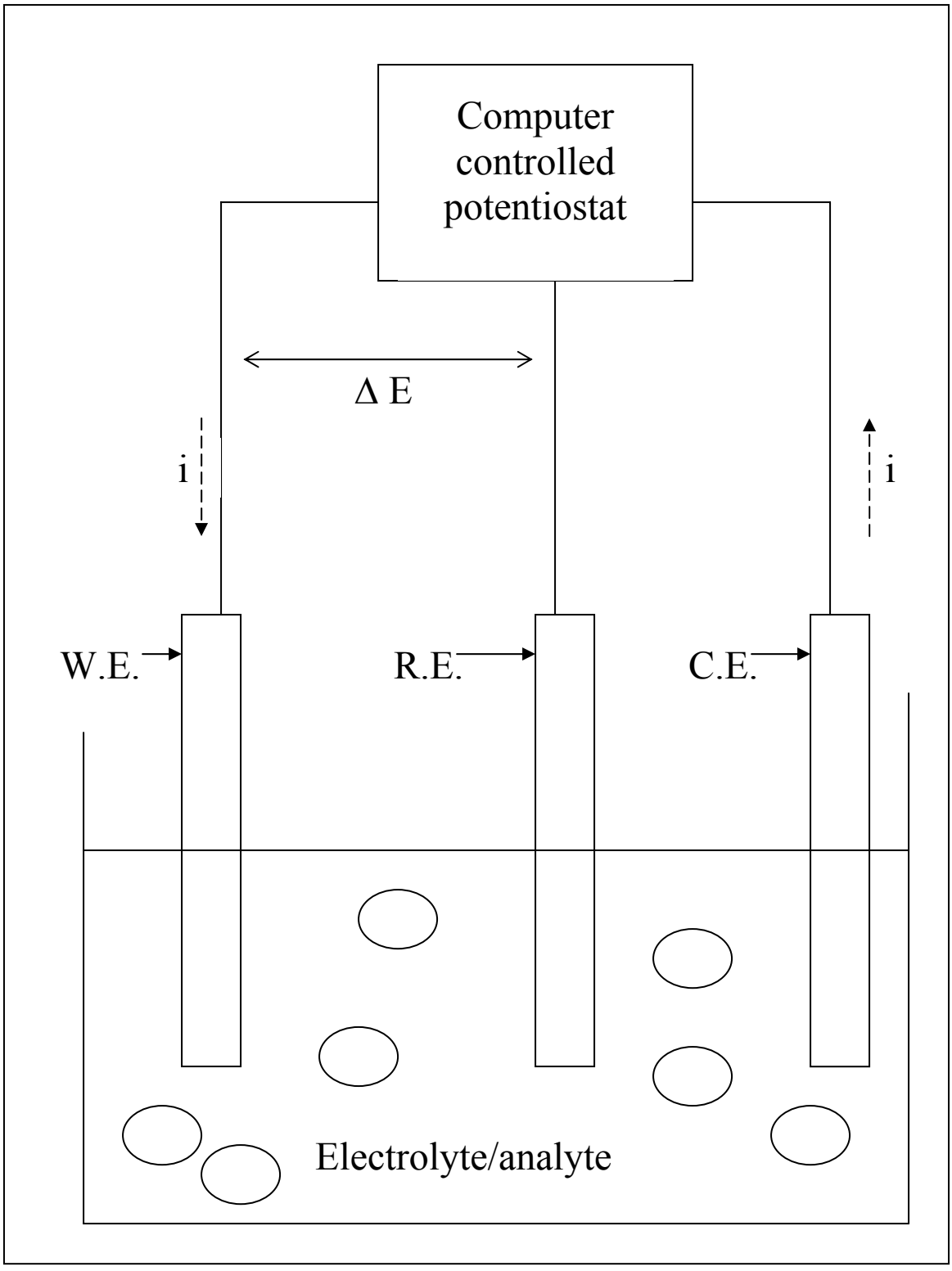

Figure 1.3 A conventional three-electrode cell: W.E. = working electrode; R. E. = reference electrode; C. E. = counter electrode; i = current.

The choice of an electrode material depends greatly on the useful potential range of the electrode in the particular solvent used and the qualities and purity of the material.

One or more of the following limits the usable potential range: [24]

- Solvent decomposition;
- Decomposition of the supporting electrolyte;
- Electrode dissolution or formation of a layer of an insulating/semiconducting substance on its surface;
- Poisoning through contact with solutions containing contaminants.

There are several reference electrodes used in electroanalytical experiments, silver | silver chloride (Ag | AgCl) being the most common. This consists of a piece of silver wire anodized with silver chloride in a glass tube. The wire is in contact with concentrated KCl or NaCl solution.[26] A semi-permeable salt bridge protects the electrode from the bulk solution. Many materials have been used as working electrodes. Mercury, carbon and "inert" (or noble) metals such as gold and platinum have been found to be essential working electrode materials. The geometry of these electrodes must also be considered. An inert conducting material, such as platinum wire or graphite rod, is usually used as the current carrying auxiliary electrode.

Supporting electrolytes are usually used in conjunction with solvents for electrochemical experiments. The choice of the solvent is based upon the solubility of the analyte including its redox activity and the solvent properties (e.g. electrical conductivity, electrochemical activity and chemical reactivity). The solvent should not react with the analyte (or products) and should not undergo electrochemical reactions over a large potential range.[23] Solvent types include water, acetonitrile, dichloromethane,

dimethylformamide (DMF), dimethylsulfoxide (DMSO) or methanol. Certain applications may require mixed solvents. Supporting electrolytes are necessary in order to: decrease the resistance of the solution; eliminate electromigration effects; maintain constant ionic strength (by eliminating the effects of erratic amounts of naturally occurring electrolyte). The inert supporting electrolyte may be an inorganic salt, a mineral acid or a buffer. While potassium chloride or nitrate and sodium hydroxide are usually used when employing water as a solvent, tetraalkylammonium salts are often utilized in organic media. Buffer systems (e.g. acetate) are used when pH control is essential. The supporting electrolyte should be prepared from highly purified reagents and must not be easily oxidized or reduced. A large excess of the electrolyte concentration is used (e.g. 0.1 – 1.0 M).[23]

1.2.3. Cyclic Voltammetry[22]

Voltammetry may be defined as an electrolysis process limited by the mass transport rate at which molecules move from the bulk of the solution to the electrode. The current is followed as a function of the potential applied using a three-electrode cell of 1-50 ml working volume. Voltammetric methods are limited to easily reducible or oxidizable compounds and are more practical for low-level quantification, possessing an extensive linear dynamic range (10^{-3} to 10^{-8} M).[22]

A more commonly used variation of the technique is cyclic voltammetry, in which the direction of the potential is reversed at the end of the first scan. This has the advantage that the product of the electron transfer reaction that occurred in the forward scan can be probed again in the reverse scan. In addition, it is a powerful tool for the determination

of formal redox potentials, detection of chemical reactions that precede or follow the electrochemical reaction and evaluation of electron transfer kinetics.

The basic shape of the current response for a cyclic voltammetry experiment is shown in Figure 1.4.[22] At the start of the experiment, the bulk solution contains only the reduced form of the redox couple (R), so that at potentials lower than the redox potential, i.e. the initial potential, there is no net conversion of R into O, the oxidized form (Point A, Figure 1.4). As the redox potential is approached, there is a net anodic current that increases exponentially with potential.[22] As R is converted into O, concentration gradients are set up for both R and O, and diffusion occurs down these concentration gradients. At the anodic peak (Figure 1.4, point B), the redox potential is sufficiently positive that any R that reaches the electrode surface is instantaneously oxidized to O. Upon reversal of the scan (Figure 1.4, point C) a net reduction of O to R occurs which causes a cathodic current that eventually produces a peak shaped response (Figure 1.4, point D).[22] If there is no reversal of potential then a Linear Sweep voltammogram is obtained.[27]

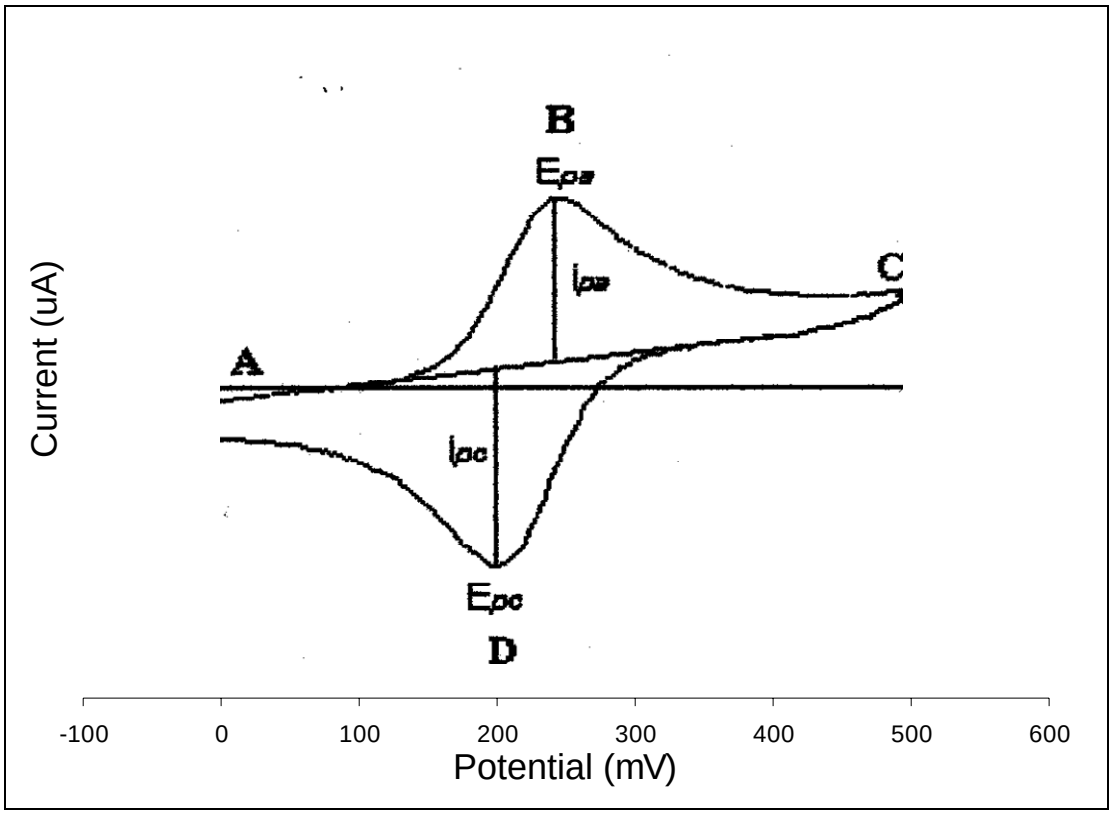

Figure 1.4 The basic shape of the current response in a cyclic voltammetry experiment.[22]

If a redox system remains in equilibrium throughout the potential scan, the electrochemical reaction is said to be reversible. This is to say equilibrium requires that the surface concentrations of O and R be maintained at the values required by the Nernst equation. Under these conditions, the following parameters characterize the cyclic voltammogram of the redox process:

- The peak potential separation (E_{pa} - E_{pc}) is equal to 59/n mV for all scan rates where n is the number of electron equivalents transferred during the redox process;
- The peak width is equal to 28.5/n mV for all scan rates;
- The peak current ratio (i_{pa}/i_{pc}) is equal to 1 for all scan rates;

- The peak current function increases linearly as a function of the square root of ν (scan rate).

For reversible systems the Nernst equation can be applied. The current of reversible reactions may be represented by the Randles-Sevcik equation 1.1:

$$i_p = 2.69 \times 10^5 n^{3/2} A D^{1/2} c \nu^{1/2} \qquad 1.1$$

where i_p is the peak current, n is the moles of electrons; A is the electrode area; D is the diffusion coefficient; c is the analyte concentration; ν is the scan rate.

By contrast, an *irreversible* reaction is one where the electrode reaction cannot be reversed. Slow electron exchange or chemical reactions at the electrode surface may result in irreversibility. A high kinetic barrier has to be overcome, achieved by the application of an extra potential (extra energy) called the overpotential (η). Cyclic voltammograms showing a single oxidation or reduction wave signify an irreversible system. A large peak current separation (> 200 mV) also indicates irreversibility.

Quasi-reversible reactions exhibit behaviours intermediate between reversible and irreversible reactions, the overpotential having a relatively small value, so that with this extra potential reactions can be reversed.[24] This phenomenon is observed when the return peak is smaller than its couple and/or a larger peak potential separation is observed in comparison to reversible systems. A peak separation of 80 to 200 mV is characteristic of a quasi-reversible system.

A summary of reversible, irreversible and quasi-reversible parameters is shown in Table 1.1.

Table 1.1 A synopsis of reversible, irreversible and quasi-reversible systems.

Parameter	Reversible	Irreversible	Quasi-reversible
E_p	Independent of ν	Shifts cathodically by $30/\alpha n$ mV per 10-fold increase in V	Shifts with ν
$E_{pc} - E_{pa}$	~ 59/n mV at 25 ^oC and independent of ν	No return peak or > 200 mV	May approach 60/n at low ν but increases as ν increases
$i_p/\nu^{1/2}$	Constant	Constant	Constant
i_{pa}/i_{pc}	Equals 1 and independent of ν	Generally no current on the reverse side	Equals 1 only for $\alpha = 0.5$

Note: α = rate of electron transfer, ν = scan rate (Vs^{-1}), V = potential (V).

1.2.4. Square Wave Voltammetry

Square Wave Voltammetry (SWV) is a useful method for studying redox reactions with overlapping waves.[28] This type of polarography is often named Osteryoung Square Wave Voltammetry. In SWV a square wave potential superimposed to a staircase potential is applied to the working electrode (Figure 1.5).[28]

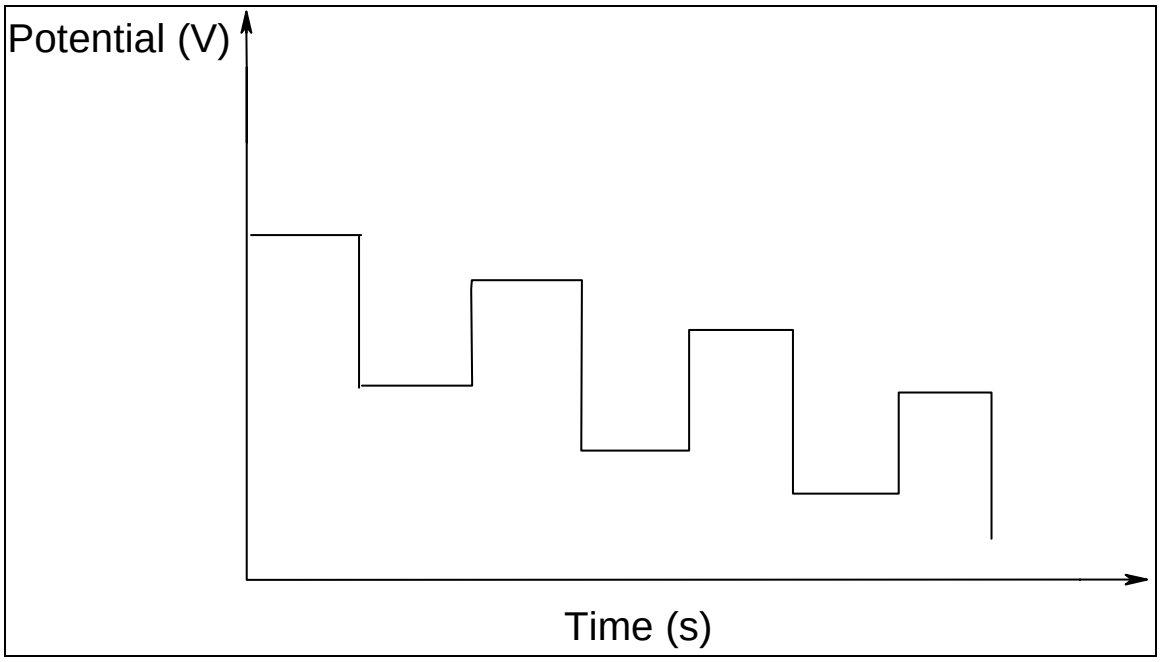

Figure 1.5 Diagrammatic representation of a Square Wave curve.

An example of a Square Wave voltammogram is shown in Figure 1.6.

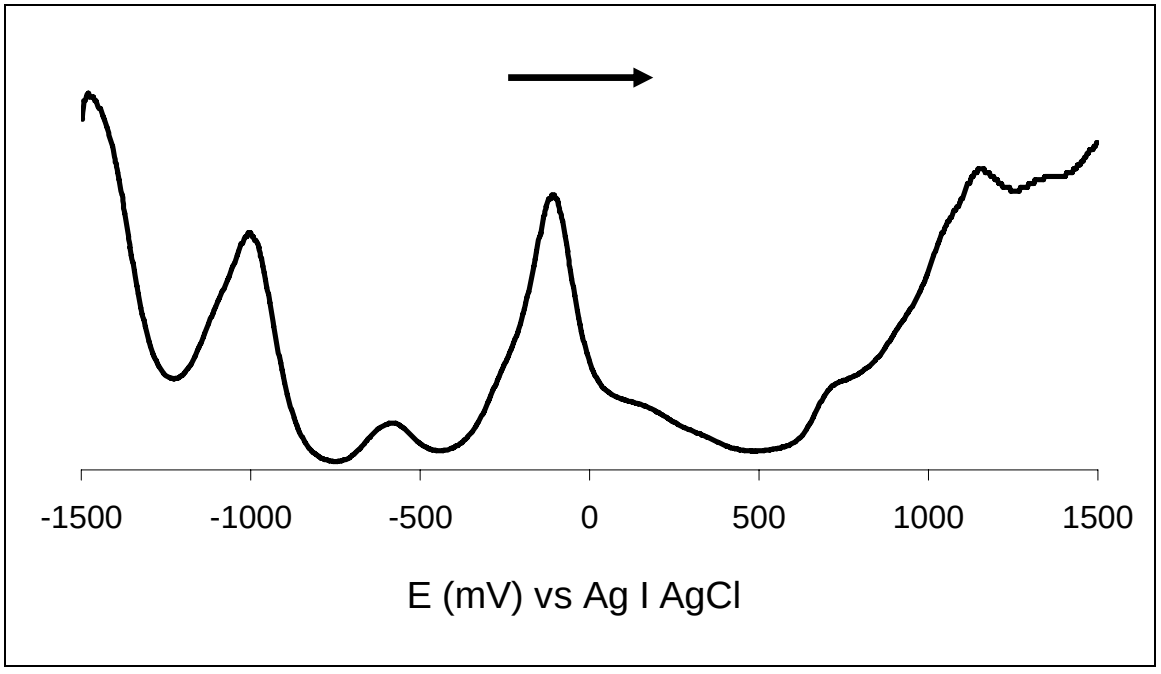

Figure 1.6 Typical Square Wave voltammogram.

For reversible processes the peaks are Gaussian shaped and the peak potentials (E_p) are equal to the half potentials ($E_{1/2}$) of the redox processes.[28] An estimate of the number of electrons (n) involved in the redox process under each peak can be obtained from the peak height (i.e. the peak current), which is approximately proportional to n. A more exact evaluation of the number of electrons involved can be calculated from the half peak widths ($W_{1/2}$) which depend on factors such as temperature and the number of electrons involved.[28] The ability to analyze both the forward and reverse currents as well as the net current in Square Wave Voltammetry proves useful as information about reaction reversibility can be obtained easily.[28]

1.2.5. Spectroelectrochemistry

Spectroelectrochemistry combines the use of electrochemistry and spectroscopy. A particular electrochemical cell, called an OTTLE (Optically Transparent Thin Layer Electrode) cell, holds the redox active compound, which is either oxidized or reduced. Product formation is then monitored *in situ* by spectroscopic techniques.[24,29] Spectroelectrochemistry may also be used to characterize the products of oxidation or reduction of redox complexes. The use of spectroelectrochemistry in MPc studies is based on the well known fact that the spectra of ring-based processes drastically affects the Q band[30] while the metal-based[20] redox processes result only in the shift in the Q band without much change in intensity. Spectroelectrochemistry may consequently be used to: monitor electron transfer reactions; investigate the stability of the oxidation or reduction products; determine the reversibility of an electrochemical reaction.

Information gathered from spectroelectrochemistry can be applied to Faraday's Law, equation 1.2:

$$Q = nFvc_o \qquad 1.2$$

where Q is the charge read from the spectroelectrochemical instrument; F is Faraday's constant, v is the volume (usually 0.5 ml), and the initial concentration, c_o, is attained from Beer's Law ($A = \varepsilon c_o l$). Hence one may find n, the number of electrons occurring in the electrochemical process.

1.3. Chemistry of Phthalocyanines

1.3.1. The origin of the Q and B bands

The ultraviolet-visible (UV-vis) absorption spectra of typical metallophthalocyanines (Figure 1.7) are exemplified by discrete bands arising from transitions within the delocalised phthalocyanine ring system. A diagrammatic illustration of an ultraviolet-visible (UV-vis) spectrum is shown in Figure 1.7.

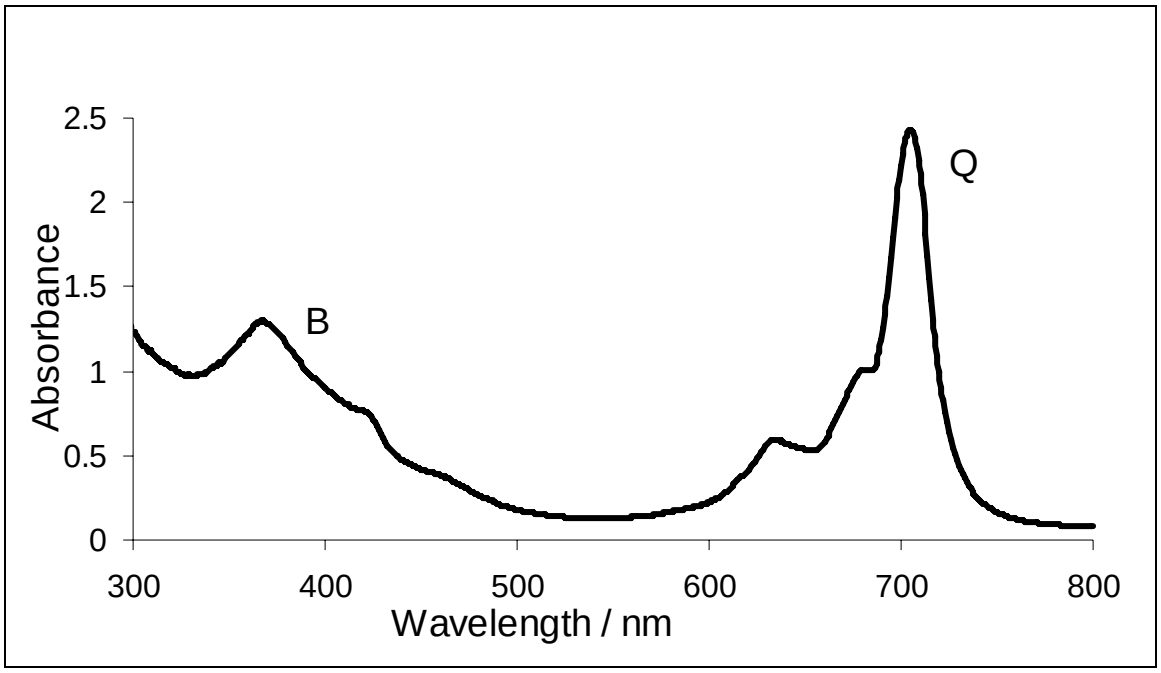

Figure 1.7 Classic electronic absorption spectra of a metallophthalocyanine, showing the B and Q bands.

Under D_{4h} symmetry, the Q band (Figure 1.7), occurring in the far end of the visible region at approximately 650 -750 nm in MPcs, has been attributed to the $\pi \rightarrow \pi^*$ electronic transition from the HOMO (highest occupied molecular orbital) to the LUMO (lowest unoccupied molecular orbital) of the Pc^{2-} ring.[31] Less intense bands in the blue end of the UV region are called B (or Soret) bands (Figure 1.7).[32,33] The B bands have been attributed to the deeper π levels $\rightarrow$ LUMO transitions. The origins of these first two $\pi \rightarrow \pi^*$ transitions are shown in Scheme 1.4.

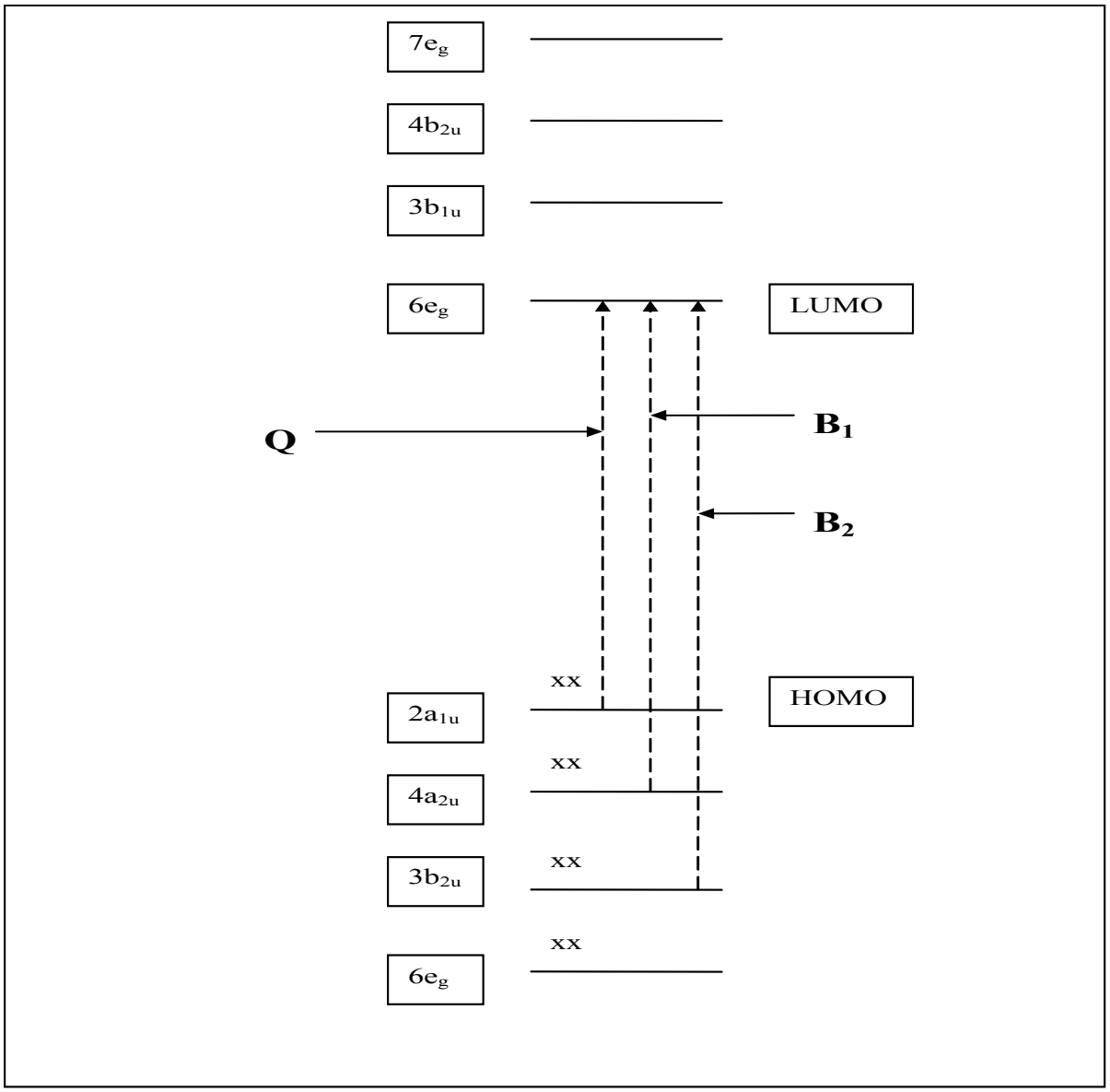

Scheme 1.4 Electronic transitions showing the derivation of the Q and B bands in phthalocyanine complexes. A 'x' represents an electron.

Gouterman's four orbital model explains that the spectra of MPc complexes are due to transition of electrons from the HOMO (highest occupied molecular orbital, π) to the LUMO (lowest unoccupied molecular orbital, π*).[34] The Q band results from the transition of electrons from the HOMO ($2a_{1u}$) to the LUMO ($6e_g$) orbital. The B bands

arise from electronic transitions from the $4a_{2u}$ and $3b_{2u}$ orbitals to the LUMO ($6e_g$) orbital (Scheme 1.4).

Both Q and B bands in alkylthio substituted Pcs are at longer wavelengths relative to unsubstituted Pcs. Such a red shift implies that the energy gaps between the HOMO and LUMO and between deeper π levels and the LUMO of alkylthio substituted Pcs are narrower than those of alkyloxy substituted Pcs.[32]

This work studies the electronic transition properties of the synthesised substituted phthalocyanines for characterization and spectroelectrochemistry purposes.

1.3.2. Electrochemistry and Spectroelectrochemistry of Phthalocyanines

The electrochemistry of metallophthalocyanine species is vast with several redox processes involved.[35,36] Diverse electrochemical properties may be achieved by incorporating different metals into the core of the Pc ring and by varying the periphery substituents.[35] Redox processes occuring in MPc complexes may hence occur at the Pc ring or at the central metal and are influenced by: the nature of the substituents on the Pc ring; the nature and oxidation state of the central metal; the nature of any axial ligands and solvents.[33]

The neutral form of Pc exists as a dianion, and may be represented as Pc^{2-}.[37] If metal orbitals lie at energies within the highest occupied molecular orbital-lowest unoccupied molecular orbital gap of the ring, oxidation or reduction, or both, may occur at the central metal.[32,38] Hence metals most commonly used in phthalocyanine electrochemistry are Co^{II}, Fe^{II}, and Mn^{II}. Typical oxidation and reduction processes of metal phthalocyanines

may then be depicted as shown below where M represents the metal, Pc the phthalocyanine ring and e^- an electron:

-Oxidation: $M^{2+}Pc^{2-} \rightarrow M^{3+}Pc^{2-} + e^-$

-Reduction: $M^{2+}Pc^{-} + e^- \rightarrow M^{+}Pc^{2-}$

Reduction of the Pc ring may occur by the successive gain of one to four electrons by the LUMO of the MPc complex, resulting in the formation of MPc^{3-}, MPc^{4-}, MPc^{5-} and MPc^{6-} species.[37] Scheme 1.5 represents the energy level diagrams of neutral, one-electron ring reduced and one-electron ring oxidized MPc complexes.

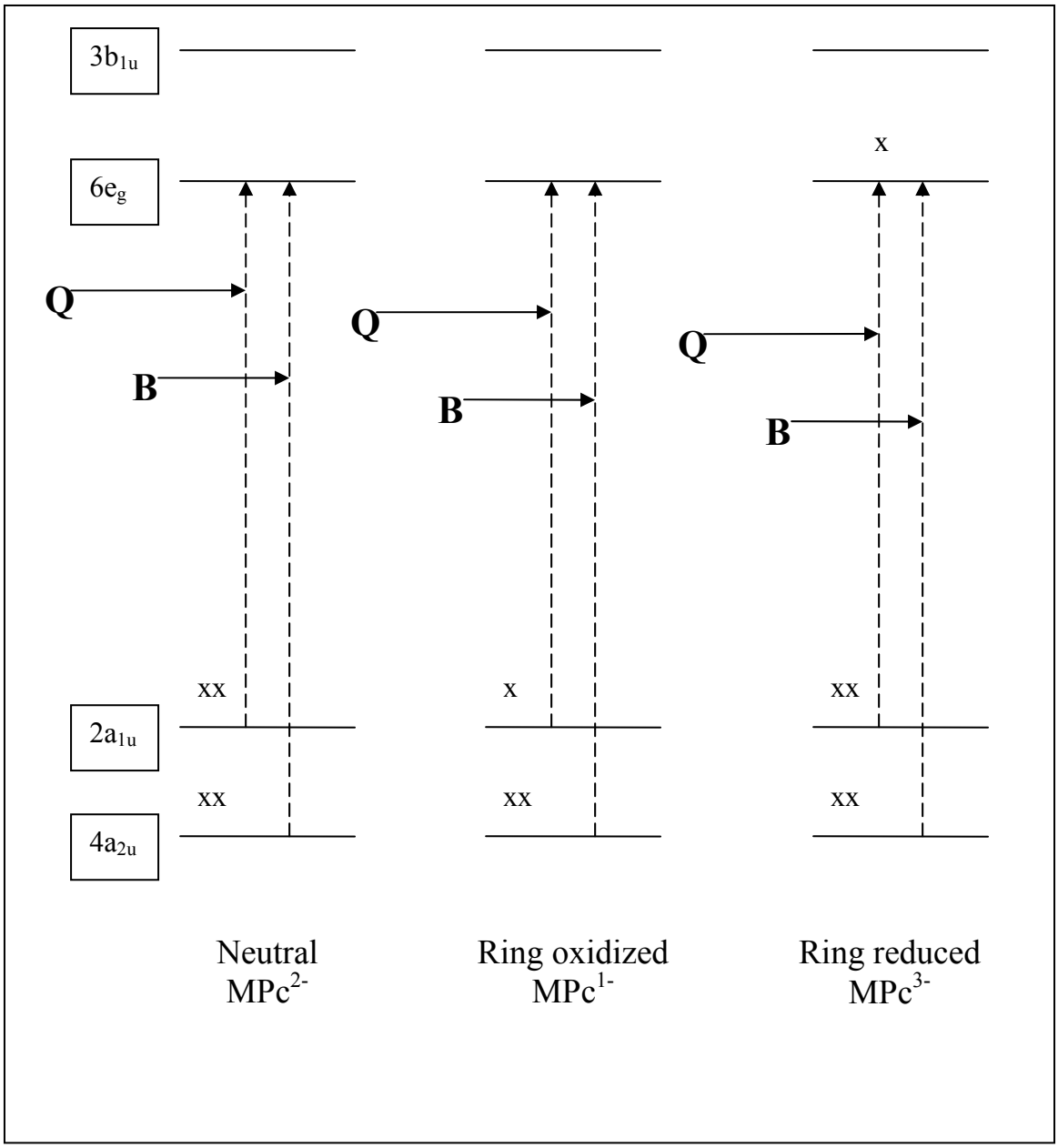

Scheme 1.5 Energy level diagrams of neutral, one-electron ring reduced and one-electron ring oxidized MPc complexes. A 'x' represents an electron.

Alterations in the oxidation state often result in reversible redox reactions and colour changes due to the ring based redox processes in MPc complexes.[38]

A shift in the Q band wavelength is due to the oxidation or reduction of the central metal in MPcs.[20] The collapse of the Q band with the formation of new/weak bands pertains to a redox reaction on the Pc ring.[30]

One may use cyclic voltammetric and spectroelectrochemical techniques in tandem to prove electron processes occurring during redox reactions. Other electrospectroscopic methods include electrochemically modulated infrared reflectance spectroscopy and UV-vis electrochemically modulated reflectance spectroscopy.

The reactions of metal-free phthalocyanines and metal phthalocyaninates (peripherally octasusbstituted with various alkylthio-groups) with silver or palladium salts were investigated using spectroelechemistry in order to study their aggregation or disaggregation effects.[15] Peripherally substituted octabutylthiophthalocyanine complexes containing Zn^{2+} and Fe^{2+} have been synthesised and their electrochemical and spectral properties have been investigated.[18] There have been a small number of patents and publications describing the use of these compounds as IR absorbers,[39,40] mainly due to the shift of their high intensity Q bands to longer wavelengths.

This work presents electrochemical and spectral attributes of novel thiol substituted phthalocyanines.

1.4. Self Assembled Monolayers

A self assembled monolayer (SAM) may be defined as an organized molecular layer in which the constituents share a universal orientation.[41] Self assembled monolayers are formed by the spontaneous absorption of molecules (thiol metallophthalocyanines in this work) onto a substrate (gold electrode surfaces in this study).[41] Self assembled

monolayers would be more comprehensively described as organized molecular assemblies or particularly thin films (one molecule thick) whose unprompted formation and stability depend on favourable, if weak, intermolecular forces, as well as forces between each of the individual component molecules and the solid substrate or support.[21] A diagrammatic representation of a self assembled monolayer consists of molecules with recognizable head and tail groups (Figure 1.8).

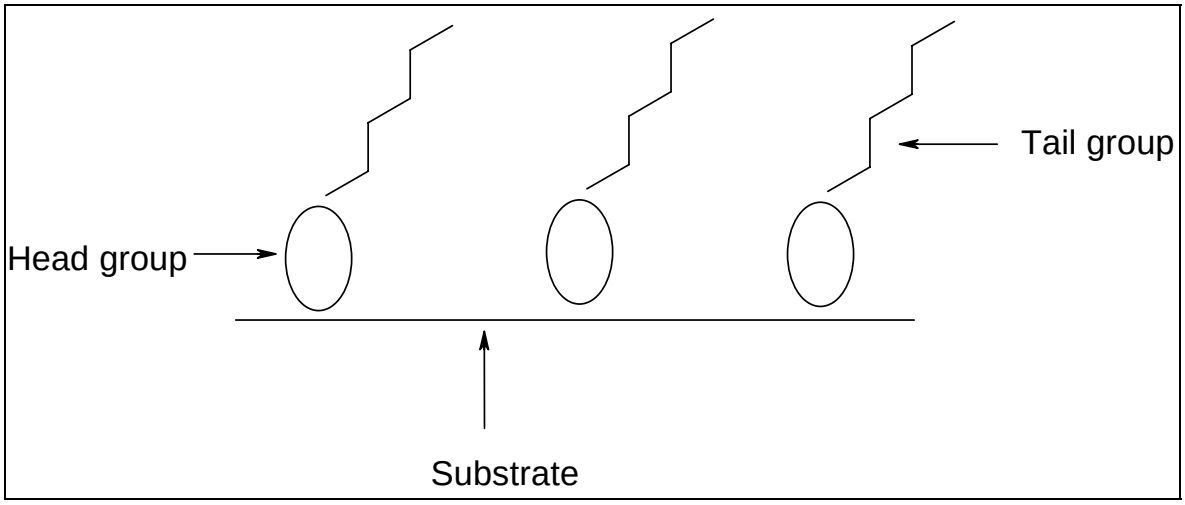

Figure 1.8 Diagrammatic representation of a self assembled monolayer attached to a substrate surface.

Self assembled monolayers are advantageous in that their formation, in addition to being spontaneous, is fast and follows relatively simple protocols.[42] The two disadvantages of self assembled monolayers are that these layers are limited to specific substrates (e.g. thiols) and in most cases are restricted to metal surfaces (e.g. gold).

SAM formation may be understood in terms of the HSAB ('hard and soft acids and bases') theory.[43] The S^{2-} anion is an example of a monodentate Lewis base as it is a ligand that donates one electron pair to one acid ion or molecule.[43] Au, functioning as a

Lewis acid, forms strong covalent bonds with the Lewis base S^{2-}. The Lewis HSAB theory hence explains why the SAM bonding between thiols and Au is so favorable and strong.

Several factors, listed below, must be considered in an attempt to achieve ideal monolayer orientation on substrate surfaces:[41]

- Substrate morphology: the degree of crystallinity of the substrate may ultimately affect the self assembled monolayer orientation. Irregular substrate morphology leads to an irregular packing of self assembled monolayers on the surface and vice versa. A rough substrate surface, relative to a smooth substrate surface, may lead to a higher density of self assembled monolayers due to an increase in available surface area.[44]
- Pre-deposition cleaning: substrate surfaces (e.g. gold electrode surfaces) are usually cleaned by sonication in an organic solvent followed by exposure to an oxidizing cleaner called 'piranha solution'. Piranha solution is prepared by mixing concentrated sulfuric acid and 30% hydrogen peroxide in a 3:1 volume ratio followed by heating. Contaminant particles adsorb to electrodes less strongly than self assembled monolayer constituents. Hence cleaning an electrode before self assembled monolayer deposition is not essential but nonetheless good practice.[41]
- Deposition solvent: solvent choice depends on several factors which may include solvent toxicity levels, solvent purity and solubility of the adsorbate in the solvent (milli molar concentrations being ideal). Otherwise all common organic solvents (e.g. ethanol) may be used appropriately for self assembled monolayer deposition.

- Deposition concentration, time and temperature: All three factors are inter-related. A high deposition concentration (e.g. milli molar levels) allows for a lower deposition time and also maybe a lower temperature environment. Lower concentrations may require longer deposition times due to mass transport limitations of the adsorbate (e.g. thiol) to the substrate (e.g. gold electrode surface).[45] The substrate is usually left in the deposition solvent for times ranging from 30 minutes to 24 hours, though longer deposition times have been reported.[46]

Thus, there has been a growing interest in thiol-derivatized metallophthalocyanines in recent years for the manufacture of self-assembled monolayers and Langmuir-Blodgett films.[47] SAMs are an incredibly versatile means of extending the functions of an electrode and have been known to offer greater advantages over other film formation techniques.[42,48] SAMs have also widely been used as metal ion sensors,[49] immunosensors[50] and biosensors.[51]

1.4.1. Characterization of Thiol derivatised MPc-SAMs

A diagrammatic representation of a thiolate-on-gold self assembled monolayer is shown in Figure 1.9.

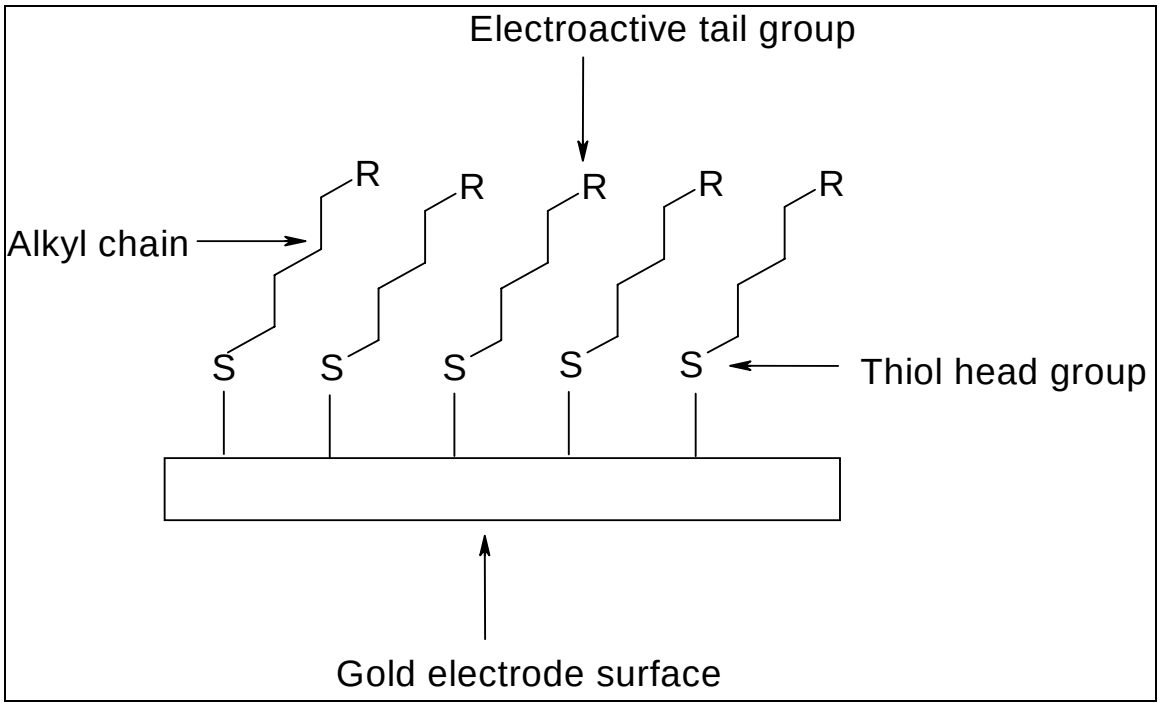

Figure 1.9 Thiolate-on-gold self assembled monolayer illustration.

Bond strengths between sulphur and the Au atom in particular have been calculated to be very high.[52] It is believed that the sulfides (e.g. from the thiol MPc-SAMs studied in this work) form monolayers on the gold surface with the C-S bonds intact.[42]

There has been work done on the modification of Au electrodes with alkyl-thiol SAMs.[53,54] Phthalocyanines substituted with sulphur groups for self assembled monolayer studies have been relatively fewer due, in a large part, to a thiol-MPc's complex development.[2,15] Studies of the electrode response of thiol-MPc functionalized electrodes in self assembled monolayer research have been reported.[47,55,56]

The characterization of MPc-self assembled monolayers is prominently based on the principle that such monolayers block a number of Faradic processes. The assembly of MPcs on conductive surfaces blocks the interfacial electron transfer i.e. formation of a MPc complex on the electrode surface is expected to introduce a barrier for the electron

transfer at the electrode surface.[57] The inhibition of the electron kinetics at the electrode interface can be monitored by different electrochemical techniques such as cyclic voltammetry. Voltammetric techniques provide a suitable and insightful type of characterization.

1.4.1.1. Ion Barrier Factor, Γ_{ibf}

Pinholes in SAM studies may be defined as "a site at which the electrode surface is exposed to the electrolyte".[41] Hence at such a site an adsorbed molecule is absent and the tails of nearby absorbed molecules do not block the site. The absence of pinholes in SAMs is commonly indicated by the inhibition of gold surface oxidation.[41] Therefore the area under the well defined reduction peak (the oxide removal or stripping peak) is considered as the factual measure of the total pinhole area available for a serene penetration of ions present in the analyte solution. By comparison of the total charges produced under the peak due to the reduction of a bare Au (Q_{Bare}) and a MPc-SAM modified electrode (Q_{SAM}), the film 'ion barrier factor' Γ_{ibf} can be obtained by using equation 1.3:

$$\Gamma_{ibf} = 1 - \frac{Q_{SAM}}{Q_{Bare}} \qquad 1.3$$

The total charge Q (C) is obtained by integrating the currents (As^{-1}). A Γ_{ibf} of unity (i.e. when $Q_{SAM} = 0$) is an indication that the Au surface is completely isolated from the aqueous solution, which is the oxygen source for gold oxide formation. This shows that

the self assembled monolayer provides an excellent barrier to permeation of the electrolyte species.[41]

1.4.1.2. Interfacial Capacitance, C_s

The interfacial capacitance, C_s, examines ion permeability through the SAM as it provides the answer as to how 'close packed' and defect-free the monolayer is.[42,54] The interfacial capacitance, C_s ($\mu F/cm^2$), is given by equation 1.4:

$$C_s = \frac{i_{ch}}{\nu A} \qquad 1.4$$

where i_{ch} is the charging current (μA), ν is the scan rate (V/s) and A is the surface area of the electrode (cm^2).

The lower the C_s value, the fewer defects there are in the SAM and thus the less permeable electrolyte ions are to the electrode surface.[41]

1.4.1.3. Inhibition of Redox Couples

Another demonstration of the blocking by SAM is the inhibition of metal deposition on the gold electrode. Metal deposition is inclusive of both bulk deposition of the metal at potentials close to the thermodynamic potential and underpotential deposition (UPD) at potentials well positive of the thermodynamic potential.[41] A cyclic voltammogram of bare gold in a Cu^{2+} aqueous electrolyte solution illustrates both facts: the start of bulk deposition of Cu is evident near the standard potential of Cu^{2+} (+0.10 V vs. SCE) during the negative-going scan and is accompanied on the return scan by a prominent stripping peak for the copper metal (at ~ +0.2 to +0.3 V vs. SCE). An ideal MPc-SAM-modified

gold electrode will hence tend to block the metal deposition and therefore the stripping processes.[41]

Thiol-MPc-SAM-modified gold electrodes should also inhibit Faradic processes of a soluble analyte, such as $Fe(NH_4)(SO_4)_2$ oxidation. The ability of a thiol-MPc-SAM to act as a barrier to the transport of $[Fe(H_2O)_6]^{3+}/[Fe(H_2O)_6]^{2+}$ redox species (from $Fe(NH_4)(SO_4)_2$ solution) is an excellent indication that this SAM film is compact and/or that the pinholes are smaller than the electroactive probe ions.

1.4.1.4. Surface Coverage studies

Determining surface coverage of an MPc SAM can be done using 2 different methods:[58]

(i) Electrochemical desorption of the alkylthiol: SAMs are known to desorb quantitatively from Au surfaces at negative potentials in strongly alkaline electrolytes (e.g. KOH). During such electrochemical desorption, a reduction peak due to the reductive desorption of the thiolate is observed. The area under this reductive peak corresponds to the coverage of the SAM.

(ii) Surface concentration may be estimated from the charge produced by a M^{III}/M^{II} (where M = metal) couple of the adsorbed MPc on an Au electrode obtained in a suitable aqueous analyte. Surface coverage (Γ) may then be calculated using equation 1.5:

$$i_p = n^2F^2A\Gamma\,(\nu)/4RT \qquad 1.5$$

where i_p is the peak current (Amps), n is the number of electrons, A is the area of the electrode (cm^2), ν is the scan rate (V/s) and the other symbols have their usual meanings. This method of surface coverage calculation was used in this work.

The orientation of the MPc-SAM can be estimated from the surface concentration coverage. MPc substituted with eight peripheral thiols or thioacetates bind to Au surfaces by adopting the so-called 'octopus' orientation.[55,56]

1.4.2. Electrocatalytic activity of MPc-SAM toward L-cysteine

Cysteine {(R)-2-amino-3-mercaptopropionic acid}, a common amino acid, is a thiol that plays vital roles as a substrate for protein synthesis and as a rate determining precursor for glutathione (an important biological molecule). L-cysteine is also used in the pharmaceutical and cosmetics industries.[59]

Electrochemical oxidation of L-cysteine at most common electrodes occurs at the extreme positive potentials with slow electron transfer kinetics, limiting the use of these electrodes for analysis. The use of MPc-SAM modified electrodes has been recognized to lower the overpotential for cysteine oxidation with fast electron transfer rates.[60,61] Table 1.2 shows the peak potentials of L-cysteine electrocatalysis (in acidic conditions) using electrodes modified with CoPc and FePc-SAM species, and also shows that lower potentials are obtained compared to CoPc on a glassy carbon electrode (GCE).

Table 1.2 Peak potentials (E_p) of L-cysteine electrocatalysis, in acidic conditions, using substituted CoPc and FePc-SAM modified electrodes.

MPc	Electrode Material	E_p / V (vs Ag|AgCl)	Reference
CoPc	SAM-GCE	0.67	62
CoOHETPc	SAM-Au	0.50	57
CoOBTPc	SAM-Au	0.42	16
FeOHETPc	SAM-Au	0.38	57
FeOBTPc	SAM-Au	0.33	58

It is accepted that the mechanism for the electrocatalytic oxidation of cysteine by MPc complexes is oxidation of the central metal in $M^{II}Pc$ forming $M^{III}Pc$ followed by electron transfer from the cysteine to the latter.[62,63] The product of oxidation of cysteine is cystine. This mechanism is depicted in equations 1.6 – 1.9:

$$M^{II}Pc^{-2} \rightarrow M^{III}Pc^{-2} + e^{-} \qquad 1.6$$

$$M^{III}Pc^{-2} + RSH \rightarrow (RSH)M^{III}Pc^{-2} \qquad 1.7$$

$$(RSH)M^{III}Pc^{-2} \rightarrow M^{II}Pc^{-2} + RS^{+} + H^{+} \qquad 1.8$$

$$2RS^{+} \rightarrow RSSR \qquad 1.9$$

where RSH represents L-cysteine and RSSR is cystine, the oxidation product of L-cysteine.[62,63]

1.4.3. Immobilization of Amine substituted MPcs on pre-formed SAMs

Cobalt tetraamino Pc (CoTAPc, **3**, Figure 1.10) may be deposited at Au electrode surfaces that have been modified with a self assembled monolayer of alkanethiol acids, using either 1-ethyl-3-(3-dimethylaminopropyl)-carbodiimide (EDC, **4**, Figure 1.10) or dithiobis(*N*-succinimidyl propionate) (DTSP, **5**, Figure 1.10) as coupling reagents. In both instances the creation of an amide bond occurs. Figure 1.10 shows the structures of the CoTAPc, thiol (mercaptopropionic acid, **6**) and coupling agents (EDC and DTSP) used in the covalent coupling studies of this work.

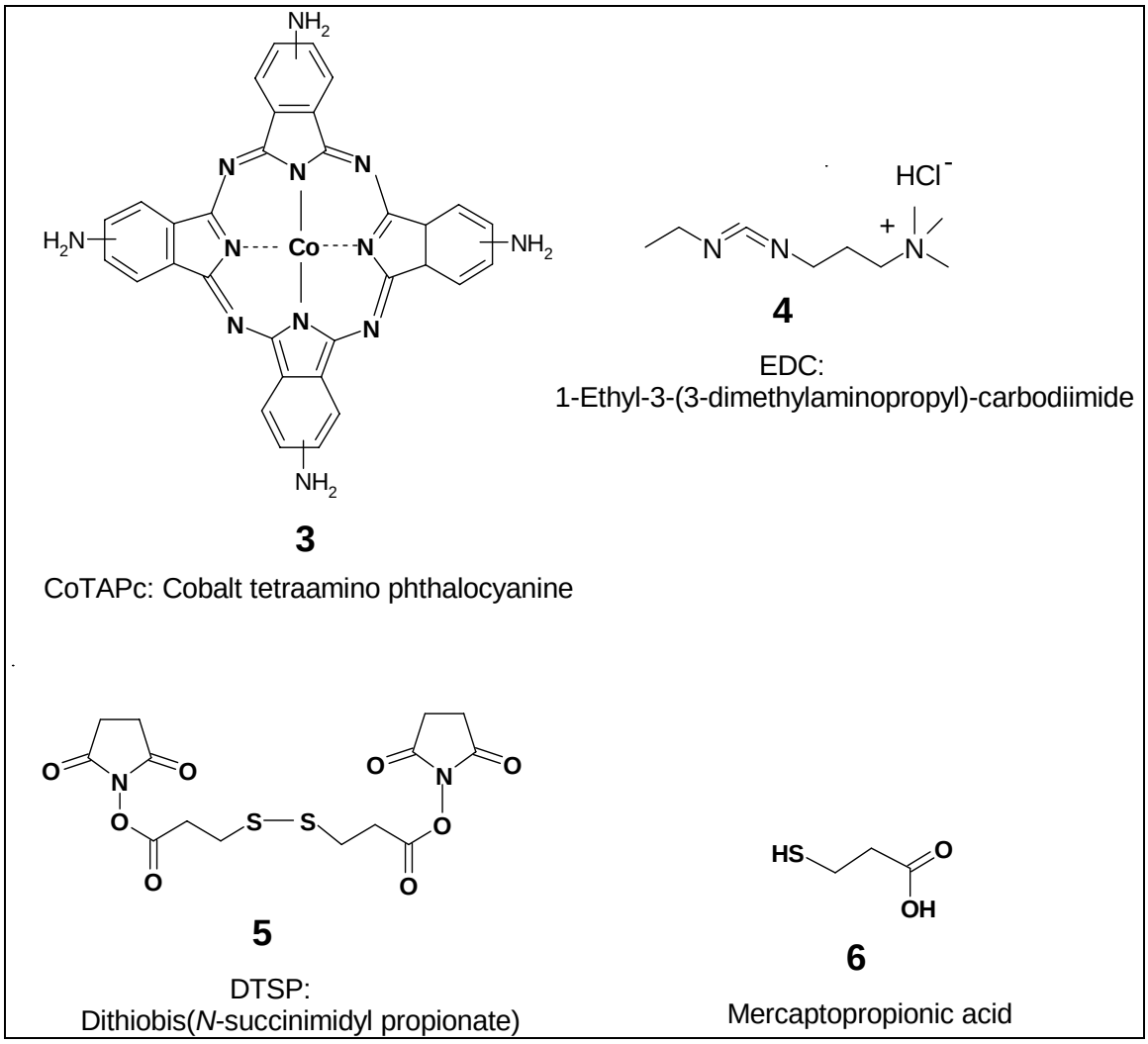

Figure 1.10 Structures of the prominent complexes used in the amino-carboxyl coupling SAM studies.

Anchoring of MPcs to SAM modified electrodes avoids complex thiol MPc synthesis whilst voltammetric techniques provide a convenient and sensitive method of characterization. Metallophthalocyanines (such as CoTAPc used in this work) exhibit a series of oxidative and reductive electron transfer processes and hence may be used as versatile electron relays for the activation of redox processes.[35,36] However, their poor solubility in aqueous media inhibits their use as diffusional electron mediators.

Nonetheless metallophthalocyanines immobilization on electrodes may yield active interfaces that may mediate electron transfer between the electrode and e.g. enzymes. In the amino-carboxyl coupling studies involving EDC, the self-assembled monolayer is formed by adsorption of the thiol functionalized molecule e.g. **6** (Figure 1.10) onto the Au electrode. EDC (**4**) is a water soluble derivative of carbodiimide.[64] Carbodiimide catalyses the formation of bonds between carboxylic acids and phosphates or amino acids. Its water soluble derivative may hence be used to form, amongst other links, peptide bonds from acids and amines.[64]

Scheme 1.6 shows an example of a possible mechanism of the activation of a thiol functionalized carboxylic group (e.g. from compound **6**) by EDC (**4**) and further reaction with an amine (from CoTAPc (**3**), used in this work) resulting in an amide bond formation.

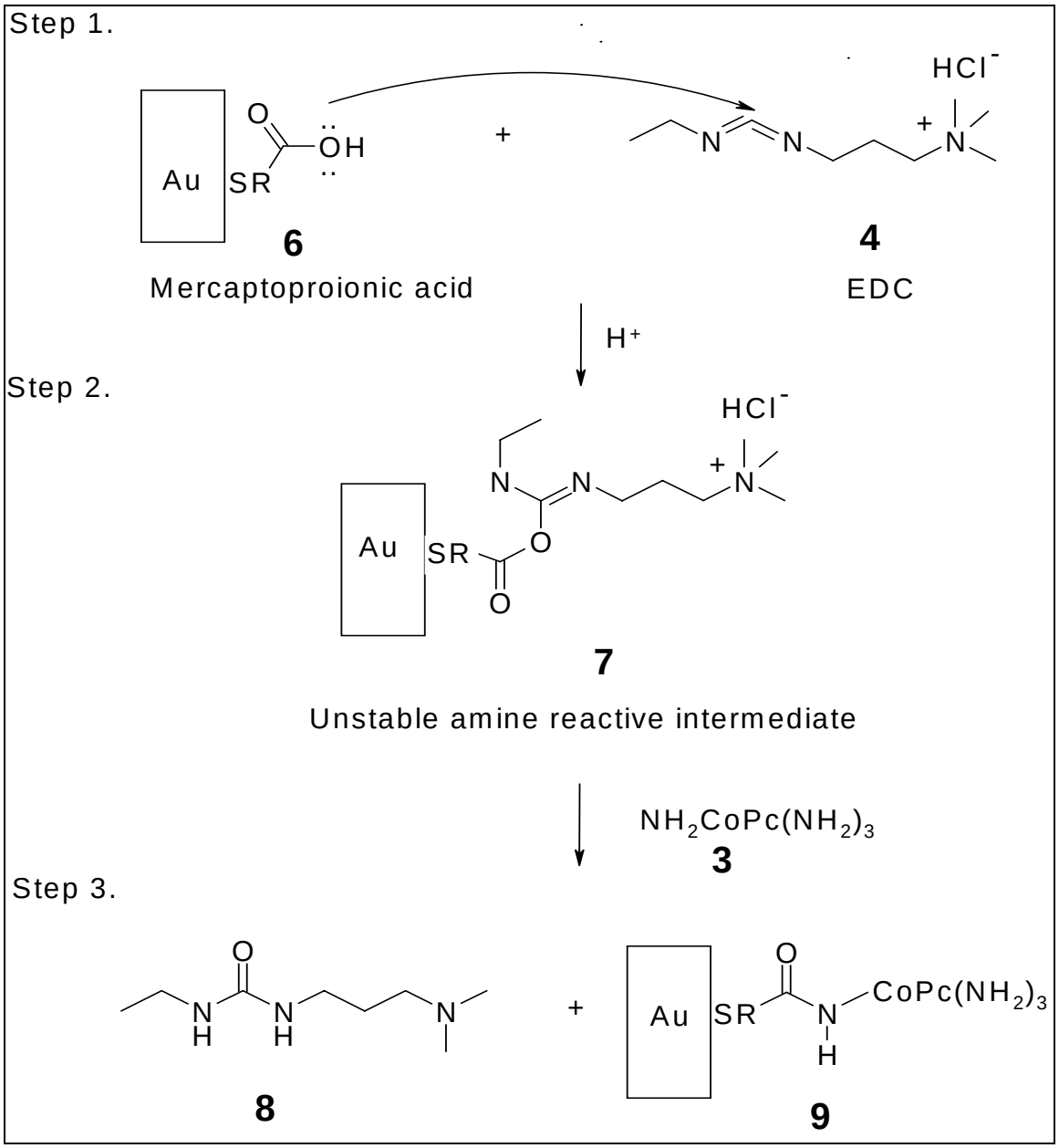

Scheme 1.6 Mechanism of the activation of a thiol functionalized carboxylic group by EDC (**4**) and further reaction with an amine (**3**) resulting in an amide bond formation (in compound **9**). R = hydrocarbon group C_2H_4; Au = gold electrode surface.

Hence in the EDC coupling mechanism, there is an initial nucleophillic addition reaction between a thiol functionalized carboxylic acid group (in **6**, Scheme 1.6) and the carbon bonded to the two nitrogens in EDC (Step 1, Scheme 1.6). This forms an unstable amine-

reactive intermediate (**7**, Scheme 1.6). The reaction of the intermediate with an amine (CoTAPc, **3**, in these studies) results in the two complexes **8** and **9** (Step 3, Scheme 1.6), one of which possesses the desired amide bond (**9**).

Amino-carboxyl coupling may be achieved at an electrode surface if the self assembled monolayer contains active ester groups.[65] These groups spontaneously react with amino groups of organic compounds. Dithiobis(*N*-succinimidyl propionate) or DTSP (**5**), otherwise known as Lomant's reagent, adsorbs onto Au surfaces through it's disulfide group. Scheme 1.7 represents the concept of a SAM formation of DTSP followed by further coupling to an amine (from CoTAPc, used in this work) resulting in an amide bond formation.

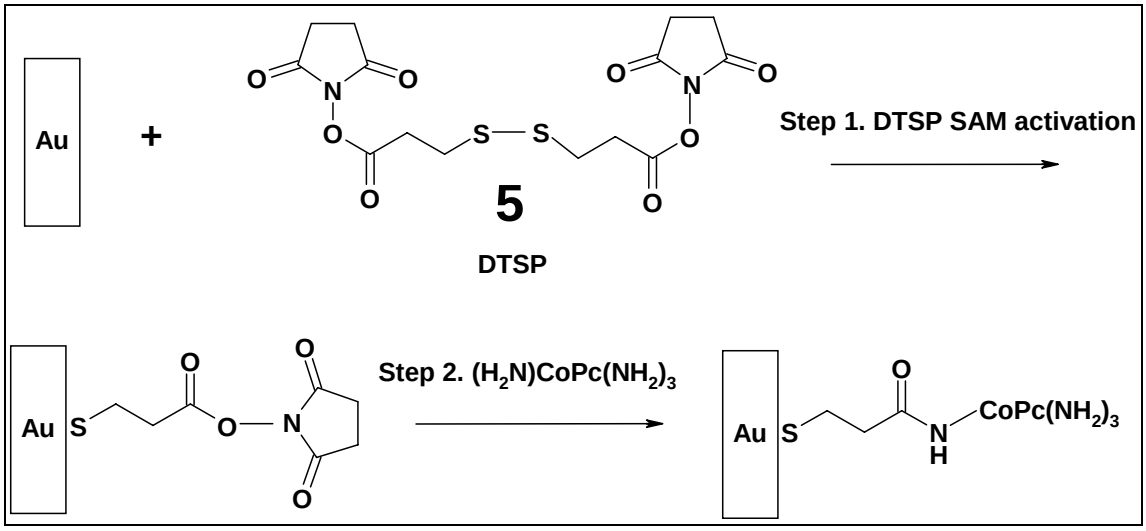

Scheme 1.7 Diagrammatic conception of DTSP (**5**) SAM coupling to an amino group of CoTAPc. Au = gold electrode surface.

The self assembly of DTSP (**5**) onto the Au electrode is shown in Step 1, Scheme 1.7. This is then followed by the carboxyl-amino coupling reaction with a CoTAPc amino

group (Step 2, Scheme 1.7). DTSP provides an easier and quicker covalent amino-carboxyl attachment relative to EDC coupling.

Direct SAM formation of FeTAPc onto a gold electrode has been used to block oxide related electrochemical reactions,[66] whereas this work (involving coupling of CoTAPc to a thiol functionalized Au electrode) aims to use CoTAPc-SAM as a possible electron mediator leading to probable detection and catalysis of oxygen.

CoTAPc has been found to form an almost complete SAM coverage on Au electrodes.[66] In simultaneously using CoTAPc and thiol SAMs on a single Au electrode, as in this work, a higher probability of complete coverage may be attained. Cyclic voltammetry experiments have shown that the stability of CoTAPc-SAM on Au electrodes to be relatively lower in comparison to CoTAPc adsorbed on Ag electrodes.[66] This lower stability was believed to be due to a low affinity of NH_2 groups (from the CoTAPc) for Au electrodes.[66] Generally, according to the HSAB theory, acids and bases interact and the most stable interactions are hard acid-hard base or soft acid-soft base.[67] Au^+ is a soft acid whilst NH_3 is a hard base; therefore this interaction is not ideally strong and may be used to explain the low affinity of amino groups for Au electrodes. Hence this work will attempt to increase stability by coupling the CoTAPc to the carboxylic acid group of a thiol functionalized electrode as opposed to merely attaching the CoTAPc to a gold electrode.

The SAM of CoTAPc on Au and Ag electrodes has been found to electrocatalyse the reduction of oxygen.[68] However this same study found the CoTAPc orientation on Au and Ag surfaces to have an impact on the formation of adducts and intermediates, resulting in the probable formation of diverse products.[68] This work (in which a CoTAPc

monolayer is attached to a thiol functionalized Au electrode) may be used to investigate and compare, with previous studies,[68] any differences in orientation and hence possible products in the electrocatalytic reduction of oxygen.

A fullerene, C_{60}, carboxylic derivative has been covalently attached to an amino-thiol functionalized Au electrode using EDC.[69] The so modified electrode was found to electrocatalyse glucose oxidation in the presence of glucose oxidase.[69] DTSP coupling has been used in the covalent immobilization of amino-containing organic molecules.[65]

No methods of CoTAPc (**3**) on thiol functionalized electrodes using EDC (**4**) or DTSP (**5**) coupling have been reported.

The use of Co and Fe metal catalysts in fuel cells, as opposed to expensive platinum, has been investigated.[70,71] Studies have shown that the Co and Fe metals, when complexed with donors and heat treated at high temperatures, show activity towards electro-reduction of oxygen.[72,73] However, the oxygen electrocatalytic reactions studied in this work do not require high temperatures and may hence provide a simple, cost effective version of fuel cells.

Part of this work may be summarised as the self assembled monolayer formation of carboxylic acid functionalized alkane-thiols on Au electrodes. This will be followed by the anchoring of CoTAPc to the carboxylic acid group of the modified Au electrode through the creation of an amide bond. Finally the electrochemical characterization and electrocatalytic effect towards the reduction of dissolved oxygen of so modified electrodes will be examined.

1.5. Summary of Thesis Aims

The aims of this thesis are summarized as:

i. Synthesis and basic chemical characterization (NMR, UV-vis spectroscopy, IR) of novel peripherally substituted octaphenylthiophthalocyaninatozinc (**10**, $ZnPc(SCH_2Ph)_8$), octaphenylthiophthalocyaninatocobalt (**11**, $CoPc(SCH_2Ph)_8$) and octaphenylthiophthalocyaninatoiron (**12**, $FePc(SCH_2Ph)_8$), Figure 1.11.

ii. Voltammetric and spectroelectrochemical characterization of the synthesized peripherally substituted octaphenylthiophthalocyaninatocobalt (**11**) and octaphenylthiophthalocyaninatoiron (**12**).

iii. Development of Au electrodes modified with the self assembled monolayers of octaphenylthiophthalocyaninatocobalt (**11**) and octaphenylthiophthalocyaninatoiron (**12**) in order to use as idyllic electrochemical sensors in the detection and catalytic oxidation of L-cysteine.

iv. The self assembly monolayer study of cobalt tetraamino Pc (**3**) coupling to pre-formed SAM Au electrodes. The respective study focuses on the chemistry and electrochemical characterization of accordingly modified electrodes. The aim of this study is to use the SAM of CoTAPc as a possible electron mediator leading to its probable use as an amperometric sensor in the detection and catalysis of oxygen.

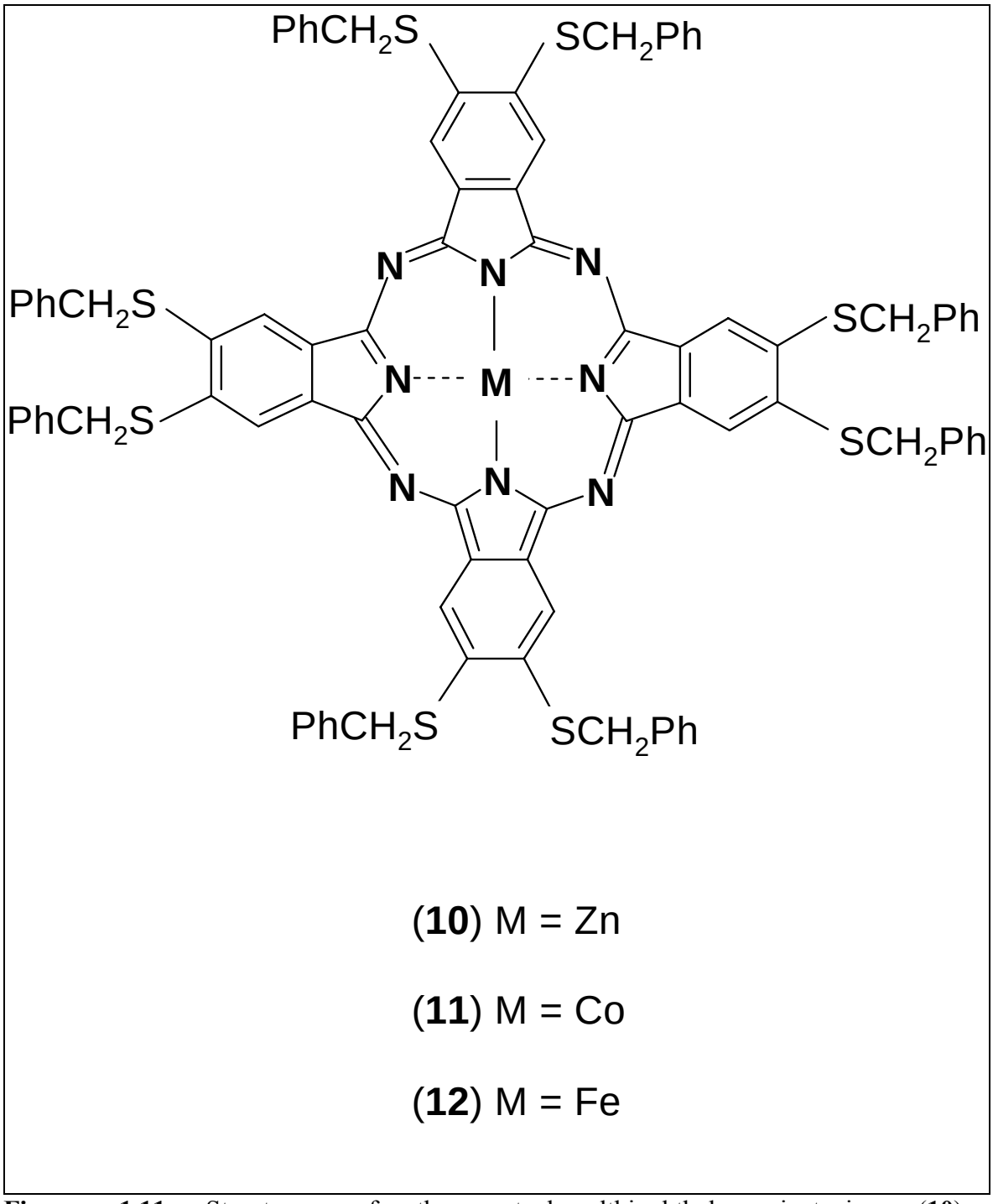

Figure 1.11 Structures of the octaphenylthiophthalocyaninatozinc (**10**), octaphenylthiophthalocyaninatocobalt (**11**) and octaphenylthiophthalocyaninatoiron (**12**) to be studied. M = Metal, Ph = Phenyl group.

CHAPTER 2: EXPERIMENTAL

2.1. Materials and Equipment

Acetic anhydride was obtained from Merck. 4,5-Dichlorophthalic acid, thionyl chloride, sodium hydride, zinc acetate and urea were purchased from Aldrich. Petroleum ether (bp 40-60^{o}C), formamide, ammonium hydroxide (25 and 35% solutions), dimethylformamide (DMF), tetrahydofuran (THF), lithium metal, iron (II) chloride hexahydrate, glacial acetic acid, cobaltous chloride hexahydrate, pH 4 buffer tablets, sodium sulphate anhydrous, cupric sulphate and potassium hydroxide pellets were procured from Saarchem. Absolute methanol, chloroform, hexane, acetone were provided by Protea Chemicals and distilled before use. Ethanol, also distilled before use, was obtained from NCP Alcohols. Phenylmethanethiol (benzyl mercaptan), 1,8-diazabicyclo(5.4.0)undec-7-ene (DBU), 1-pentanol, mercaptopropionic acid, dithiobis(*N*-succinimidyl propionate) (DTSP), 1-ethyl-3-(3-dimethylaminopropyl)-carbodiimide (EDC), dimethylsulfoxide (DMSO) and pH 12 buffer solution were purchased from Fluka. Ethylene glycol was obtained from NT Laboratory. Tetrabutylammonium perchlorate (TBAP), employed as an electrolyte in electrochemistry, was recrystallized from ethanol before use. L-cysteine was purchased from Sigma. Deionised water was obtained from a Millipore-Q-system. Nitrogen gas was purchased from Afrox. Cobalt tetratamino phthalocyanine (CoTAPc), synthesised according to literature methods,[74] was available in our laboratory.

IR spectra (KBr pellets) were recorded on a Perkin-Elmer spectrum 2000 FTIR spectrometer. ^{1}H-nuclear magnetic resonance (NMR, 400 MHz) spectra were obtained using Bruker EMX 400 NMR spectrometer. UV-visible spectra were recorded on a Varian 500 UV/visible/NIR spectrophotometer. MALDI-TOF spectra were obtained with

Perspective Biosystems Voyager DE-PRO Biospectrometry Workstation and possessing Delayed Extraction at the University of Cape Town, Cape Town, South Africa.

Spectroelectrochemical data were recorded using an optically transparent thin-layer electrochemical (OTTLE) cell, connected to a BioAnalytical System (BAS) 27 voltammogram. All other electrochemical experiments were performed on either BioAnalytical System (BAS) B/W 100 Electrochemical Workstation or PARSTAT 2273 potentiostat from AMETEK (controlled by the Powersuite software, run on a DELL Pentium computer).

2.2. Electrochemical methods

2.2.1. Electrochemical characterization of MPcs

Cyclic voltammetry and square wave voltammetry studies were recorded using a BioAnalytical System (BAS) B/W 100 Electrochemical Workstation. A conventional three electrode system consisting of a glassy carbon electrode (GCE) (3.00 mm diameter) as a working electrode, Ag|AgCl pseudo reference electrode and a platinum wire counter electrode were employed. All electrochemical experiments were performed at 25.0 ± 1.0 ^{o}C using freshly distilled DMF containing TBAP. For these studies the solutions were purified of any oxygen by bubbling purified nitrogen prior to experiments and the electrochemical cell was kept under nitrogen atmosphere throughout the analyses. The unmodified GCE was polished with alumina on a Buehler-felt pad followed by washing thoroughly with deionized water collected from a Milli-Q Water System. The GCE was then rinsed with DMF before transferring into the electrochemical cell.

2.2.2. Direct Self Assembled Monolayer of MPc on Au

The SAM studies involved first polishing the gold electrode (∅ = 1.6 mm) using aqueous slurries of alumina (< 10 micron) on a SiC-emery paper (type 2400 grit), and then to a mirror finish on a Buehler-felt pad. The Au electrode was then ultrasonicated (in an Integral Systems ultrasonicator) in ethanol so as to remove residual alumina particles trapped at the surface. The electrode was then etched for approximately two minutes in hot 'Piranha' solution (1:3 (v/v) 30 % H_2O_2 and concentrated H_2SO_4). This 'Piranha' solution treatment serves to eradicate any organic impurity on the electrode. Finally the Au electrode was rinsed in copious amounts of ultrapure Millipore water followed by the deposition solvent. This pre-treatment was followed immediately by placing the electrode in a 3 ml DMF solution of the thiol-derivatised MPc (1 x 10^{-3} M concentration) for 24 hours at room temperature. The thiol-derivatised MPc deposited on the Au electrode were either octaphenylthiophthalocyaninatocobalt (**11**) or octaphenylthiophthalocyaninatoiron (**12**). Upon removal from the deposition solution, the electrode was rinsed with DMF before any electrochemical analysis.

2.2.3. Amino-carboxyl covalent coupling SAM studies

These studies were done at Gent University (Belgium) on PARSTAT 2273 potentiostat from AMETEK, which was controlled by the Powersuite software, run on a DELL Pentium computer.

Gold disc electrodes (∅ = 1.6 mm) from BioAnalytical Systems were used. Prior to SAM deposition the gold surfaces were subjected consecutively to a mechanical, chemical and electrochemical pre-treatment. First a mechanical treatment was performed with scouring

of the electrode surface on SiC-emery paper (Buehler-felt pad from BioAnalytical Systems) of 1200 grit, followed by polishing on different polishing cloths (BioAnalytical Systems) covered with 1 and 0.05 μm Al_2O_3 powder for 5 minutes each. Any remaining polishing powder was removed from the surface by ultrasonic treatment in a Branson 3210 ultrasound bath. In a second step, the electrode surface was etched chemically by dipping the electrode in a piranha solution (1:3 (v/v) 30 % H_2O_2 and concentrated H_2SO_4) for 30 seconds. Finally the electrode surface was pre-treated electrochemically by performing a continuous scanning procedure between –0.6 V and 0.7 V vs. Ag|AgCl until a stable voltammetric curve was obtained (typically 50 scans).

Formation of the DTSP-SAM was done by dipping the electrode surface in a de-aerated DMSO solution of 1 x 10^{-2} mol L^{-1} DTSP (**5**) for 30 minutes. Coupling of the CoTAPc (**3**) at the DTSP (**5**) layer was obtained by dipping the electrode in DMSO containing 1 x 10^{-3} mol L^{-1} of CoTAPc (**3**) for 90 minutes. After each pre-treatment step the electrode surface was thoroughly rinsed with DMSO to remove weakly adsorbed DTSP (**5**) or CoTAPc (**3**) species.

Modification of the gold electrode with a mercaptopropionic acid SAM was done by dipping the Au surface in an aqueous solution of 2 x 10^{-2} mol L^{-1} $HS(CH_2)_2COOH$ (**6**) for 2 hours. The EDC (**4**) coupling reaction was then performed to bind the CoTAPc (**3**) at the mercaptopropionic acid (**6**) layer by dipping the electrode in an EtOH/DMSO (1:1) solution containing 1 x 10^{-3} mol L^{-1} CoTAPc (**3**) and 5 x 10^{-3} mol L^{-1} EDC (**4**) for 4 hours. Weakly adsorbed species were again removed by rinsing with water and an EtOH/DMSO mixture, respectively, before any electrochemical analysis.

2.3. Synthesis

2.3.1. Synthesis of 4,5-dichloro-1,2-dicyanobenzene (14), Scheme 3.1

4,5-Dichloro-1,2-dicyanobenzene (**14**) was synthesized from **13** according to literature methods.[2] Yield: 61 %. IR (KBr) ν, cm^{-1}: 3086, 2238 (nitrile), 1575, 1536, 1467, 1350, 1258, 1222, 1142. ^{1}H NMR (DMSO-d_6): δ, ppm: 8.50 (s, 2H, benzyl).

2.3.2. Synthesis of 1,2-bis(*S*-benzylthio)-4,5-dicyanobenzene (15), Scheme 3.1

To a suspension of sodium hydride (3 g, 124 mmol) in dry DMF (80 ml), benzyl mercaptan (15 ml) was added under N_2 while keeping the temperature between 10 and 15 ^{o}C. The mixture was brought to room temperature and **14** (12 g, 61 mmol) was then added in small portions. The reaction mixture was left overnight under N_2 while stirring. The product was collected by filtration and recrystallized from $CHCl_3$/MeOH. Compound **15** was then dissolved in MeOH and heated under reflux, then $CHCl_3$ was added to the mixture and heating under reflux continued. This procedure was repeated once. Finally the product was recrystallized to give **15** as a pale yellow powder, which was dried in vacuum. Yield: 39 %. IR (KBr) ν, cm^{-1}: 3033, 2227 (nitrile), 1561, 1492, 1456, 1344, 1237, 1113. ^{1}H NMR (DMSO-d_6): δ, ppm: 8.20 (s, 2 H, benzyl), 7.30 (m, 10 H, phenyl), 4.30 (s, 4 H, methylene).

2.3.3. Synthesis of octaphenylthiophthalocyaninatozinc (10), Scheme 3.2

Dry 1-pentanol (5 ml) was heated under N_2 atmosphere to 125 ^{o}C, then **15** and Li metal (treated in methanol) were added. The solution was heated for 3 hrs. The dark green

solution was diluted in hexane and filtered. The precipitate $Li_2Pc(SCH_2Ph)_8$ was washed with H_2O, MeOH, acetone and finally MeOH. The precipitate was then washed with 30 ml glacial acetic acid, water and $CHCl_3$ (in order to demetallate dilithium Pc to form **16**) then dried in vacuum. Complex **16** was not characterised further, but was used for the synthesis of compound **10**. A DMF suspension of **16** (0.115 g, 7.7 x 10^{-5} mol) and zinc acetate (0.034 g, 1.5 x 10^{-4} mol) was heated under stirring (130 ^{o}C) for 15 minutes. After cooling to room temperature, the solution was poured into ice-water mix (200 ml). The precipitated product was collected by centrifugation and treated with hot methanol, acetone, ethanol and methanol again. The precipitate **(10)** was purified by column chromatography (THF effluent). Yield: 11 %. UV-vis (DMF): λ_{max}, nm (log ε) 633 (4.11), 706 (4.99). The yield was too low to allow any further characterization.

2.3.4. Synthesis of octaphenylthiophthalocyaninatocobalt (11), Scheme 3.2

A mixture of **15** (2.5 g, 6.7 mmol), anhydrous $CoCl_2$ (0.22 g, 1.7 mmol) and ethylene glycol (13 ml) was heated and stirred at 200 ^{o}C for 4 hours under N_2. After cooling to room temperature, the reaction mixture was treated with ethanol to precipitate the dark green product and then filtered. The precipitate **11** was intensively washed with acetone and hexane. Yield: 55 %. IR (KBr) ν, cm^{-1}: 3852, 1698, 1561, 1115, 1067, 960, 746, 687. ^{1}H NMR (DMSO-d_6): δ, ppm: 8.20 (s, 8 H, Pc), 7.20 (m, 40 H, phenyl), 4.60 (m, 16 H, methylene). UV-vis (DMF): λ_{max}, nm (log ε) 327 (4.61), 619 (4.31), 686 (4.45). MS (MALDI-TOF), $C_{88}H_{64}CoN_8S_8$: *m/z*, calcd. for $[CoPc(SCH_2Ph)_8 + H]^+$ 1549.8, found 1549.7.

2.3.5. Synthesis of octaphenylthiophthalocyaninatoiron (12), Scheme 3.2

A mixture of **15** (1.52 g, 4 mmol), $FeCl_2.4H_2O$ (0.21 g, 1 mmol) and urea (0.386 g, 6.25 mmol) was heated and stirred at 150 ^oC for 90 minutes. After cooling to room temperature, the reaction mixture was heated with hot ethanol and filtered. The dark green crude product was purified by treating with $CHCl_3$ followed by Soxhlet extraction with ethanol, methanol and acetone. Compound **12** was treated with hot methanol, ethanol and acetone then dried in vacuum. Yield: 55 %. IR (KBr) ν, cm^{-1}: 3676, 1653, 1118, 1069, 962, 777, 747, 694. ^1H NMR (DMSO-d_6): δ, ppm: 8.00 (s, 8 H, Pc), 7.50 (m, 40 H, phenyl), 4.50 (m, 16 H, methylene). UV-vis (DMF): λ_{max}, nm (log ε) 359 (4.80), 451 (4.33), 623 (4.29), 690 (4.80). MS (MALDI-TOF), $C_{88}H_{64}FeN_8S_8$: *m/z*, calcd. for $[FePc(SCH_2Ph)_8 + H]^+$ 1546.8, found 1546.4.

CHAPTER 3: RESULTS AND DISCUSSION

Part of this work has been published and is not referenced in this thesis:

1. Matemadombo, F.; Maree, M. D.; Ozoemena, K. I.; Westbroek, P.; Nyokong, T. **Synthesis, Electrochemical and Spectroelectrochemical studies of Octaalkylthiosubstituted Phthalocyanines** *J. Porphyrins Phthalocyanines* **2005**, *9*, 484.

3.1. Synthesis and Characterization

An outline of the synthetic procedures for phthalonitriles **14**, **15** and phthalocyanines **16**, **10**, **11, 12** are given in Schemes 3.1 and 3.2 respectively.

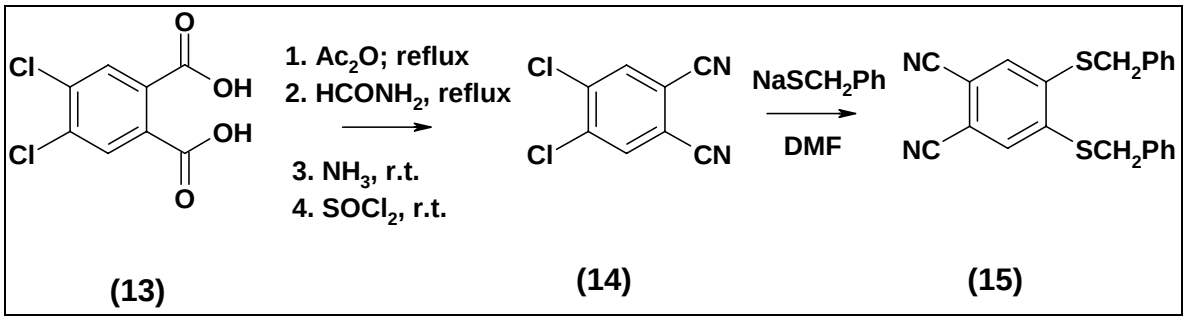

Scheme 3.1 Synthetic procedure for the phthalonitriles **14** and **15**.

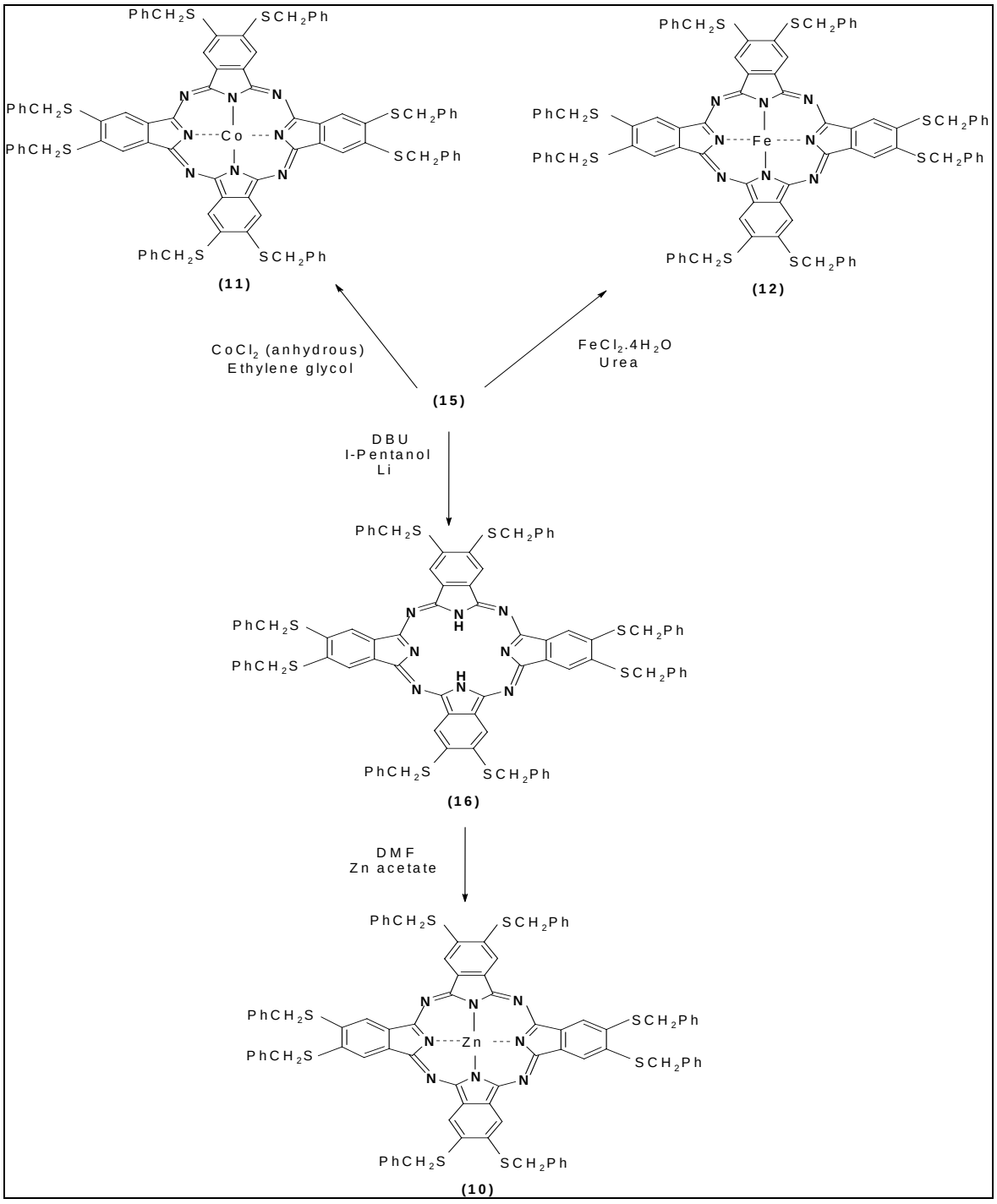

Scheme 3.2 Synthetic procedure for the unmetallated octaphenylthiophthalocyanine ($H_2Pc(SCH_2Ph)_8$, **16**), octaphenylthiophthalocyaninatozinc ($ZnPc(SCH_2Ph)_8$, **10**), octaphenylthiophthalocyaninatocobalt ($CoPc(SCH_2Ph)_8$, **11**) and octaphenylthiophthalocyaninatoiron ($FePc(SCH_2Ph)_8$, **12**) complexes.

3.1.1. Starting Materials

The compound 4,5-dichloro-1,2-dicyanobenzene (**14**) was synthesized, using a common literature method,[2] starting from 4,5-dichlorophthalic acid (**13**)**,** with an overall yield of 61 %. Synthesis of **14** initially involved the conversion of the starting reagent 4,5-dichlorophthalic anhydride to an imide then a diamide, as reported in literature.[2] Compound **14** is also available commercially. Synthesis of the aromatic dibenzyl sulfide 1,2-bis(*S*-phenylthio)-4,5-dicyanobenzene (**15**), done according to reported procedures,[75] involved the conversion of the dichlorophthalonitrile (**14**) into the corresponding 1,2-bis(*S*-benzylthio)-4,5-dicyanobenzene (**15**) in a 39 % yield. Synthesis of the aromatic dibenzyl sulfide (**15**) using sodium hydride and benzyl mercaptan proved to be more successful (especially with respect to a purer product) as opposed to the nucleophillic displacement reaction using an excess of thiols in the presence of an excess of potassium carbonate.[2]

Table 3.1 lists the NMR and IR data of complexes **14** and **15**.

Table 3.1 Characterization data of phthalonitriles synthesized in this work.

Complex	**IR (KBr):** ν**, cm^{-1}**	**^{1}H NMR (DMSO-d$_6$):** δ**, ppm**
14	3086, 2238 (nitrile), 1575, 1536, 1467, 1350, 1258, 1222, 1142.	8.50 (s, 2 H, benzyl).
15	3033, 2227 (nitrile), 1561, 1492, 1456, 1344, 1237, 1113.	8.20 (s, 2 H, benzyl), 7.30 (m, 10 H, phenyl), 4.30 (s, 4 H, methylene).

A prominent band at 2238 cm^{-1} in the IR spectrum of **14** corresponded to the nitrile group, Figure 3.1.

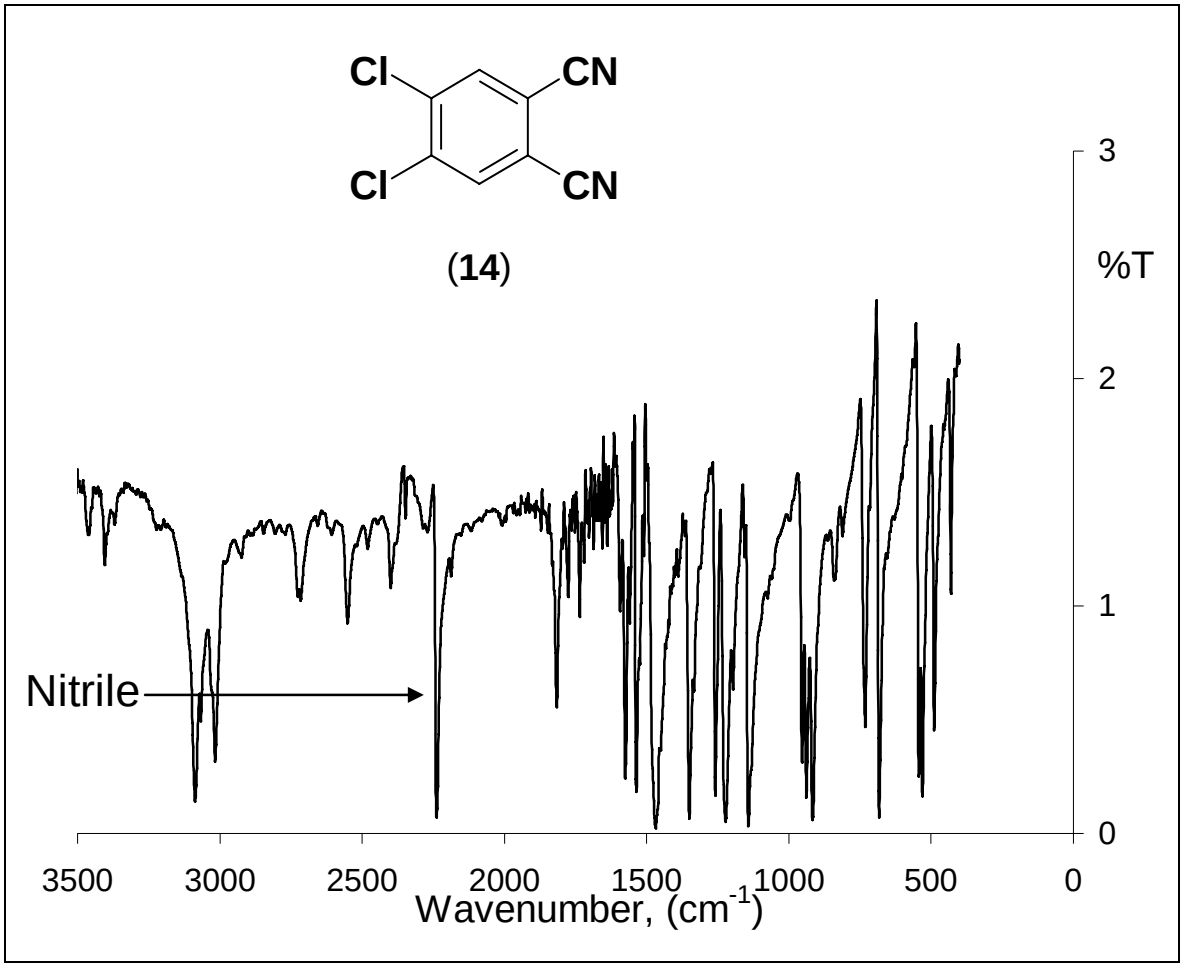

Figure 3.1 IR spectrum of compound **14**.

The CN band in the IR spectrum of **15** was observed, as expected, at 2227 cm^{-1}, Figure 3.2.

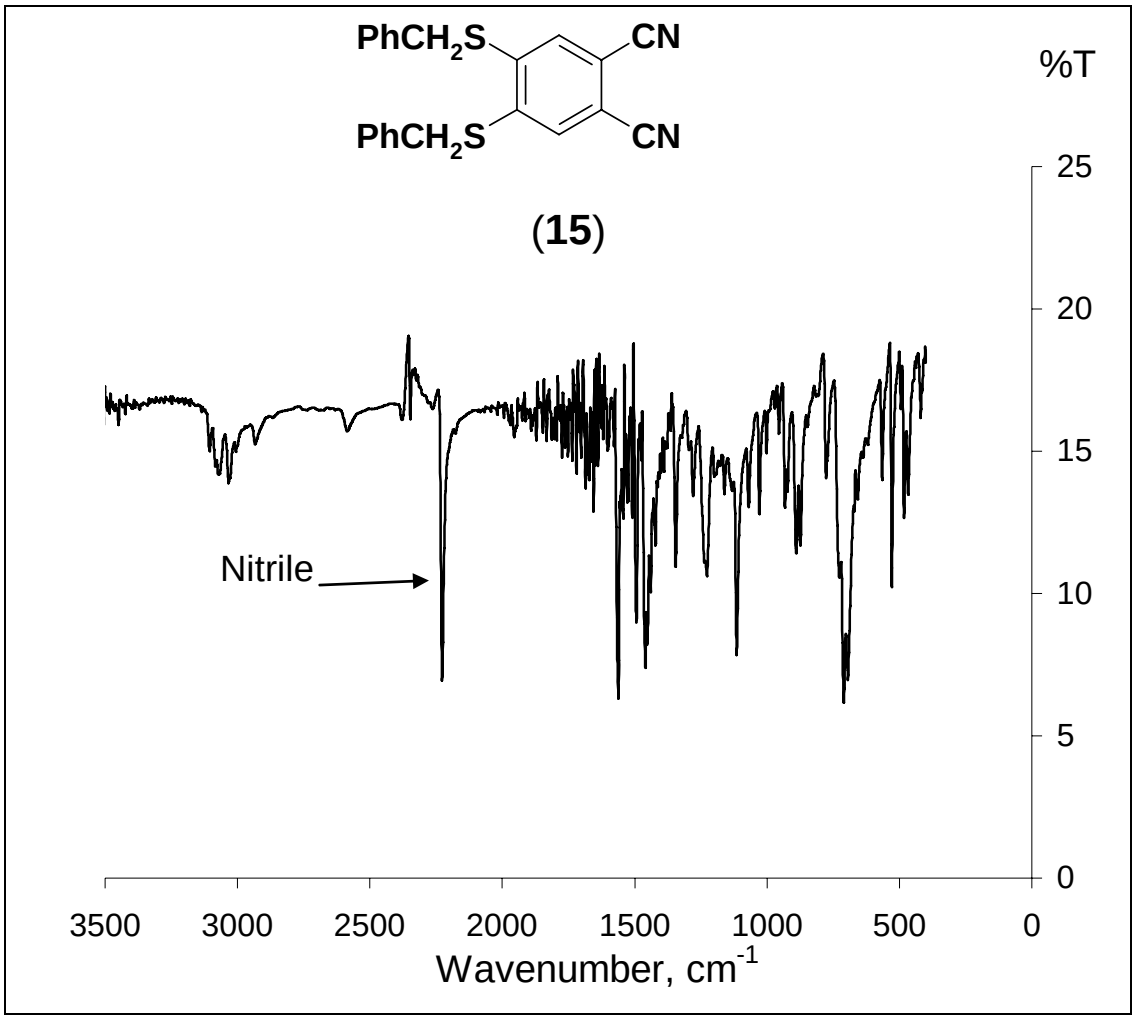

Figure 3.2 IR spectrum of compound **15**.

A singlet, analogous to the benzyl proton of **14**, occurred in the downfield ^{1}H NMR region of the spectrum (8.50 ppm), Figure 3.3.

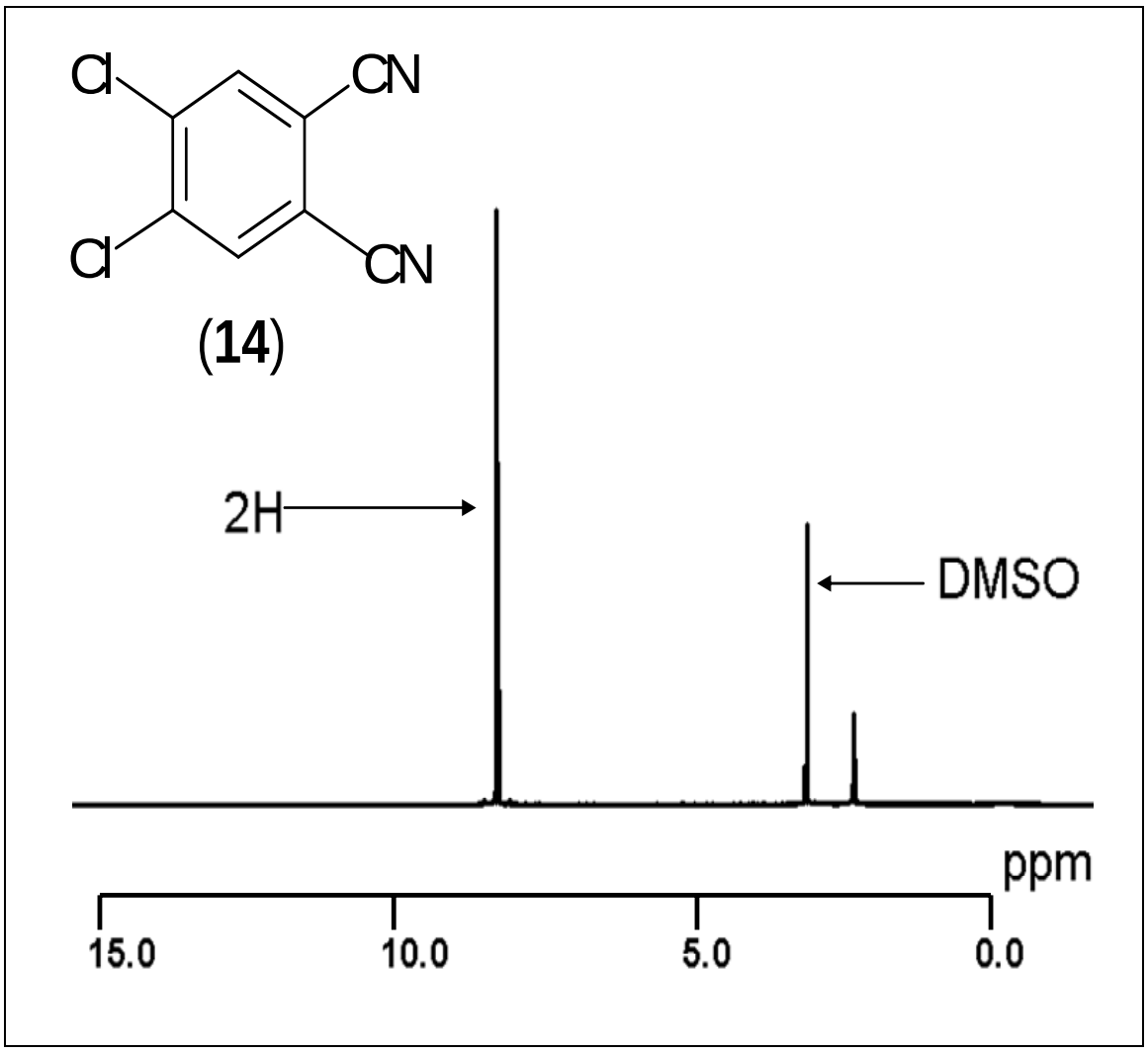

Figure 3.3 NMR spectrum of compound **14**. 2H = two phenyl hydrogens.

The benzyl protons of **15** appeared as a singlet at 8.20 ppm in the ^{1}H NMR spectrum, Fig 3.4. A multiplet pertaining to the phenyl protons of **15** at 7.30 ppm also appeared in the ^{1}H NMR spectrum. As anticipated, the methylene protons appeared as a singlet at 4.30 ppm in the ^{1}H NMR spectrum of **15**.

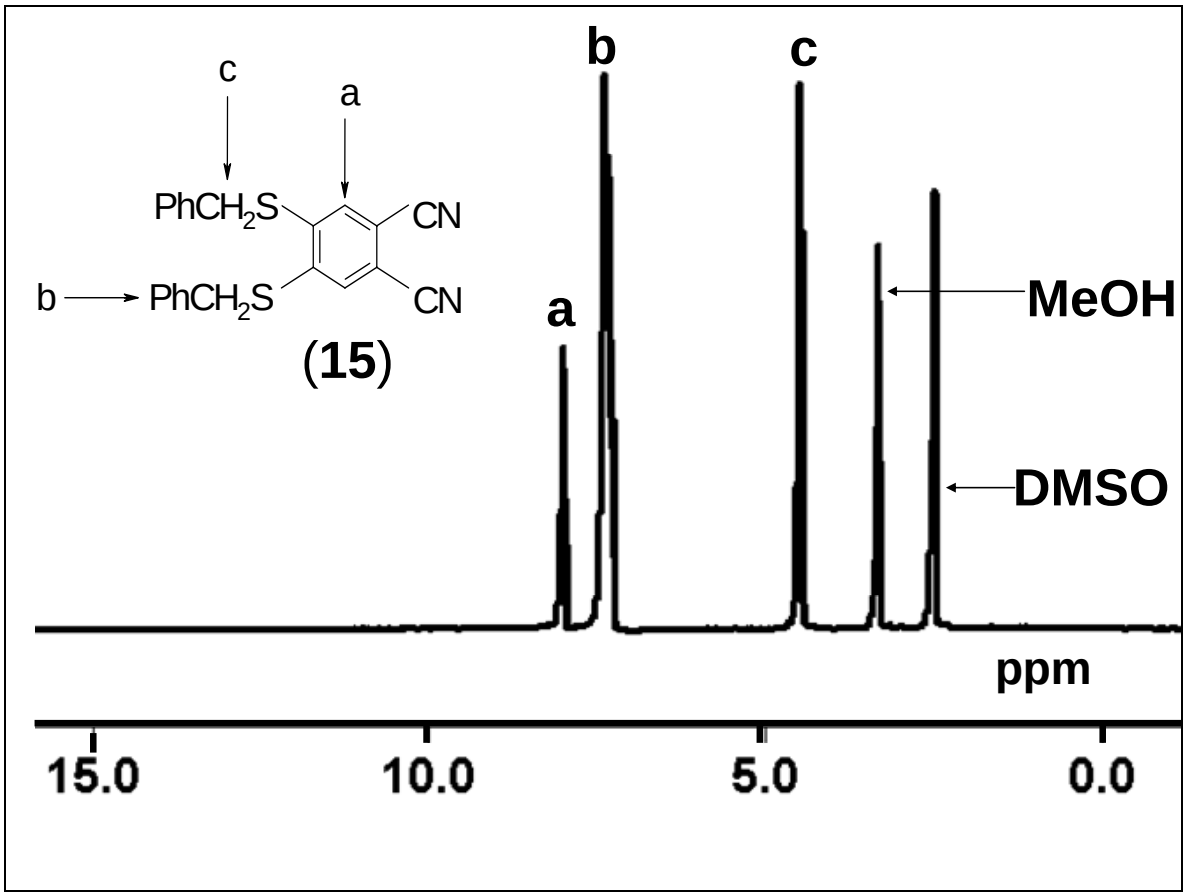

Figure 3.4 NMR spectrum of compound **15**. Ph = Phenyl group.

3.1.2. Phthalocyanines

Synthesis of octabenzylthiophthalocyaninatozinc (**10**) was done according the established procedures.[2] A clean product was obtained using the reported method largely due to the fact that crude (**10**) was soluble in most volatile organic solvents, and could hence easily be purified using column chromatography. However, this purification step had the

disadvantage of resulting in a low yield (11 %). As complex **10** had such a low yield and is not useful for electroanalysis (because Zn is not an electroactive metal) no further characterization was done on this molecule.

Octaphenylthiophthalocyaninatocobalt (**11**) was synthesized according to the reported synthesis of octakis(alkylthio)-substituted phthalocyanines.[16] It was important to use the anhydrous form of the metal salt ($CoCl_2$) as this was found to effect a purer product. Anhydrous $CoCl_2$ was obtained by heating commercially available cobaltous chloride hexahydrate to 140 ^{o}C resulting in the loss of the six water molecules. Octaphenylthiophthalocyaninatocobalt (**11**) was not entirely soluble in several organic solvents, even after intensive heating, and hence needed to be purified by numerous rigorous washings with acetone and hexane. Octaphenylthiophthalocyaninatoiron (**12**) gave better yields when synthesized using the urea method as opposed to other methods.[2] Purification was performed by treating crude **12** with hot alcohols. Complexes **10**, **11** and **12** were found to be soluble in common organic solvents such as DMF, DMSO and THF. Table 3.2 lists the characterization data of complexes **11** and **12**.

Table 3.2 Characterization data of MPcs synthesized in this work.

Complex	**IR (KBr): ν, cm^{-1}**	**^{1}H NMR (DMSO-d_6): δ, ppm**	**UV-vis (DMF): λ_{max}, nm (log ε)**
$CoPc(SCH_2Ph)_8$ (**11**)	3852, 1698, 1561, 1115, 1067, 960, 746, 687.	8.20 (s, 8 H, Pc), 7.20 (m, 40 H, phenyl), 4.60 (m, 16 H, methylene).	327 (4.61), 619 (4.31), 686 (4.45).
$FePc(SCH_2Ph)_8$ (**12**)	3676, 1653, 1118, 1069, 962, 777, 747, 694.	8.00 (s, 8 H, Pc), 7.50 (m, 40 H, phenyl), 4.50 (m, 16 H, methylene).	359 (4.80), 451 (4.33), 623 (4.29), 690 (4.80).

The absence of a prominent nitrile band at ~2200 cm^{-1} in the IR spectra of $CoPc(SCH_2Ph)_8$ (**11**) and $FePc(SCH_2Ph)_8$ (**12**) (Table 3.2) confirms, to a certain extent, the presence of MPc and therefore successful conversion of 1,2-bis(*S*-phenylthio)-4,5-dicyanobenzene (**15**) (displaying a nitrile peak in its IR spectrum, Table 3.1) into an MPc. Nonetheless, supplementary characterization techniques are necessary to corroborate this conversion.

Broad peaks in the ^{1}H NMR spectrums of the Pc complexes studied in this work are due to the aggregation occurring at the high concentrations used[76] and to the paramagnetic nature of the central metal ions. However, vigilant integration of the observed ^{1}H NMR peaks gave the expected number of protons. The Pc protons in the ^{1}H NMR spectrum of **11** occurred as a broad singlet at 8.20 ppm, Figure 3.5. The phenyl protons of **11** occurred in the downfield ^{1}H NMR region. At 4.60 ppm the protons pertaining to the methylene group of **11** appeared as a multiplet in the ^{1}H NMR spectrum, Figure 3.5.

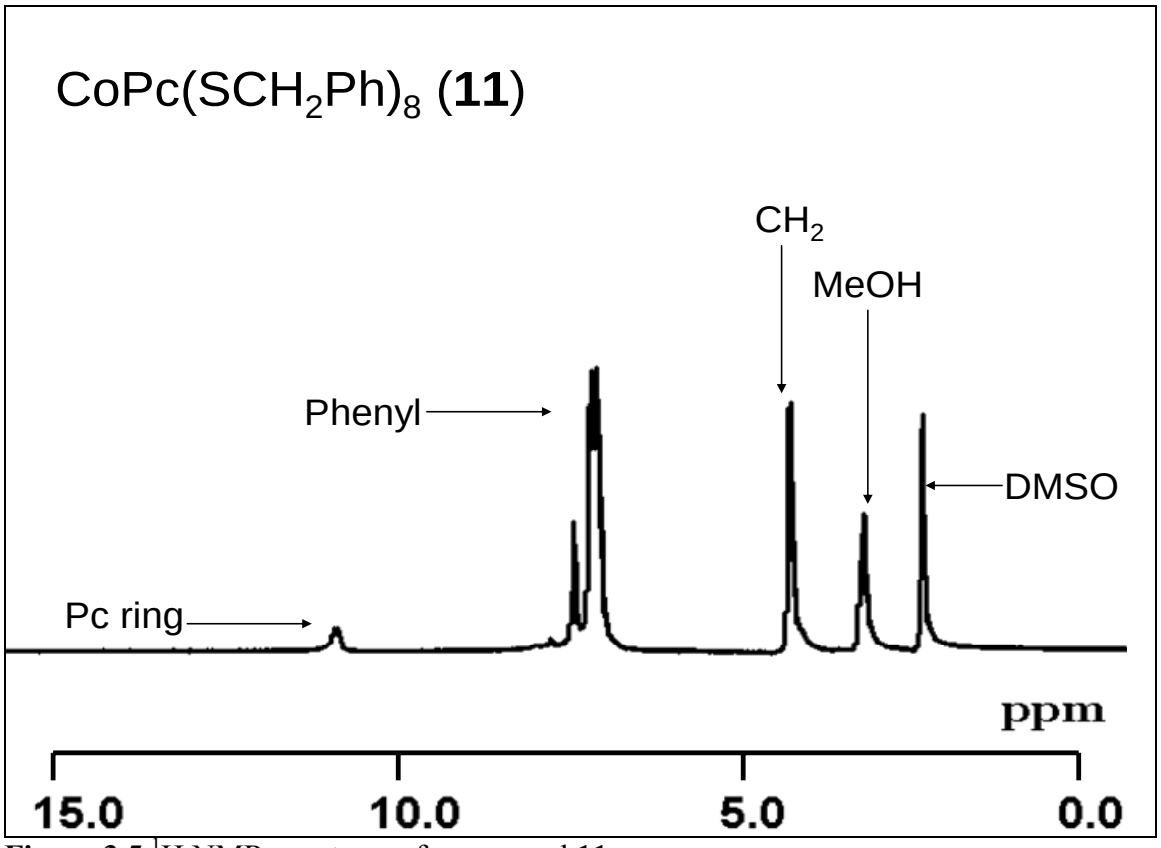

Figure 3.5 ^{1}H NMR spectrum of compound **11**.

The Pc protons occurred as a broad singlet at 8.00 ppm for compound **12**, Figure 3.6. The phenyl protons moreover appeared downfield as a broad multiplet in the ^{1}H NMR spectrum of **12**. The methylene protons of **12** occurred up-field at 4.50 ppm, Figure 3.6.

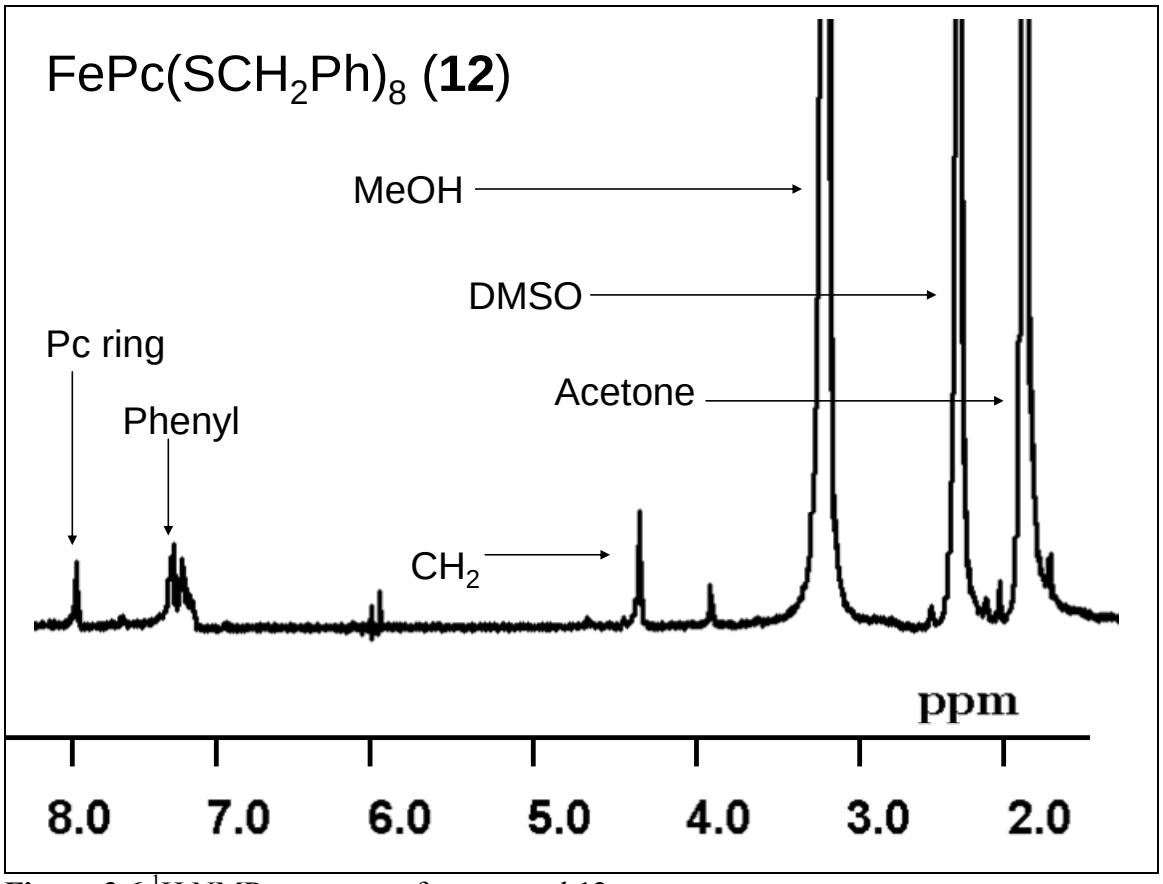

Figure 3.6 ^{1}H NMR spectrum of compound **12**.

UV-Visible spectra of the Pc complexes **10**, **11** and **12** in freshly distilled organic solvents are shown in Figures 3.7 – 3.9 respectively.

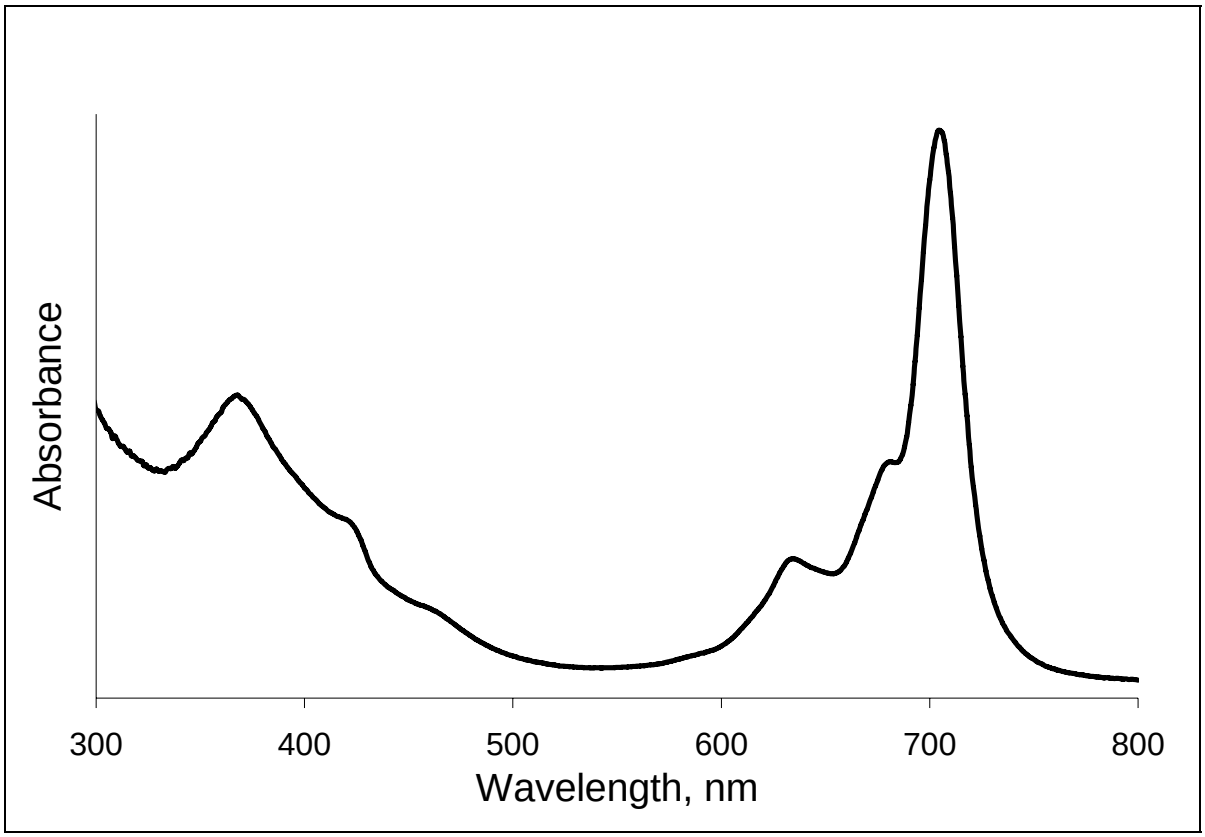

Figure 3.7 UV-visible spectrum of compound **10** in freshly distilled DMF.

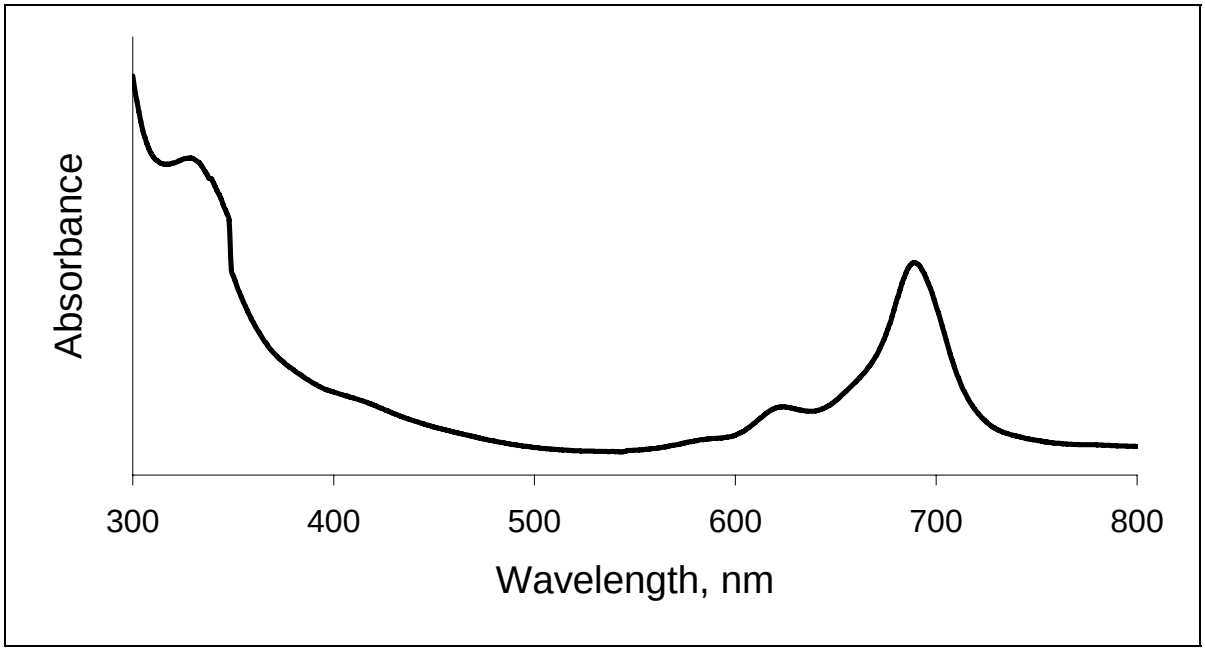

Figure 3.8 UV-visible spectrum of compound **11** in freshly distilled THF.

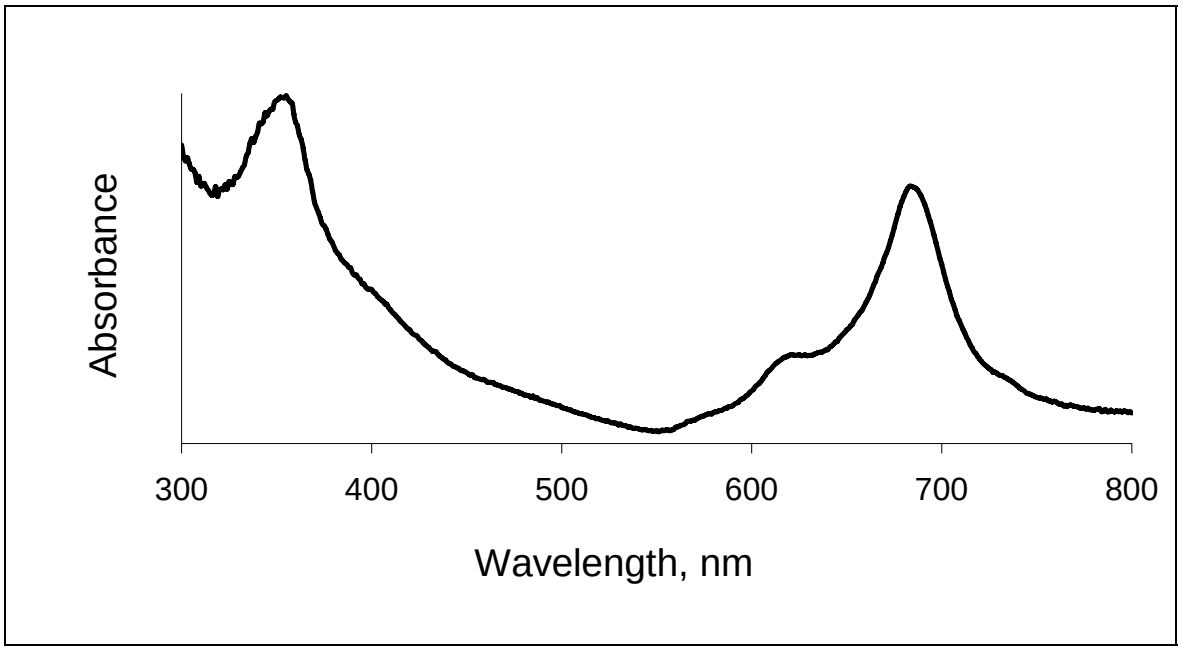

Figure 3.9 UV-visible spectrum of compound **12** in freshly distilled DMF.

The Q bands occurred in the visible region at 706 nm (for compound **10**), 686 nm (for compound **11**) and 690 nm (for compound **12**) in the respective organic solvents**.** The characteristic B band occurring in the UV regions for compounds **10** (372 nm), **11** (327 nm) and **12** (359 nm) result from the deeper π levels to LUMO transitions.[76] The Q band wavelength values of compounds **11** and **12** are red shifted relative to unsubstituted CoPc or FePc[33] due to effects of the phenylthiol substituents. As is typical of MPc complexes, an increase in concentration was found to result in aggregation of all the Pc complexes studied in this work, resulting in the splitting of the Q band. The ε value of compounds **10**, **11** and **12** were hence determined at low concentrations (< 10^{-6} M). The spectra of iron phthalocyanines has been a subject of several reports[77,78] and much controversy. The formation of μ-oxo, Fe(II)Pc or Fe(III)Pc species has been reported for the same types of complexes such as Cl_{16}PcFe.[77] Hence it is important to determine the oxidation state of the central metal ion for each preparation of a FePc species. The formation of Fe(II)Pc

species in this work is evident by the presence of a typical charge transfer band in the 450 nm region.[33]

The mass spectra by the MALDI-TOF technique on the synthesized compounds **11** and **12** verified the anticipated structures. Molecular ions in **11** and **12** were identified at *m/z*: 1549.7 $[M + 1]^+$ and *m/z*: 1546.4 $[M + 1]^+$, respectively.

3.2. Electrochemistry and Spectroelectrochemistry

Cyclic (CV) and square wave (SWV) voltammetry (recorded at Rhodes University using a BioAnalytical System (BAS) B/W 100 Electrochemical Workstation) of complexes **11** and **12** were performed in DMF containing 0.1 M TBAP and the data are listed in Table 3.3.

Table 3.3 Redox potentials (V) for complexes **11** and **12** measured in DMF containing 0.1 M TBAP. Values from SWV maxima. Scan rate = 100 mVs^{-1}.

Complex	$M^{III}Pc^{0}$/ $M^{III}Pc^{-1}$ (**VI**)	$M^{III}Pc^{-1}$/ $M^{III}Pc^{-2}$ (**V**)	$M^{III}Pc^{-2}$/ $M^{II}Pc^{-2}$ (**IV**)[a]	$M^{II}Pc^{-2}$/ $M^{I}Pc^{-2}$ (**III**)[a]	$M^{I}Pc^{-2}$/ $M^{I}Pc^{-3}$ (**II**)	$M^{I}Pc^{-3}$/ $M^{I}Pc^{-4}$ (**I**)
$CoPc(SCH_2Ph)_8$ (**11**)		1.16	0.72 (0.72)	- 0.096 (- 0.38)	-0.58	-1.0
$FePc(SCH_2Ph)_8$ (**12**)	1.14	0.60	0.25 (0.26)	-0.26 (-0.49)	-0.70	- 1.3

[a]Values in brackets are for Co and Fe octabutylthiometallophthalocyanine.[57]

SWV shows peak potentials relatively more clearly, as expected. CV and SWV for complex **11** are shown in Figure 3.10.

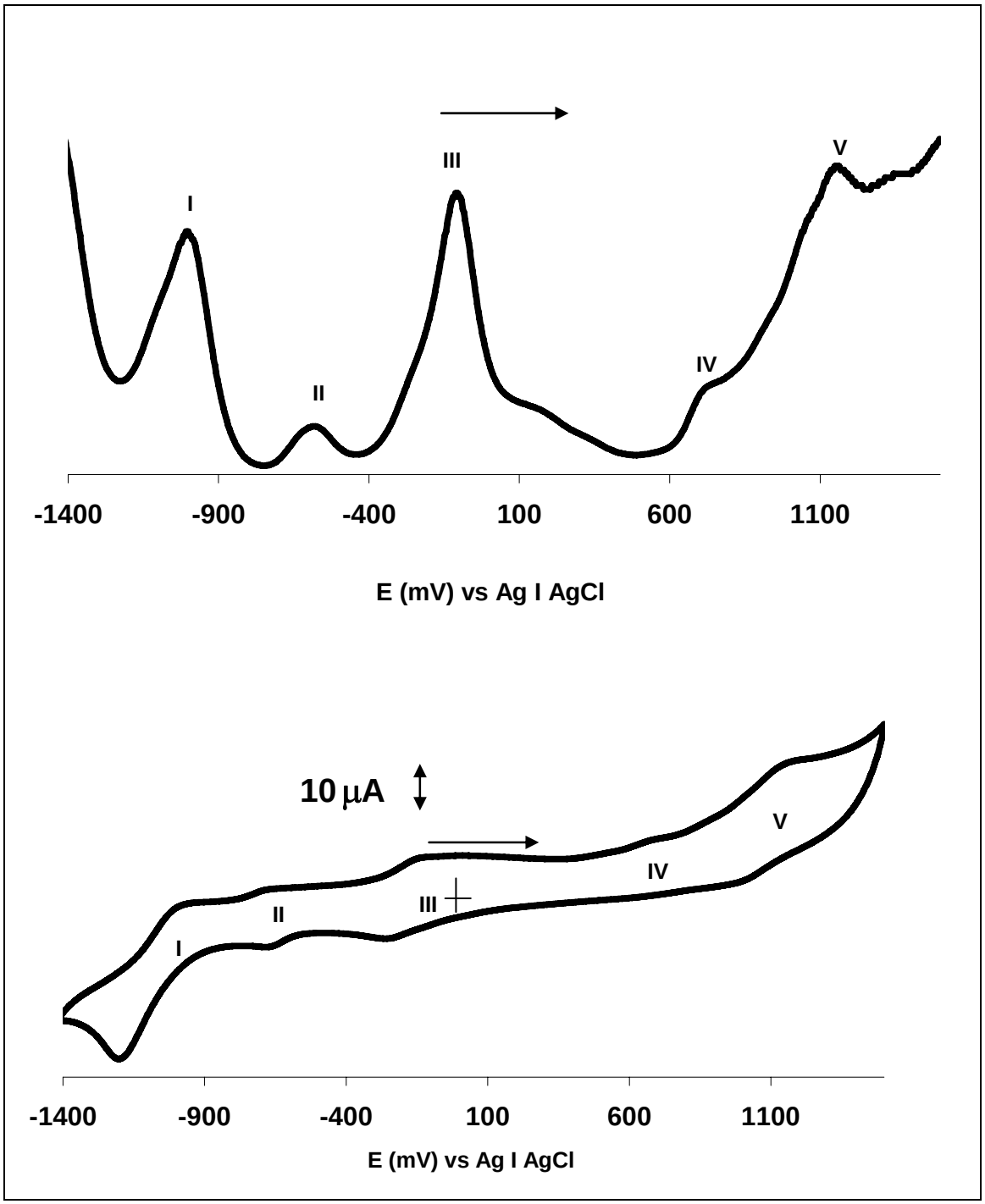

Figure 3.10 Cyclic and square wave (top) voltammograms on a GCE, for complex **11** in DMF containing TBAP. Scan rate = 100 mV/s.

The couples exhibited reversible to quasi-reversible behavior in that the ratio of cathodic to anodic peak currents were not unity (e.g. processes **I**, **IV** and **V**) and the anodic to cathodic peak potential separations (ΔE) were larger than 90 mV in some cases (ΔE = 90 mV was obtained for the ferrocenium/ferrocene internal standard). The lack of reversibility for the thiosubstituted phthalocyanine complexes has been reported before.[18] Couple **II** gave a ΔE of ~ 0 mV, suggesting adsorption behavior of complex **11**. Sharp peaks in the CV of thiol substituted MPc complexes have been observed before,[18] and such behavior is attributed to the formation of adsorbed species. The plot of the peak current versus square root of the scan rate was linear suggesting diffusion controlled behavior for all couples except **II**, which showed adsorption behavior.

Spectroelectrochemistry was employed to assign the CV couples of complex **11**. The UV-visible spectral changes of complex **11** are shown in Figure 3.11.

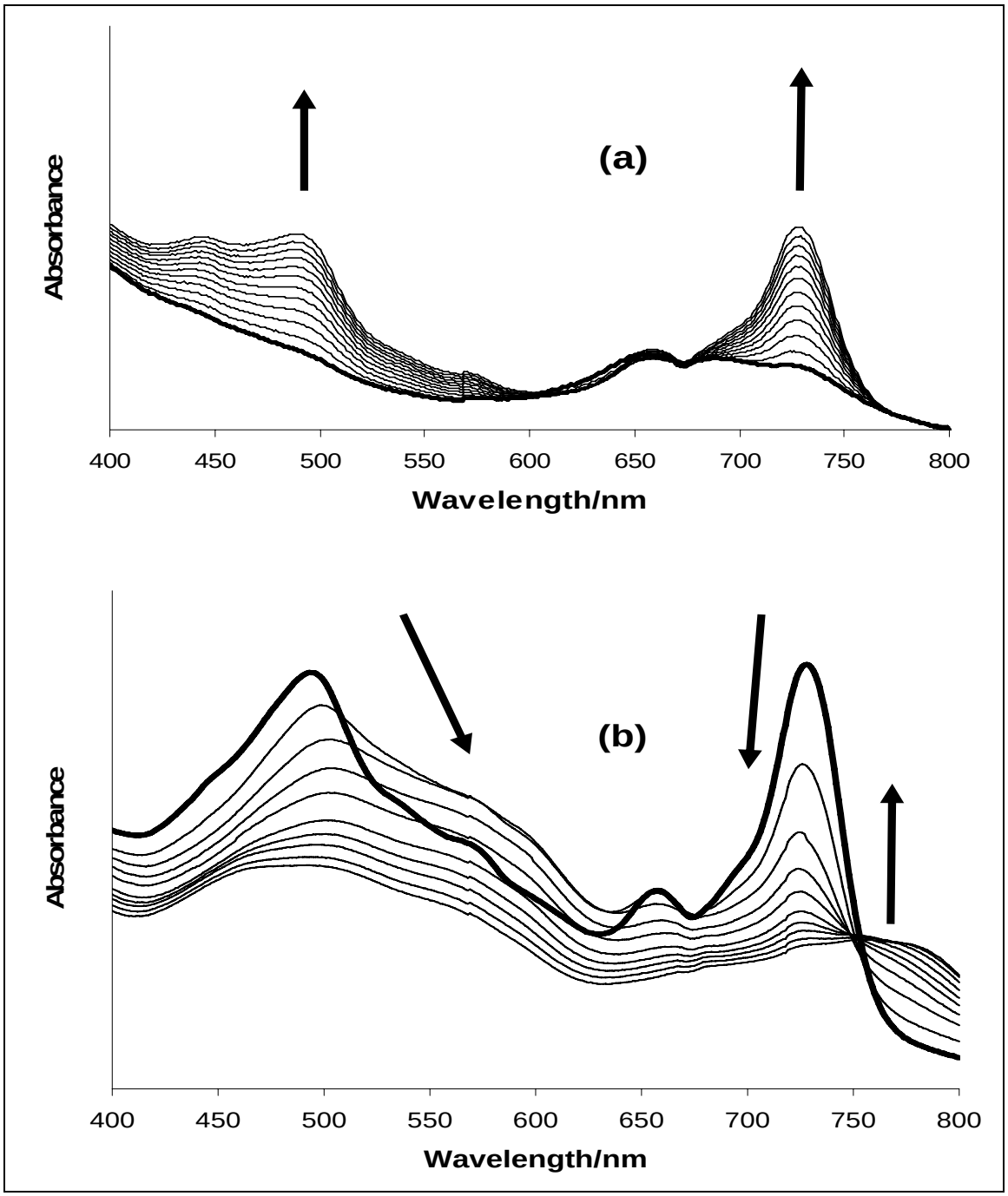

Figure 3.11 Typical UV-visible spectral changes observed using OTTLE cell during reduction of complex **11**. The spectra were recorded continuously during the electrolysis. (a) Applied potential -0.5 V. (b) Applied potential – 1.0 V {the first spectrum is the same as the last spectrum in (a)}. Electrolyte: DMF containing TBAP.

With respect to complex **11**, reduction at potentials more negative than couple **III** (- 0.5 V) resulted in the spectral changes shown in Figure 3.11(a). At the high concentrations employed for OTTLE studies, the complex is highly aggregated as seen in the first trace in Figure 3.11(a), with monomer peak at 680 nm, and the peak due to aggregated species at 655 nm. Upon reduction, the monomeric peak shifted from 680 nm to 726 nm and increased considerably in intensity. The spectral changes show that upon reduction the Pc molecules become disaggregated. New intense peaks between 400 and 500 nm are characteristic of $Co^{I}Pc$ species.[33] Also the shift in the Q band without decreasing in intensity is typical of metal based reduction in MPc complexes. Thus spectral changes shown in Figure 3.11(a) clearly confirm that couple **III** is due to the reduction of $Co^{II}Pc$ to $Co^{I}Pc$. The reduction was partly reversible in that applying zero volts resulted in the regeneration of the starting spectrum. Further reduction of the species formed in Figure 3.11(a) at potentials more negative than couple **II** resulted in spectral changes shown in Figure 3.11(b), which consisted of the decrease in the Q band and the shifting of the band at 490 nm to longer wavelengths, new bands were formed in the 500 to 650 nm region. The decrease in the Q band is characteristic of ring-based processes. Bands in the 500 to 600 nm region are typical[30] for ring based reduction and the formation of a Pc^{-3} species. Thus reduction at potentials of couple **II** results in the formation of $Co^{I}Pc^{-3}$ species. The 0 mV value of the cathodic to anodic peak separation shows the reduction of $Co^{I}Pc^{-2}$ to $Co^{I}Pc^{-3}$ results in adsorption of the latter to the electrode. Couple **I** is then due to the subsequent formation of the $Co^{I}Pc^{-4}$ species. Table 3.3 summarizes the assignments of the couples.

For complex **11**, oxidation at potentials more positive than couple **IV** resulted in spectral changes shown in Figure 3.12, consisting of an increase in the peak due to the monomer which displayed a wavelength shift from 680 to 697 nm.

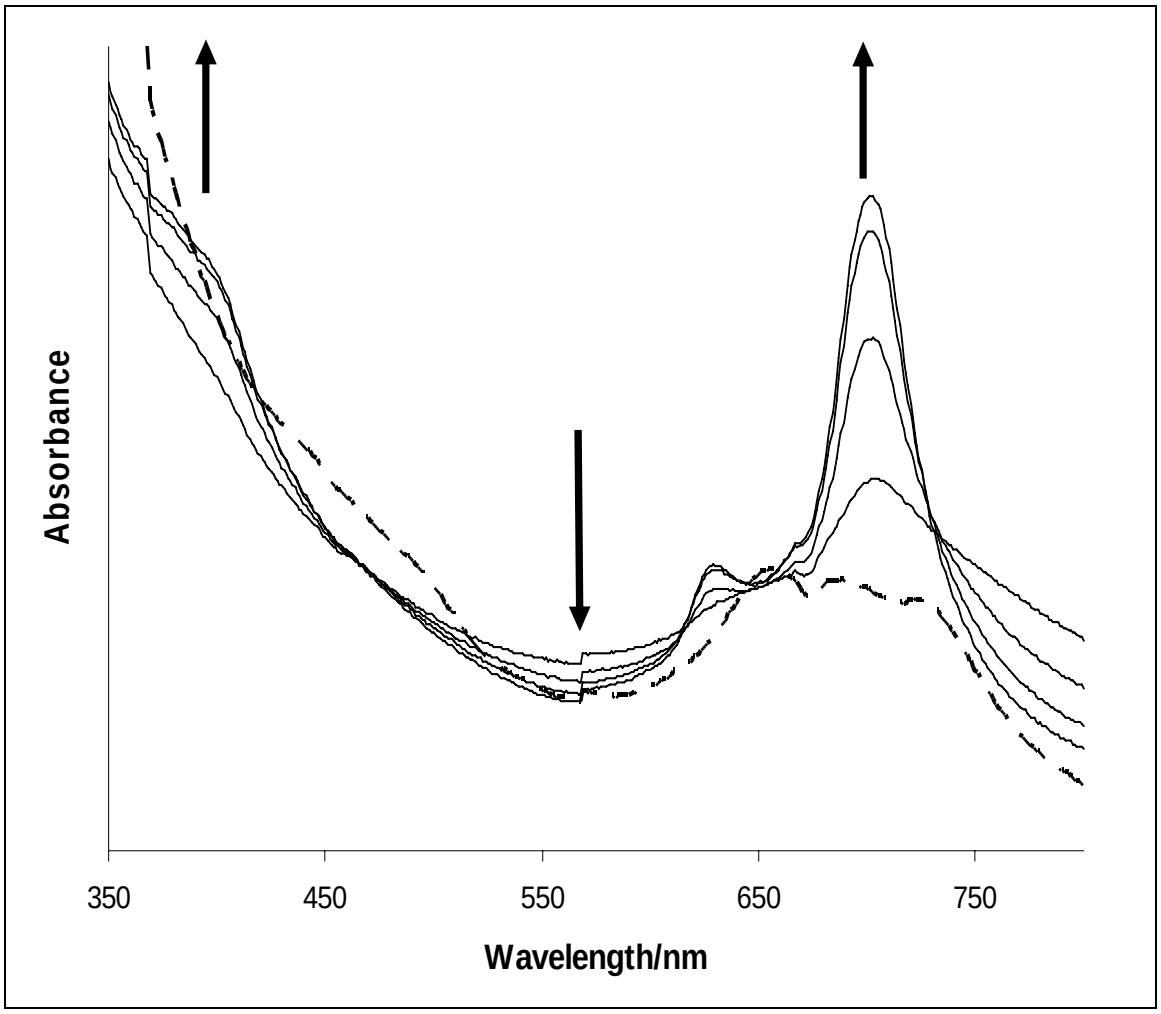

Figure 3.12 Typical UV-Visible spectral changes observed using OTTLE cell during oxidation of complex **11**. The spectra were recorded continuously during the electrolysis. Applied potential + 1.0 V.

As with Figure 3.11(a), the starting spectra of Figure 3.12 is typical of the aggregated species with two bands associated with the monomer (at lower energy) and the

aggregated species (at higher energy), due to the high concentrations employed for the OTTLE cell. Since there was an increase in Q band intensity, the spectral changes in Figure 3.12 are due to the oxidation of Co(II) to the Co(III) species, showing that at potentials of couple **IV** metal oxidation occurs, and that the couple is due to $Co^{III}Pc^{-2}/Co^{II}Pc^{-2}$. The subsequent oxidations are expected to be on the ring in comparison with literature.[79]

Figure 3.13 shows the CV and SWV for complex **12** in DMF containing 0.1 M TBAP.

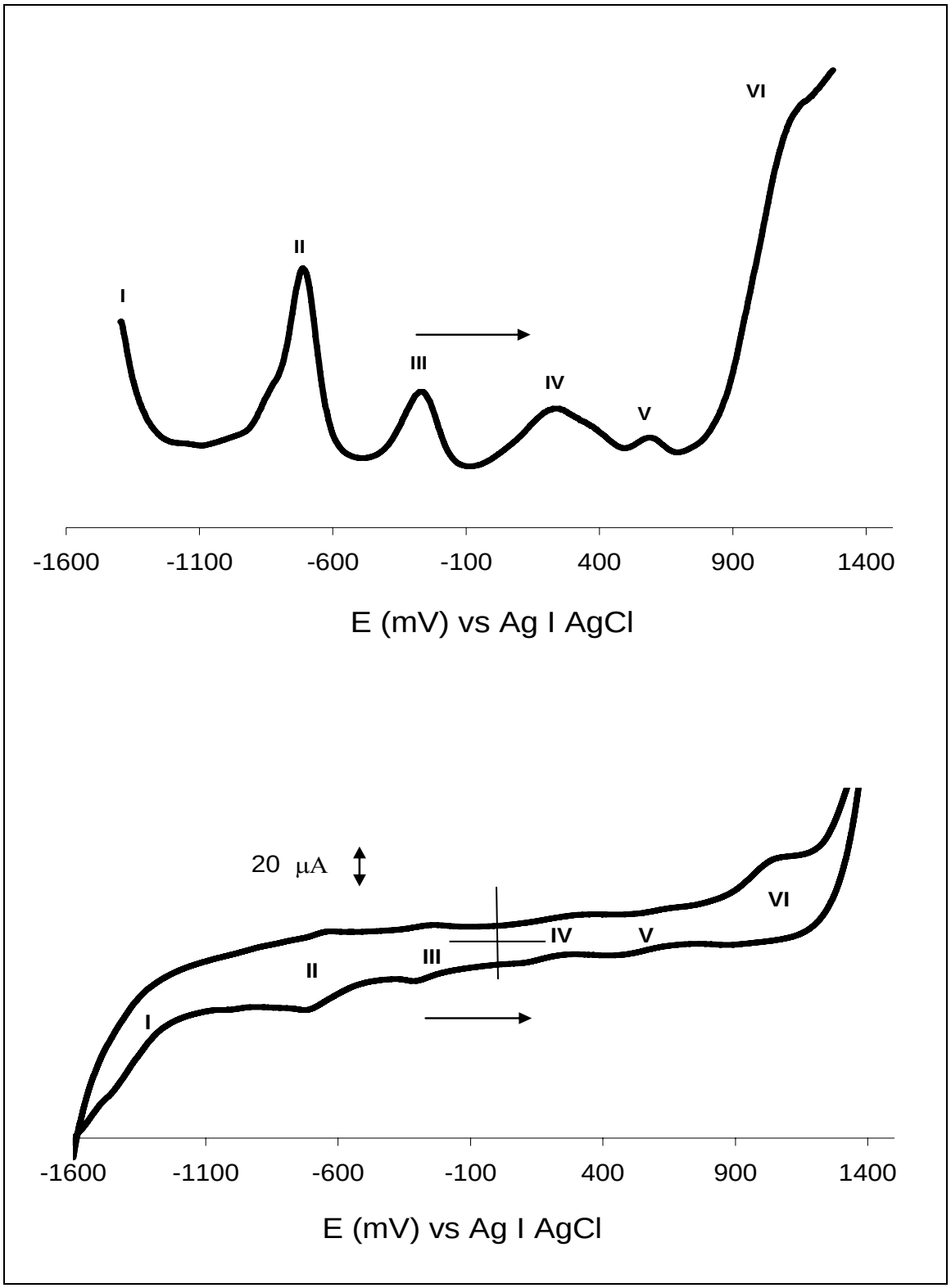

Figure 3.13 Cyclic and square wave (top) voltammograms on a GCE, for complex **12** in DMF containing 0.1 M TBAP. Scan rate = 100 mV/s.

From Figure 3.13 six processes were observed. As with the CoPc species above, the couples exhibited reversible to quasi-reversible behavior in that the ratio of cathodic to anodic peak currents were not unity and ΔE values were larger than the 90 mV observed for ferrrocenium/ferrocene standard. The plot of peak current versus square root of the scan rate was linear for all couples hence confirming diffusion control.

The potentials for first reduction of complexes **11** and **12** are much less negative than those of other thiol substituted CoPc and FePc complexes (Table 3.3), suggesting that the phenylthiol substituents confer ease of reduction on the CoPc and FePc species.

Spectroelectrochemistry (OTTLE) for complex **12** at potentials more negative than couple **III** gave spectral changes shown in Figure 3.14.

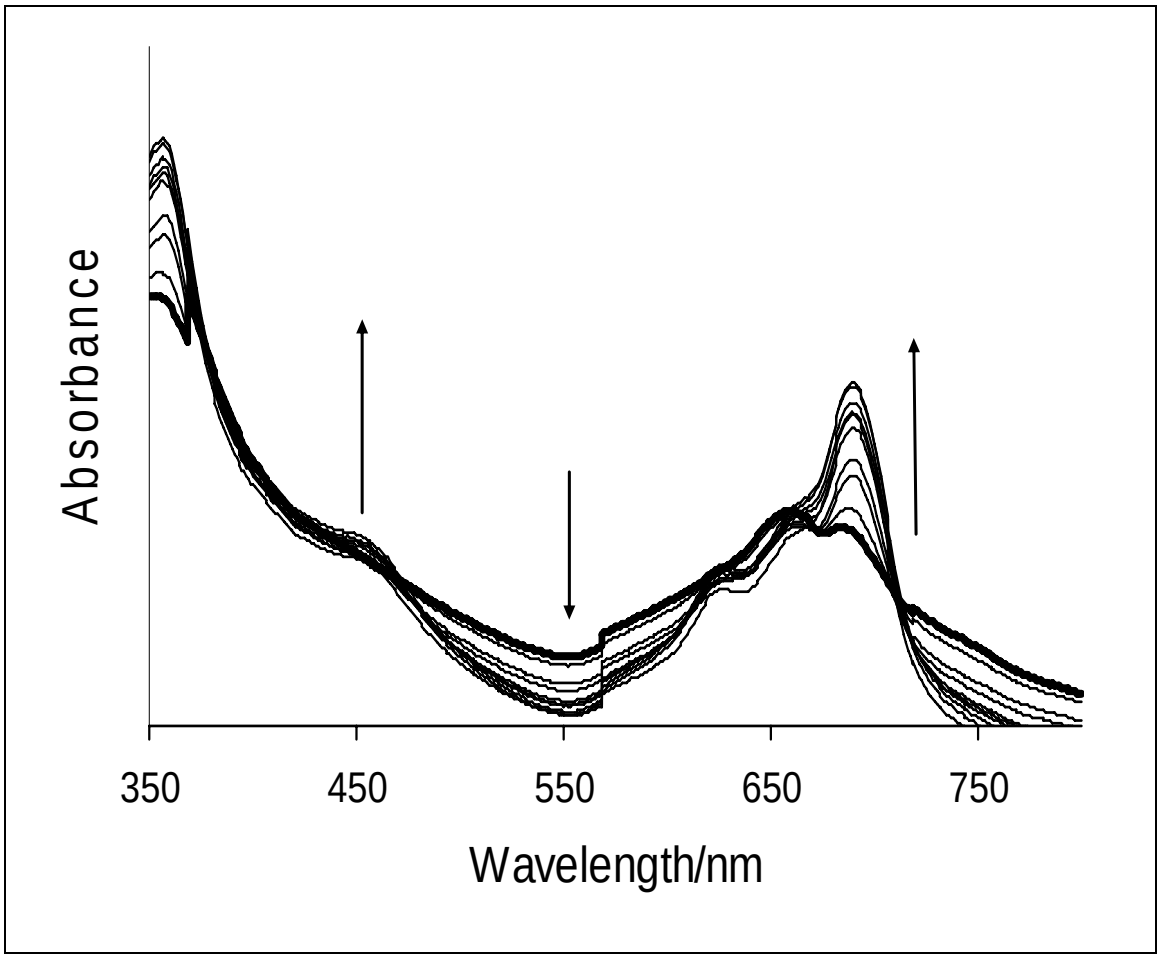

Figure 3.14 Typical UV-Visible spectral changes observed using OTTLE cell during reduction of complex **12**. The spectra were recorded continuously during the electrolysis. Applied potential -0.5 V. Electrolyte: DMF containing TBAP.

Again, from Figure 3.14, complex **12** shows aggregation at the concentrations employed for the OTTLE cell, as shown by the broad and split Q band before electrolysis. Upon reduction, the peak due to the monomer increased and shifted slightly to longer wavelengths, while the band at 450 nm associated with charge transfer in axially ligated Fe(II)Pc complexes decreased in intensity. The disappearance of this band suggests a change in the oxidation state of the central Fe(II) metal. Generally, in phthalocyanine chemistry, the lack of disappearance of the Q band on reduction or oxidation suggests a

metal-based process. Thus the spectral changes shown in Figure 3.14 are typical of metal-based reduction, suggesting the formation of the Fe(I) species. The spectra of Fe(I)Pc species is not well known. It has been reported[20] that the presence of Fe(I) disturbs the π-π* spectrum of the Pc resulting in a weak Q band and a pink solution. This work however shows that a strong Q band is still present following reduction of Fe(II)Pc to Fe(I)Pc, probably due to the influence of the ring substituents. The spectroelectrochemical studies hence confirm that couple **III** is due to $Fe^{II}Pc^{-2}/Fe^{I}Pc^{-2}$.

Reduction of complex **12** at potentials of couple **II** resulted in the decrease in the Q band and the formation of bands in the 500 to 600 nm region, typical of ring reduction in MPc complexes and suggesting the formation of the $Fe^{I}Pc^{-3}$ species. Further reductions are expected to occur on the ring, and the assignments are listed in Table 3.3. Attempts to oxidize complex **12** resulted in the formation of a broad Q band, probably due to the fact that the Fe(III)Pc species is characterized by a split Q band.

3.3. Direct Self Assembled Monolayer of MPc on Au

Table 3.4 summarizes the characterization parameters of the $CoPc(SCH_2Ph)_8$ (**11**) and $FePc(SCH_2Ph)_8$ (**12**) self assembled monolayers on gold electrode surfaces studied in this work.

Table 3.4 A synopsis of the characterization parameters of the $CoPc(SCH_2Ph)_8$ (**11**) and $FePc(SCH_2Ph)_8$ (**12**) self assembled monolayers on gold electrode surfaces.

Parameter	**$CoPc(SCH_2Ph)_8$-SAM (11)**	**$FePc(SCH_2Ph)_8$-SAM (12)**
Ion Barrier Factor, Γ_{ibf}	~ 1	0.98
Interfacial Capacitance, C_s ($\mu F/cm^2$)	500	~ 800
Surface Coverage, Γ ($x10^{-10}$ mol/cm^2)	1.55	4.24

3.3.1. Characterization of $CoPc(SCH_2Ph)_8$ (11) and $FePc(SCH_2Ph)_8$ (12) SAMs

This work may be summarized as the self assembly monolayer (SAM) study of $CoPc(SCH_2Ph)_8$ (**11**) and $FePc(SCH_2Ph)_8$ (**12**) on gold electrode surfaces and may be divided in 2 parts:

(i) The characterization of the formed self assembly monolayers: as stated in the introduction self assembled monolayers of metallophthalocyanines block a number of Faradic process which include: gold surface oxidation; underpotential deposition (UPD) of metals (most commonly copper) and Fe^{III}/Fe^{II} redox processes.[41] These parameters are used to analyze the extent and veracity of the MPc SAMs in this work. Co and Fe central metals were used in the phthalocyanines as these metals display ideal redox activities.

(ii) Electrocatalytic effects of MPc-SAM modified gold electrodes towards L-cysteine. Voltammetric techniques provide methods for characterization of SAMs and analysis and hence cyclic voltammetry was used for the characterization of the SAMs.

The aim of this part of the work is to study MPc complexes self-assembled to gold electrode surfaces in order to envisage any further technological uses e.g. as sensors.

3.3.1.1. Ion Barrier Factor, Γ_{ibf}

The ion barrier factor (Γ_{ibf}) is obtained by a comparison of the total charge under the peak of a SAM modified electrode (Q_{SAM}) with that of an unmodified electrode (Q_{Bare}). The charge values are obtained by integrating the currents under the redox peaks (either cathode or anode). The ion barrier factor (Γ_{ibf}) may hence be represented using equation 3.1, introduced as equation 1.3 in chapter 1:

$$\Gamma_{ibf} = 1 - \frac{Q_{SAM}}{Q_{Bare}} \qquad 3.1$$

An ion barrier factor of unity indicates an ideal barrier to ion and solvent permeability afforded by the SAM.

Figure 3.15 shows the cyclic voltammograms of an unmodified gold electrode in 1 M Na_2SO_4 in pH 4 buffer solution (curve i), a gold electrode modified with the SAM of $CoPc(SCH_2Ph)_8$ (curve ii) and a gold electrode modified with the SAM of $FePc(SCH_2Ph)_8$ (curve iii).

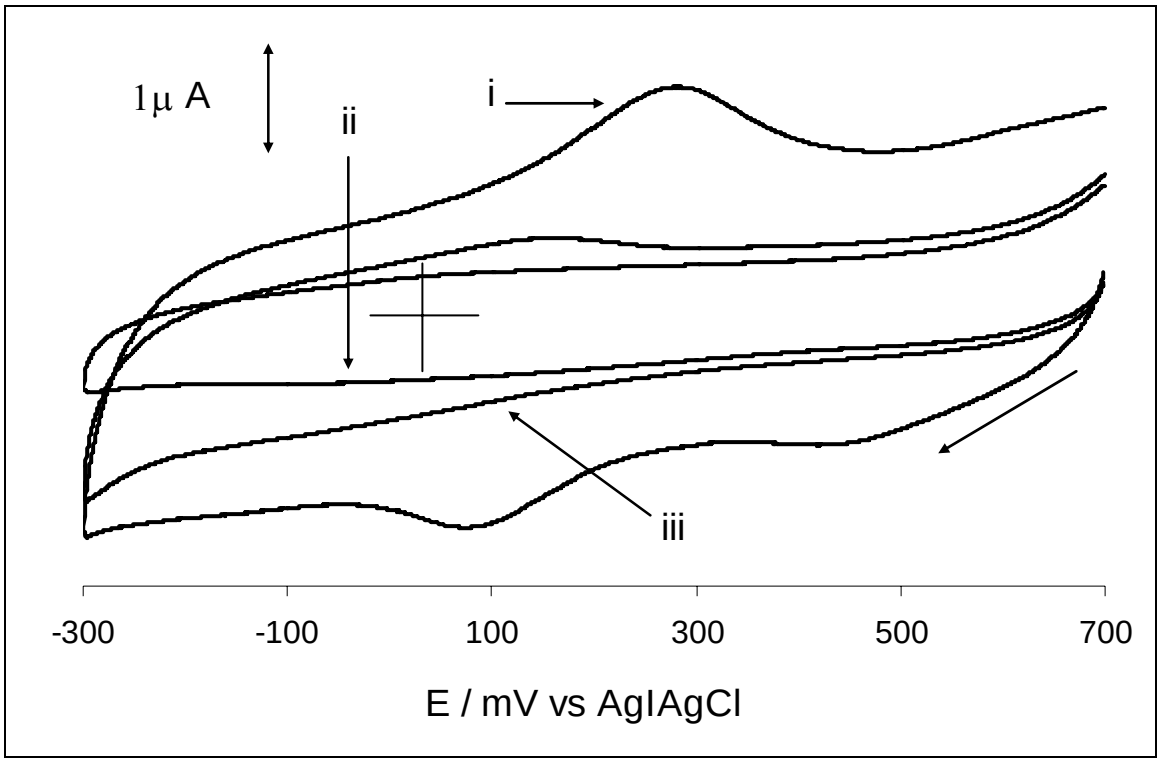

Figure 3.15 Cyclic voltammograms of a gold electrode before modification (i), after modification with the SAM of $CoPc(SCH_2Ph)_8$ (**11**) (ii) and after modification with the SAM of $FePc(SCH_2Ph)_8$ (**12**) (iii). Electrolyte = 1 M Na_2SO_4 in pH 4 buffer solution. Scan rate = 100 mV/s.

The peaks observed on an unmodified Au electrode (Figure 3.15, curve i) are due to the Au oxide redox reaction. From Figure 3.15 ion barrier factors of unity and 0.98 (using equation 3.1) for the $CoPc(SCH_2Ph)_8$-SAM and $FePc(SCH_2Ph)_8$-SAM, respectively, were obtained. These results hence confirm the fact that both SAMs are well packed, have a strong passivating aptitude and act as an efficient barrier to ion permeability.

3.3.1.2. Interfacial Capacitance, C_s

A defined potential window of a cyclic voltammogram, in which no peaks are observed for both an unmodified and modified gold electrode, will have a charging current (i_{ch}) whose value may be used to calculate the interfacial capacitance (C_s) from equation 3.2, introduced in chapter 1 as equation 1.4:

$$C_s = \frac{i_{ch}}{\nu A} \qquad 3.2$$

where i_{ch} is the charging current (μA), ν is the scan rate (V/s) and A is the surface area of the electrode (cm^2).

A SAM modified gold electrode should display a lower interfacial capacitance (C_s) relative to an unmodified gold electrode. The lower the C_s value for a SAM modified electrode, the less defects are present in the SAM.

Figure 3.15 above, showing the cyclic voltammograms of an unmodified gold electrode in 1 M Na_2SO_4 in pH 4 buffer solution (curve i) and after coating with the SAM of $CoPc(SCH_2Ph)_8$ (**11**) (curve ii) or $FePc(SCH_2Ph)_8$ (**12**) (curve iii), was used to estimate the C_s values in the potential window of -0.3 V to -0.1 V. The C_s value of the $CoPc(SCH_2Ph)_8$-SAM modified electrode (Figure 3.15, curve ii) was lower (C_s = 500 μFcm^{-2}) compared to the C_s value of the unmodified Au electrode (C_s = 1500 μFcm^{-2}) as expected. This fact pertains to a closely packed, relatively defect free formed $CoPc(SCH_2Ph)_8$-SAM. The C_s value of the $FePc(SCH_2Ph)_8$-SAM modified electrode (Figure 3.15, curve iii) was also lower (C_s = ~ 800 μFcm^{-2}) compared to the C_s value of the unmodified Au electrode (Figure 3.15, curve i) (C_s = 1500 μFcm^{-2}) also as expected. Hence albeit the C_s values of $CoPc(SCH_2Ph)_8$-SAM and $FePc(SCH_2Ph)_8$-SAM

demonstrate that the SAMs are closely packed on the gold electrode surface, the higher C_s value relative to the $CoPc(SCH_2Ph)_8$-SAM shows that the latter is not as defect free as the former. This fact is illustrated in Figure 3.15 where the cyclic voltammogram of the SAM of $CoPc(SCH_2Ph)_8$ (Figure 3.15, curve ii) shows lower currents than that of $FePc(SCH_2Ph)_8$-SAM (Figure 3.15, curve iii). It must also be noted (though true comparison is difficult) that the C_s values obtained in this work are relatively higher than those obtained in literature.[58] This may be explained by the fact that the substituents of the Pcs studied in this work possess bulky phenolic groups which may hence lower the compactness, hence increasing the C_s value, to a large extent.

3.3.1.3. Underpotential Deposition (UPD) of Copper

Figure 3.16 shows how the SAMs of $CoPc(SCH_2Ph)_8$ (**11**) (curve ii) and $FePc(SCH_2Ph)_8$ (**12**) (curve iii) inhibit the Faradic process of Cu metal deposition onto a gold electrode relative to an unmodified gold electrode (curve i).

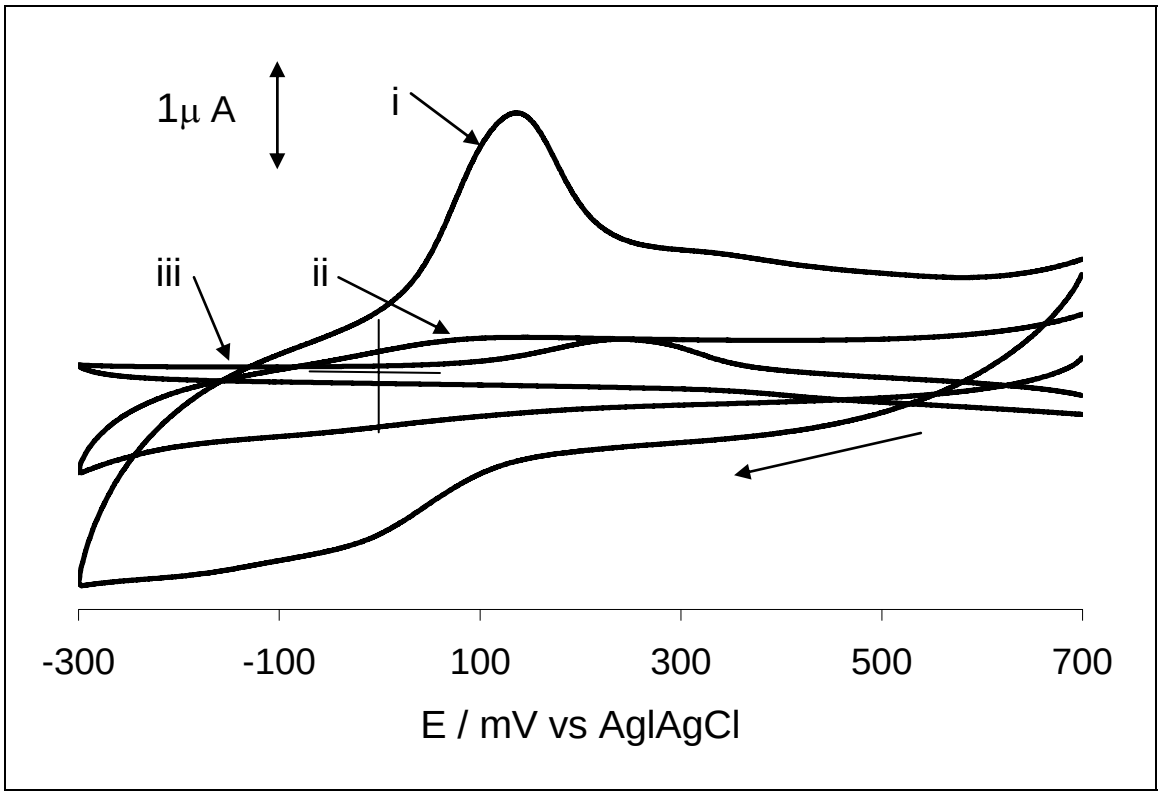

Figure 3.16 Cyclic voltammograms showing the response of a gold electrode to the underpotential deposition of copper on an unmodified gold electrode (i), after coating with $CoPc(SCH_2Ph)_8$-SAM (ii) and after coating with $FePc(SCH_2Ph)_8$-SAM (iii). Electrolyte = 1 mM $CuSO_4$ in pH 4 buffer. Scan rate = 100 mVs^{-1}.

The bulk deposition of copper began at approximately +0.1 V vs Ag|AgCl during the negative going scan of the unmodified gold electrode (Figure 3.16, curve i). A large underpotential deposition (UPD) stripping peak for the Cu metal is observed at +0.15 V on the return scan (Figure 3.16, curve i). This peak has a characteristic shape and occurs in a similar potential window as previously published.[41,80] Hence voltammogram (i) in Figure 3.16 represents the UPD of Cu in the forward direction and stripping of the so formed monolayer of Cu in the reverse direction. A negligible current response is observed on the cyclic voltammograms of $CoPc(SCH_2Ph)_8$-SAM (Figure 3.16, curve ii)

and FePc$(SCH_2Ph)_8$-SAM (Figure 3.16, curve iii) relative to that of the unmodified Au electrode (Figure 3.16, curve i). This confirms the fact that the CoPc$(SCH_2Ph)_8$-SAM and FePc$(SCH_2Ph)_8$-SAM cover the gold surface well as the gold surface is no longer accessible to the Cu solution and hence no redox reaction is clearly observed. The idyllic blocking characteristics of CoPc$(SCH_2Ph)_8$-SAM and FePc$(SCH_2Ph)_8$-SAM displayed in Figure 3.16 also indicate that the SAMs are almost pinhole-free. From Figure 3.16, the ion barrier factor (Γ_{ibf}) of the CoPc$(SCH_2Ph)_8$-SAM and FePc$(SCH_2Ph)_8$-SAM were calculated using Equation 3.1 (given above) and were found to be 0.98 and 0.99 respectively. This shows that approximately 2% and 1% of the gold surface is not covered with the CoPc$(SCH_2Ph)_8$-SAM or FePc$(SCH_2Ph)_8$-SAM showing that the SAMs are compact and virtually defect-free.

3.3.1.4. Inhibition of Fe^{III}/Fe^{II} Redox Processes

Figure 3.17 shows the cyclic voltammograms of $[Fe(H_2O)_6]^{3+}/[Fe(H_2O)_6]^{2+}$ on CoPc$(SCH_2Ph)_8$-SAM modified electrode (curve ii), FePc$(SCH_2Ph)_8$-SAM modified electrode (curve iii) and on an unmodified Au electrode (curve i).

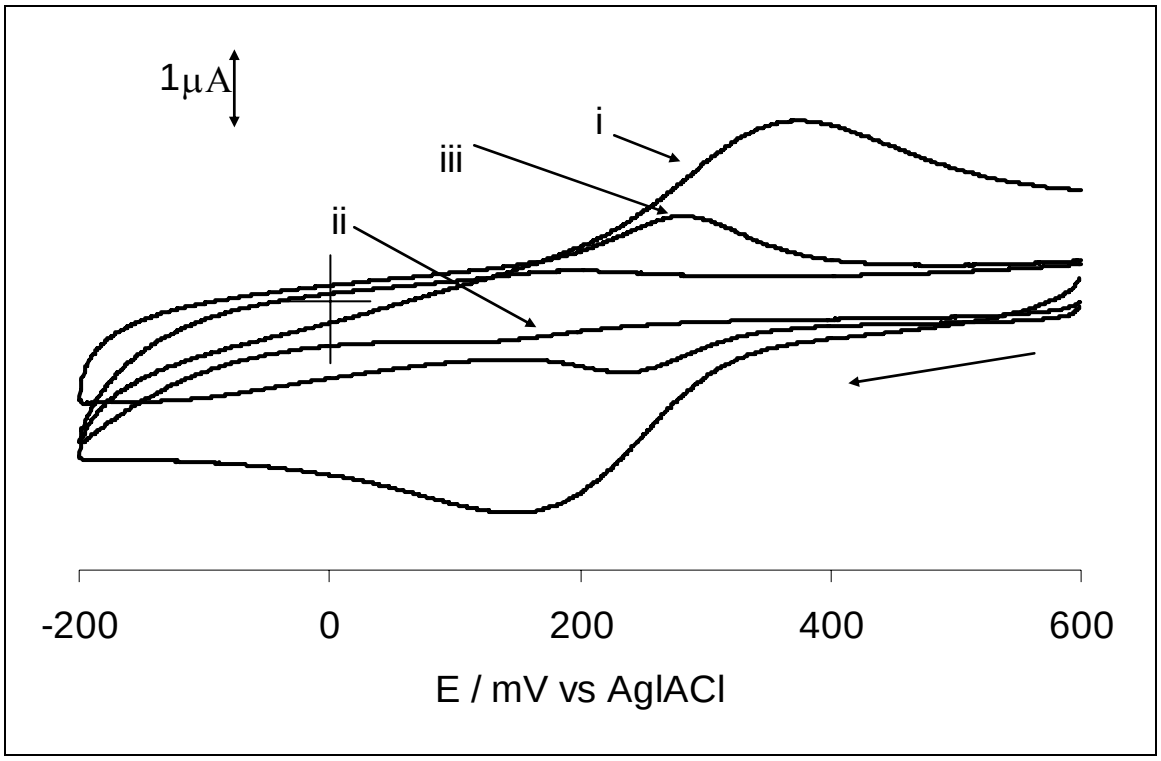

Figure 3.17 Cyclic voltammograms of 1 mM $Fe(NH_4)SO_4$ in 1 M $HClO_4$ on a gold electrode before modification (i), after coating with $CoPc(SCH_2Ph)_8$-SAM (ii) and after coating with $FePc(SCH_2Ph)_8$-SAM (iii). Scan rate = 100 mVs^{-1}.

$Fe(NH_4)SO_4$ in $HClO_4$ was used as the analyzing electrolyte as its redox couple $[Fe(H_2O)_6]^{3+}/[Fe(H_2O)_6]^{2+}$ displays a relatively (*cf* $[Fe(CN)_6]^{3-}/[Fe(CN)_6]^{4-}$) lower electron transfer rate constant (hence mass transport does not determine the reaction rate, even at small overpotentials).[81] From Figure 3.17 it may be observed that the Faradic couple $[Fe(H_2O)_6]^{3+}/[Fe(H_2O)_6]^{2+}$ occurring in the +0.1 V to +0.4 V region (curve i) is largely inhibited in the case of a gold electrode modified with $CoPc(SCH_2Ph)_8$-SAM (curve ii) or $FePc(SCH_2Ph)_8$-SAM (curve iii). The latter shows less inhibition of the redox process. Figure 3.17 shows a prominent $[Fe(H_2O)_6]^{3+}/[Fe(H_2O)_6]^{2+}$ redox peak couple (curve i) on an unmodified Au electrode. It may be inferred that the

$CoPc(SCH_2Ph)_8$-SAM film is more compact and acts as a better barrier to the transport of these ions than the $FePc(SCH_2Ph)_8$-SAM.

3.3.1.5. Surface Coverage, Γ

Figures 3.18 and 3.19 show cyclic voltammograms of $CoPc(SCH_2Ph)_8$-SAM and $FePc(SCH_2Ph)_8$-SAM respectively in 1 M $HClO_4$. The peak at ~ 100 mV in Figure 3.18 is assigned to Co^{II}/Co^{I} in comparison with literature.[57] The Co^{III}/Co^{II} couple was not observed probably because it occurs at potentials > 0.7 V but SAMs desorb at these potentials. The Co^{III}/Co^{II} couple is expected to catalyze RSH (cysteine) oxidation. The Fe^{III}/Fe^{II} peak was observed at 0.25 V in comparison with literature.[82] This is also confirmed by solution studies and Figure 3.13, where the $Fe^{III}Pc^{-2}/Fe^{II}Pc^{-2}$ peak occurs at 250 mV. The ΔE (at ν = 200 mV/s) for Co^{II}/Co^{I} and Fe^{III}/Fe^{II} were 188 mV and 100 mV, higher than the expected 0 V for absorbed species indicating slow electron transfer processes (ΔE = 0 was observed at low scan rates for Fe^{III}/Fe^{II}, Figure 3.19). The cyclic voltammograms shown in Figures 3.18 and 3.19 were similar to those observed in pH 4 buffer alone.

Surface coverage (Γ) may be calculated using equation 3.3, introduced as equation 1.5 in chapter 1:

$$i_p = n^2F^2A\Gamma\,(\nu)/4RT \qquad 3.3$$

where i_p is the peak current (Amps), n is the number of electrons, A is the area of the electrode (cm^2), ν is the scan rate (V/s) and the other symbols have their usual meanings.

The Γ values of the electroactive $CoPc(SCH_2Ph)_8$-SAM and $FePc(SCH_2Ph)_8$-SAM were estimated from the peak corrected current (i_{pcorr}) under the reductive [$Co^{II}Pc^{-2}/Co^{I}Pc^{-2}$] and [$Fe^{III}Pc^{-2}/Fe^{II}Pc^{-2}$] redox peaks (Figures 3.18 and 3.19 respectively). The peak corrected current (i_{pcorr}) was calculated by subtracting the background current from the observed current. The peak corrected current (i_{pcorr}) increased linearly as a function of scan rate as shown in Figures 3.18 and 3.19 inserts, as expected for adsorbed species.

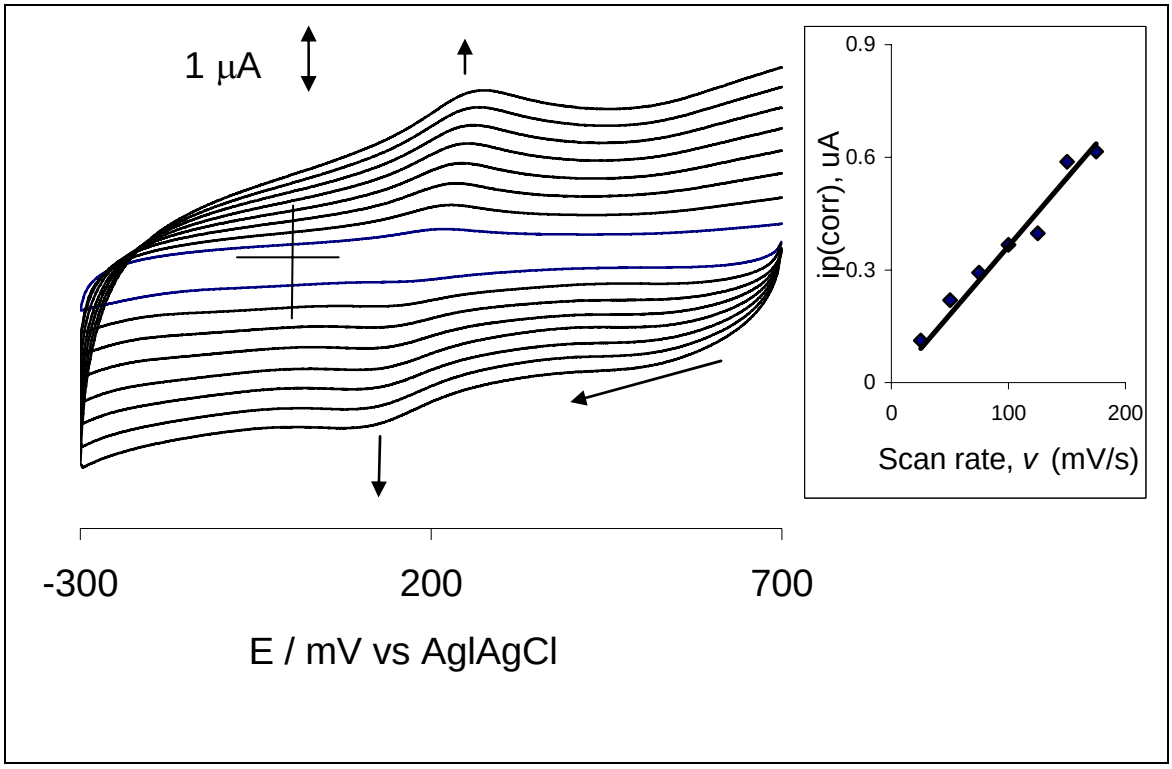

Figure 3.18 Cyclic voltammograms of a $CoPc(SCH_2Ph)_8$-SAM modified gold electrode showing the dependence of peak currents on scan rates in a 1 M $HClO_4$ solution. Insert = plot showing peak corrected current (i_{pcorr}) versus the scan rate (ν) of the $CoPc(SCH_2Ph)_8$-SAM modified gold electrode in 1 M $HClO_4$ solution.

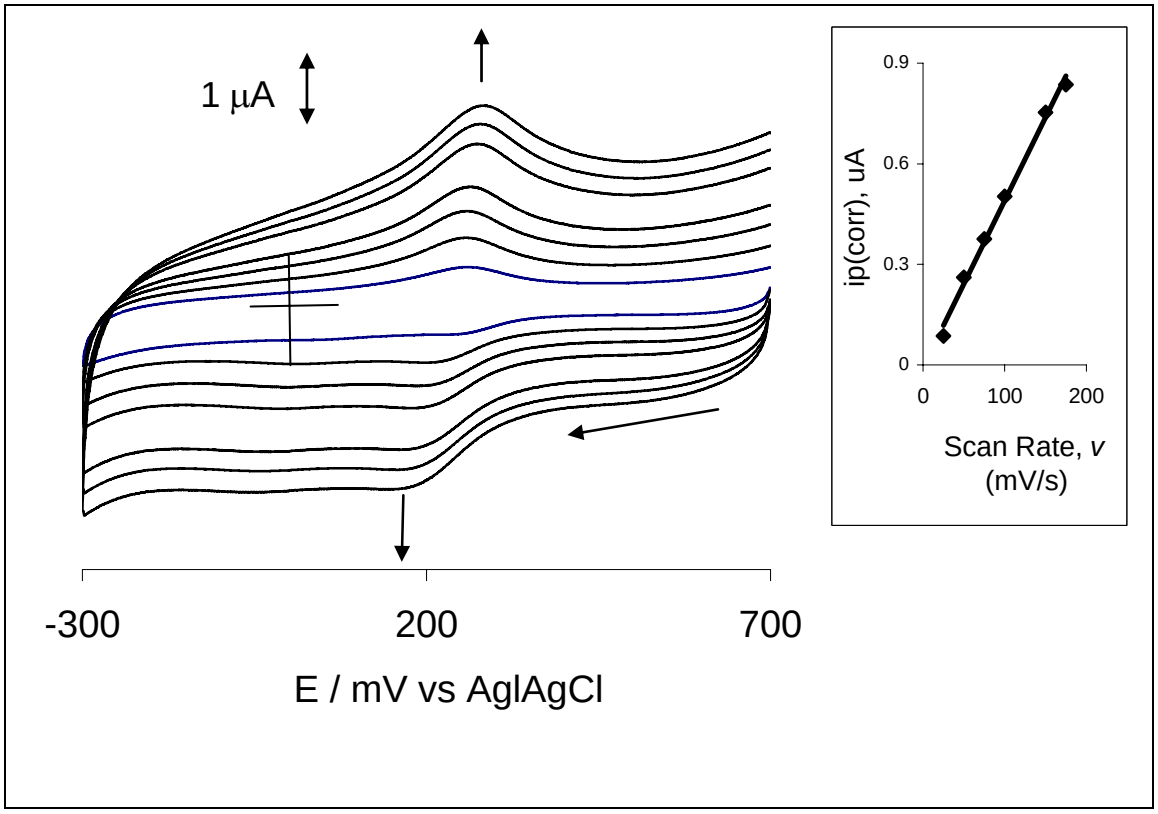

Figure 3.19 Cyclic voltammograms of a $FePc(SCH_2Ph)_8$-SAM modified gold electrode showing the dependence of peak currents on scan rates in a 1 M $HClO_4$ solution. Insert = plot showing corrected current (i_{pcorr}) versus the scan rate (ν) of the $FePc(SCH_2Ph)_8$-SAM modified gold electrode in 1 M $HClO_4$ solution.

The slopes of the straight line obtained from Figures 3.18 and 3.19 (inserts) were then used in equation 3.3 to calculate the surface coverage (Γ) value of $CoPc(SCH_2Ph)_8$-SAM and $FePc(SCH_2Ph)_8$-SAM. The Γ values of $CoPc(SCH_2Ph)_8$-SAM and $FePc(SCH_2Ph)_8$-SAM were 1.55 x 10^{-10} mol/cm^2 and 4.24 x 10^{-10} mol/cm^2 respectively and are within the range (10^{-10} mol/cm^2) reported for other metallophthalocyanine macrocycles adsorbed as monolayers.[80, 83-85]

3.3.2. Electrocatalytic activity of MPc-SAM modified Au electrodes towards L-Cysteine

L-cysteine electrochemical oxidation generally occurs at extreme positive potentials with slow electron transfer kinetics presenting disadvantages for its analysis. Using metallophthalocyanine-chemically modified electrodes (MPc-CMEs) decreases the potential at which L-cysteine oxidation occurs with fast electron transfer rates.[63]

The potential window used in the cyclic voltammogram L-cysteine study had to be carefully chosen. Preliminary studies in pH 4 buffer proved that a potential window that was too narrow would result in the absence of $MPc(SCH_2Ph)_8$-SAM catalyzed L-cysteine oxidation peak; whilst a potential that was too wide (Figure 3.20) resulted in the desorption of the $MPc(SCH_2Ph)_8$-SAM from the gold electrode surface. This latter fact is clearly observed as, in a wide potential window, the sharp gold oxide stripping peak occurring at ~ 400 mV (Figure 3.20) is prominent.

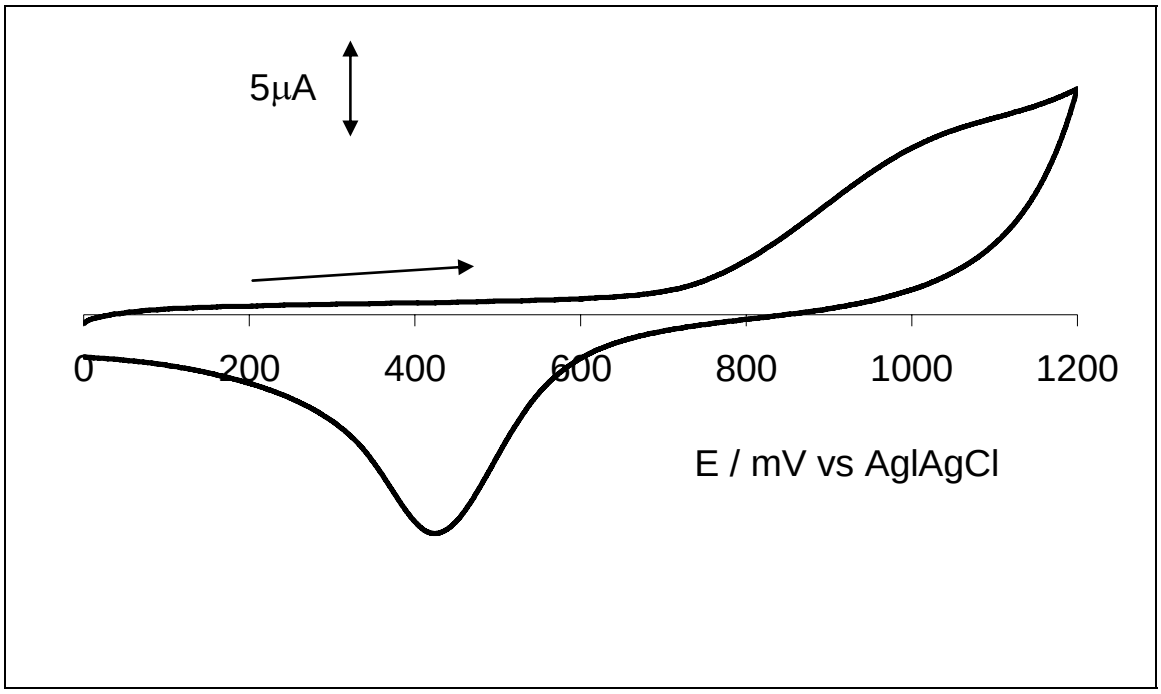

Figure 3.20 Cyclic voltammogram of a $FePc(SCH_2Ph)_8$-SAM modified gold electrode in pH 4 buffer solution run in a wide potential window (0-1200 mV).

3.3.2.1. Electrocatalytic activity of $CoPc(SCH_2Ph)_8$-SAM towards L-Cysteine

Figure 3.21 shows the cyclic voltammograms of an unmodified gold electrode in an L-cysteine solution (curve i) and a $CoPc(SCH_2Ph)_8$-SAM modified gold electrode in pH 4 buffer solution containing increasing concentrations of L-cysteine (curves ii - iv). Studies were performed in pH 4 as this was the pH producing the most defined voltammetric peaks. Also note the potential window used allowed the observation of the L-cysteine peak whilst simultaneously inhibiting the stripping of the $CoPc(SCH_2Ph)_8$-SAM from the gold electrode surface (as proven by the absence of the gold oxide stripping peak).

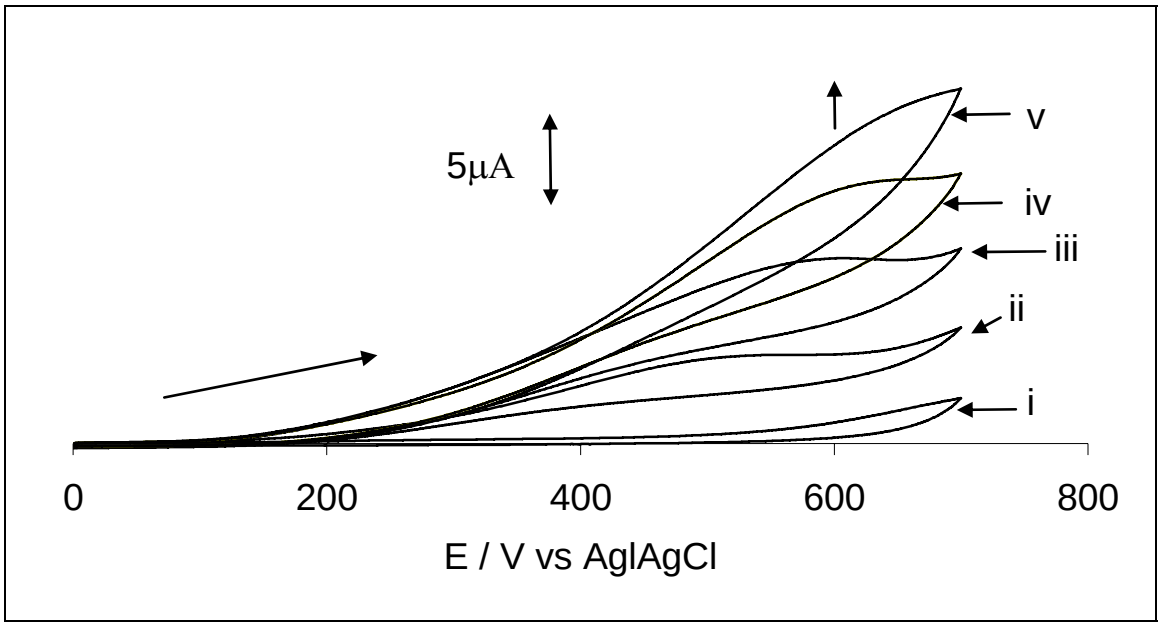

Figure 3.21 Typical cyclic voltammograms of an unmodified gold electrode run in 1.20 x 10^{-5} M L-cysteine (i) and a $CoPc(SCH_2Ph)_8$-SAM modified gold electrode in pH 4 buffer solution containing: 9.41 x 10^{-6} M (ii); 1.77 x 10^{-5} M (iii); 2.09 x 10^{-5} M (iv); 2.23 x 10^{-5} M (v) L-cysteine.

From Figure 3.21 the cyclic voltammogram of an unmodified gold electrode run in an L-cysteine solution (i) displayed no peaks as expected. It is observed from Figure 3.21 that the anodic peak potential at approximately + 0.6 V vs Ag|AgCl increases with an increase in L-cysteine concentration proving that the $CoPc(SCH_2Ph)_8$-SAM catalyses the oxidation of L-cysteine to cystine. A proposed mechanism of this oxidation process is similar to the generally accepted mechanism: initially there is the oxidation of the central metal in $M^{II}Pc$ forming $M^{III}Pc$ followed by electron transfer from cysteine to $M^{II}Pc$ (cystine being the oxidation product of cysteine).[63] This is in good agreement with the results obtained in Figure 3.10 for solution electrochemistry: it is observed that the $Co^{III}Pc/Co^{II}Pc$ peak occurs at ~ 0.7 V in solution which is in the same region as that of

cysteine oxidation (0.6 V). As stated earlier this peak is not observed on $CoPc(SCH_2Ph)_8$-SAM (Figure 3.18) due to desorption. Hence it may be deduced that the $CoPc(SCH_2Ph)_8$-SAM is electrochemically catalyzing the oxidation of cysteine.

As the $Co^{III}Pc/Co^{II}Pc$ process (in solution) of $CoPc(SCH_2Ph)_8$-SAM occurs in the same potential region as that of cysteine oxidation, the catalytic oxidation of L-cysteine by $CoPc(SCH_2Ph)_8$-SAM through the $Co^{III}Pc/Co^{II}Pc$ couple may be represented by equations 3.4 to 3.7:

$$Co^{II}(SCH_2Ph)_8Pc^{-2} \rightarrow Co^{III}(SCH_2Ph)_8Pc^{-2} + e^- \quad 3.4$$

$$Co^{III}(SCH_2Ph)_8Pc^{-2} + RSH \rightarrow (RSH)Co^{III}(SCH_2Ph)_8Pc^{-2} \quad 3.5$$

$$(RSH)Co^{III}(SCH_2Ph)_8Pc^{-2} \rightarrow Co^{II}(SCH_2Ph)_8Pc^{-2} + RS^+ + H^+ \quad 3.6$$

$$2RS^+ \rightarrow RSSR \quad 3.7$$

where RSH represents L-cysteine and RSSR is cystine, the oxidation product of L-cysteine.

In order to prove the coordination of L-cysteine to $Co^{III}Pc(SCH_2Ph)_8$ (equation 3.5), a shift in the Q band to lower wavelength was observed when L-cysteine was added to $Co^{III}(SCH_2Ph)_8Pc^{-2}$ (generated by bromine oxidation), Figure 3.22. Such shifts are typical of axial ligand coordination in MPc complexes.[32]

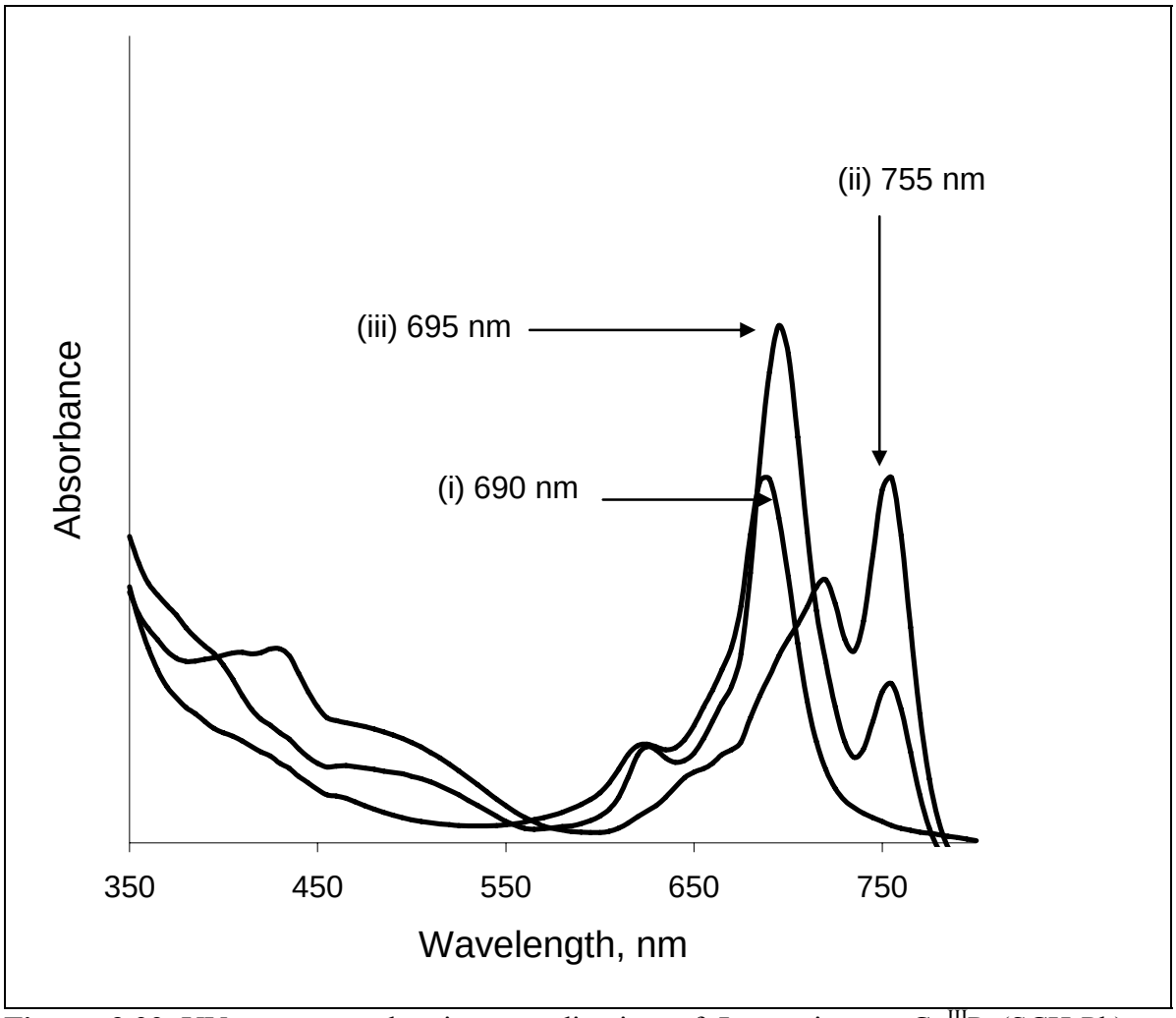

Figure 3.22 UV spectrum showing coordination of L-cysteine to $Co^{III}Pc(SCH_2Ph)_8$ through a shift in the Q band maxima of $Co^{III}Pc(SCH_2Ph)_8$ solution (curve ii) on addition of L-cysteine solution (curve iii). Curve (i) represents the $Co^{II}Pc(SCH_2Ph)_8$ solution. Solvent = THF.

Figure 3.23 shows the dependence of peak current on the square root of the scan rate for 1.45×10^{-3} M L-cysteine on $CoPc(SCH_2Ph)_8$-SAM in acidic pH, the linearity confirming diffusion control for L-cysteine.

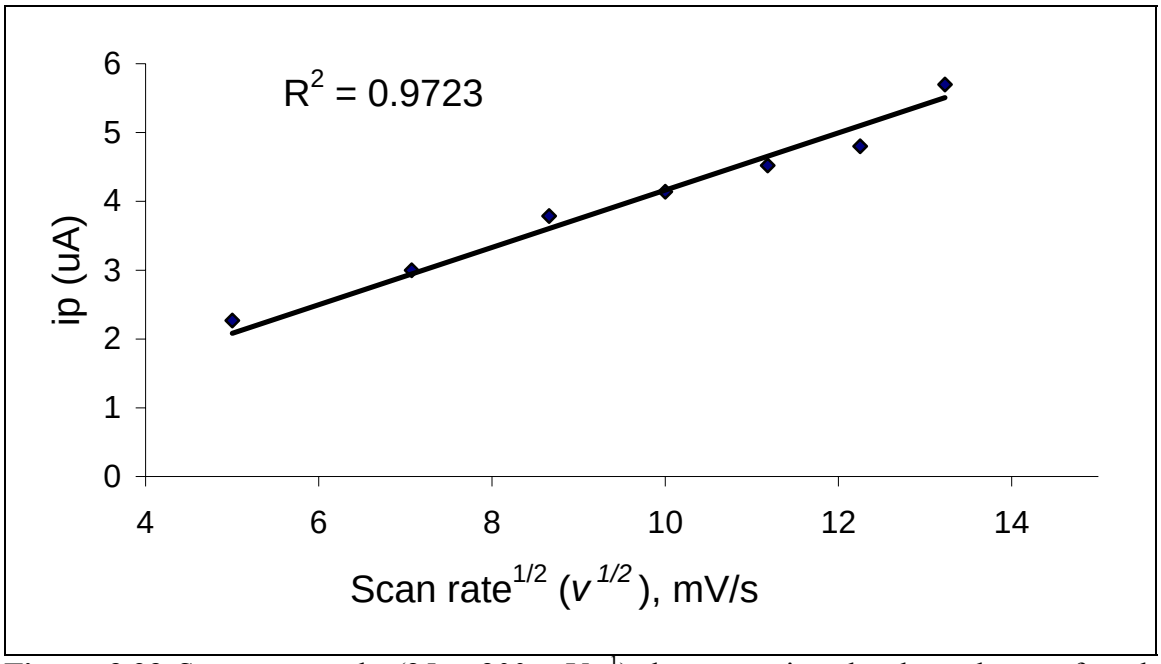

Figure 3.23 Scan rate study (25 – 200 mVs^{-1}) demonstrating the dependence of peak current on scan rate of a $CoPc(SCH_2Ph)_8$-SAM modified gold electrode in a 1.45 x 10^{-3} M L-cysteine acidic solution.

3.3.2.2. Electrocatalytic activity of $FePc(SCH_2Ph)_8$-SAM towards L-Cysteine

Figure 3.24 shows the cyclic voltammograms of a $FePc(SCH_2Ph)_8$-SAM modified gold electrode in pH 4 buffer solution containing increasing L-cysteine concentrations (curves ii – v). Figure 3.24 insert shows the cyclic voltammogram of an unmodified gold electrode run in 1.20 x 10^{-5} M L-cysteine (curve i). Note the potential windows used allowed the observation of the L-cysteine peak whilst simultaneously inhibiting the stripping of the $FePc(SCH_2Ph)_8$-SAM from the gold electrode surface (as proven by the absence of the gold oxide stripping peak).

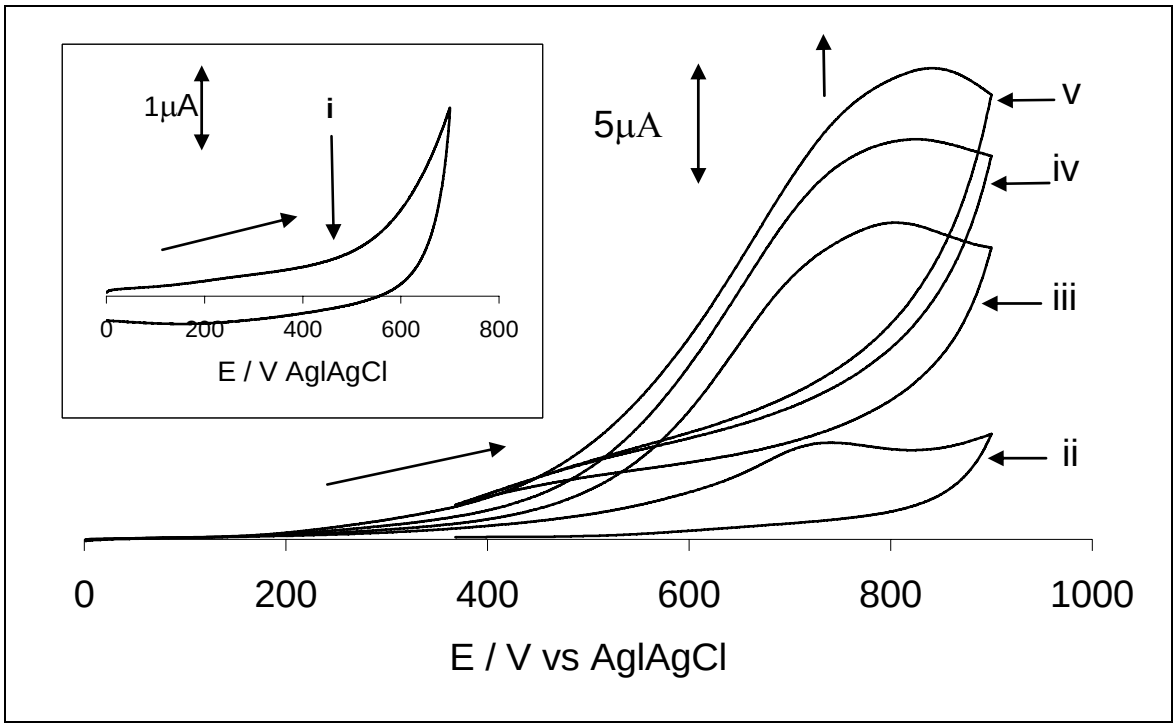

Figure 3.24 Cyclic voltammograms of a $FePc(SCH_2Ph)_8$-SAM modified gold electrode in pH 4 buffer solution containing: 2.48 x 10^{-3} M (ii); 3.30 x 10^{-3} M (iii); 4.10 x 10^{-3} M (iv); 4.13 x 10^{-3} M (v) L-cysteine. Insert = cyclic voltammogram of an unmodified gold electrode run in 1.20 x 10^{-5} M L-cysteine (i).

From Figure 3.24 the cyclic voltammogram of an unmodified gold electrode run in an L-cysteine solution (i, insert) displayed no peaks as expected. From Figure 3.24 it can be seen that, at the concentrations and potential window used, the L-cysteine oxidation peak occurs at ~ 700 mV. However, in most cases, L-cysteine oxidation catalysis by CMEs is due to metal based processes.[82] Figures 3.13 and 3.19 show that the L-cysteine oxidation is more positive than the Fe^{III}/Fe^{II} couple at 0.25 V, but L-cysteine oxidation is still within the stability range for the Fe^{III}/Fe^{II} peak. Such behavior of the catalytic peak being more positive than the redox peak has been observed before.[82] The catalytic oxidation of

L-cysteine by the process $Fe^{III}Pc^{-2}/Fe^{II}Pc^{-2}$ of the $FePc(SCH_2Ph)_8$-SAM may be represented by equations 3.8 to 3.11:

$$Fe^{II}(SCH_2Ph)_8Pc^{-2} \rightarrow Fe^{III}(SCH_2Ph)_8Pc^{-2} + e^- \quad 3.8$$

$$Fe^{III}(SCH_2Ph)_8Pc^{-2} + RSH \rightarrow (RSH)Fe^{III}(SCH_2Ph)_8Pc^{-2} \quad 3.9$$

$$(RSH)Fe^{III}(SCH_2Ph)_8Pc^{-2} \rightarrow Fe^{II}(SCH_2Ph)_8Pc^{-2} + RS^+ + H^+ \quad 3.10$$

$$2RS^+ \rightarrow RSSR \quad 3.11$$

where RSH represents L-cysteine and RSSR is cystine, the oxidation product of L-cysteine.

The coordination of L-cysteine to $Fe^{III}Pc(SCH_2Ph)_8$ (equation 3.9) was proven by a shift in the Q band maximum when L-cysteine was added to a solution of $Fe^{III}Pc(SCH_2Ph)_8$ in DMF (generated by $Fe^{II}Pc(SCH_2Ph)_8$ oxidation with Br_2, Figure 3.25) and as explained above the 15 nm shift is typical of axial ligand coordination.[32]

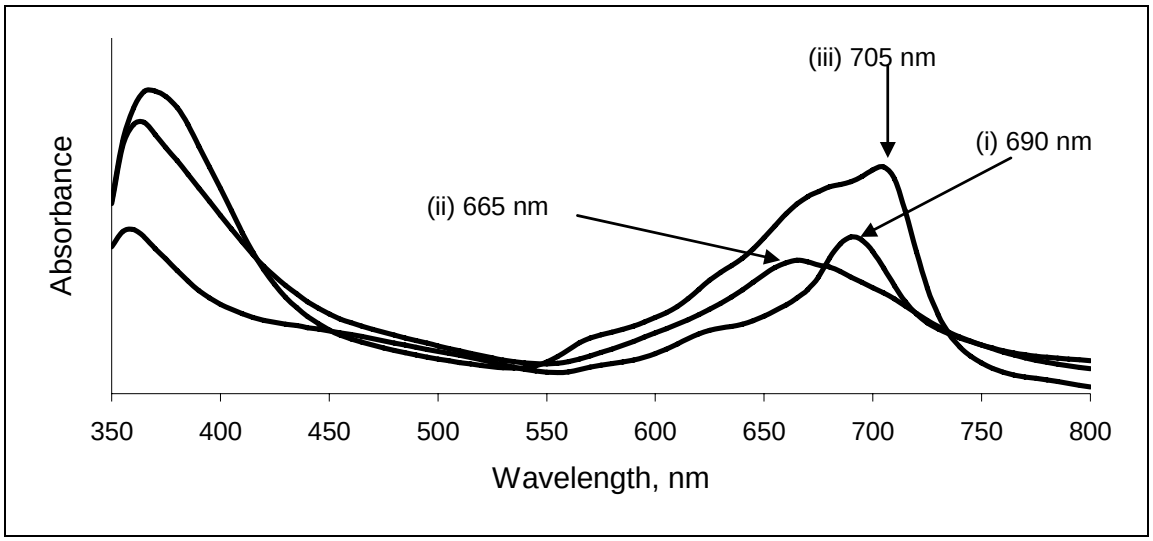

Figure 3.25 UV spectrum showing coordination of L-cysteine to $Fe^{III}Pc(SCH_2Ph)_8$ through a shift in the Q band maxima of $Fe^{III}Pc(SCH_2Ph)_8$ solution (ii) on addition of L-cysteine solution (iii). Spectrum (i) represents the $Fe^{II}Pc(SCH_2Ph)_8$ solution. Solvent = DMF.

3.4. Immobilization of Amine substituted MPcs on pre-formed SAMs

Amine substituted cobalt phthalocyanine (CoTAPc, **3**) was deposited on gold surfaces by using an interconnecting layer of a SAM of mercaptopropionic acid (**6**) or Lomant's reagent (dithiobis(*N*-succinimidyl propionate), **5**). In both cases the new bond formed is obtained by the creation of an amide. The layers were characterized using cyclic voltammetry.

These studies were done at Gent University (Belgium) on PARSTAT 2273 potentiostat from AMETEK, which was controlled by the Powersuite software, run on a DELL Pentium computer. Noise was observed on a number of cyclic voltammogramms. The studies were repeated several times but the noise persisted. However, consistent results proved the curves gave reliable information on the processes being studied.

3.4.1. Bare gold electrode study

Figure 3.26 shows a range of cyclic voltammograms recorded at a freshly pre-treated gold electrode in pH 12 buffer solution at room temperature and at a scan rate of 50 mV s^{-1}.

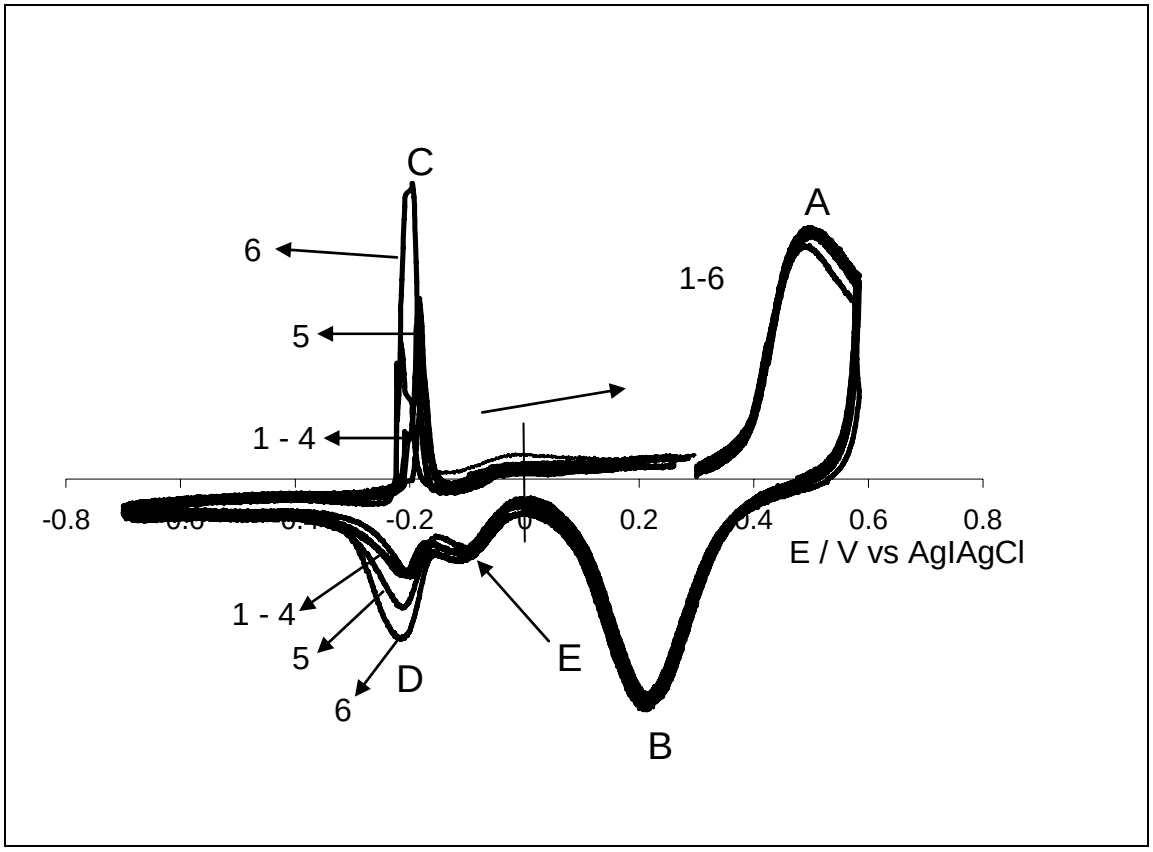

Figure 3.26 Current-potential curves recorded at a bare gold electrode in pH 12 buffer as a function of scan number: (1) 2; (2) 3; (3) 5; (4) 10; (5) 20 and (6) 50 scans. Scan rate = 50 mV s^{-1}.

From Figure 3.26 the voltammograms 1 to 6 represent the following scan numbers of the experiment: 2, 3, 5, 10, 20 and 50. The oxidation wave (A) observed at potentials more positive than 0.4 V vs. Ag|AgCl corresponds to the formation of gold oxide.[86-90] Its return peak is detected with a peak potential around 0.3 V vs. Ag|AgCl (peak B). The regeneration of the metallic gold surface in this peak can be expected as complete since the charge exchanged in both reactions (peak A and B) is similar and equals about

11.1±0.2 μQ. Note also that this charge is independent of scan number indicating a well-defined and reproducible regeneration process of the metallic gold surface.

Oxidation peak C and reduction peak D were not expected to occur. These peaks can be attributed to gold ad-atom oxidation-reduction reactions.[86,91-93] Ad-atoms are gold atoms that are present at the surface of the gold electrode but do not truly belong to the crystallographic structure, therefore these atoms are more reactive and subject to oxidation at less positive potentials compared to common atoms (which are oxidized at much more positive potentials, i.e. > 0.4 V vs. Ag|AgCl). The occurrence of gold ad-atoms from scan 2 of this experiment is not common. A possible explanation for the high amount of ad-atoms at the gold surface can be found in the type of experiment. Frequently an increase of ad-atoms at gold surfaces is observed when electrochemical scanning over a wide potential range and/or chemical etching[94,95] is performed. Additional experiments, similar to those shown in Figure 3.27, reveal indeed that scanning over a large potential range is the cause of the presence of gold ad-atoms at the electrode surface. It can be seen from the current-potential curve (scan 50) recorded in a potential window limited up to 0.5 V vs. Ag|AgCl and shown in Figure 3.27 that gold ad-atoms are absent and do not start to occur as a function of scan number.

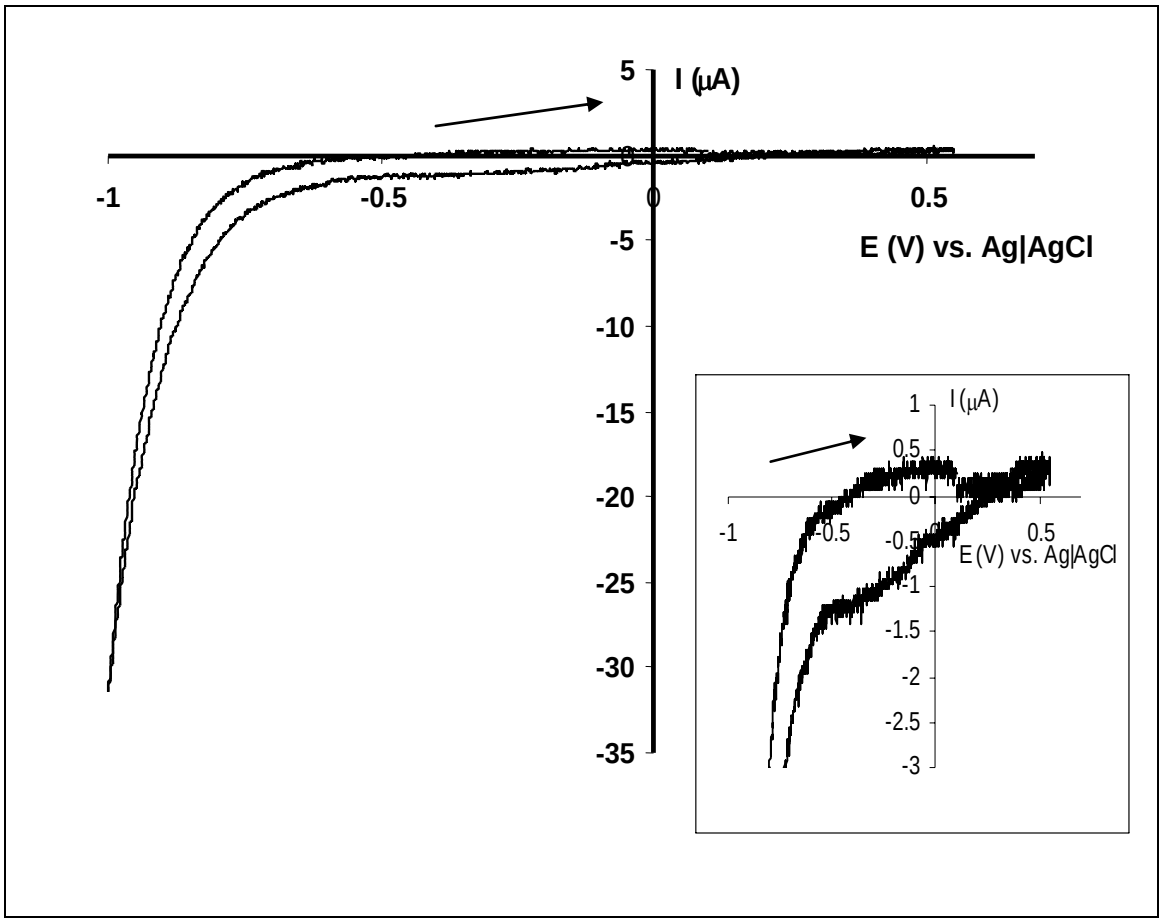

Figure 3.27 Current-potential curve of the 50th scan recorded at a bare gold electrode in pH 12 buffer solution. No ad-atom formation is observed around E = -0.1 V vs. Ag|AgCl (see also insert) ν = 50 mV s^{-1}.

In addition, it especially shows that the formation of gold oxide (at E > 0.5 V vs. Ag|AgCl) promotes ad-atom formation. Although the peak heights of the ad-atom oxidation and reduction reaction (peaks C and D in Figure 3.26) are quite different, the charge exchanged under these peaks is similar and equals about 2.3±0.1 μQ. The peak potentials are shifted over about 60 mV for both C and D for all scan numbers, while the

half-wave potentials are almost identical (-90 mV vs. Ag|AgCl). This result shows that the oxidation/reduction reaction of gold ad-atoms is a reversible process.

Finally, a reduction peak E with peak potential around 0 V vs. Ag|AgCl is observed and is probably due to a residue of dissolved oxygen that is present in the buffer solution. This was confirmed by repeating the experiments reported in Figures 3.26 and 3.27, in an aerated solution. Current-potential curves recorded in aerated solutions are given in Figure 3.28.

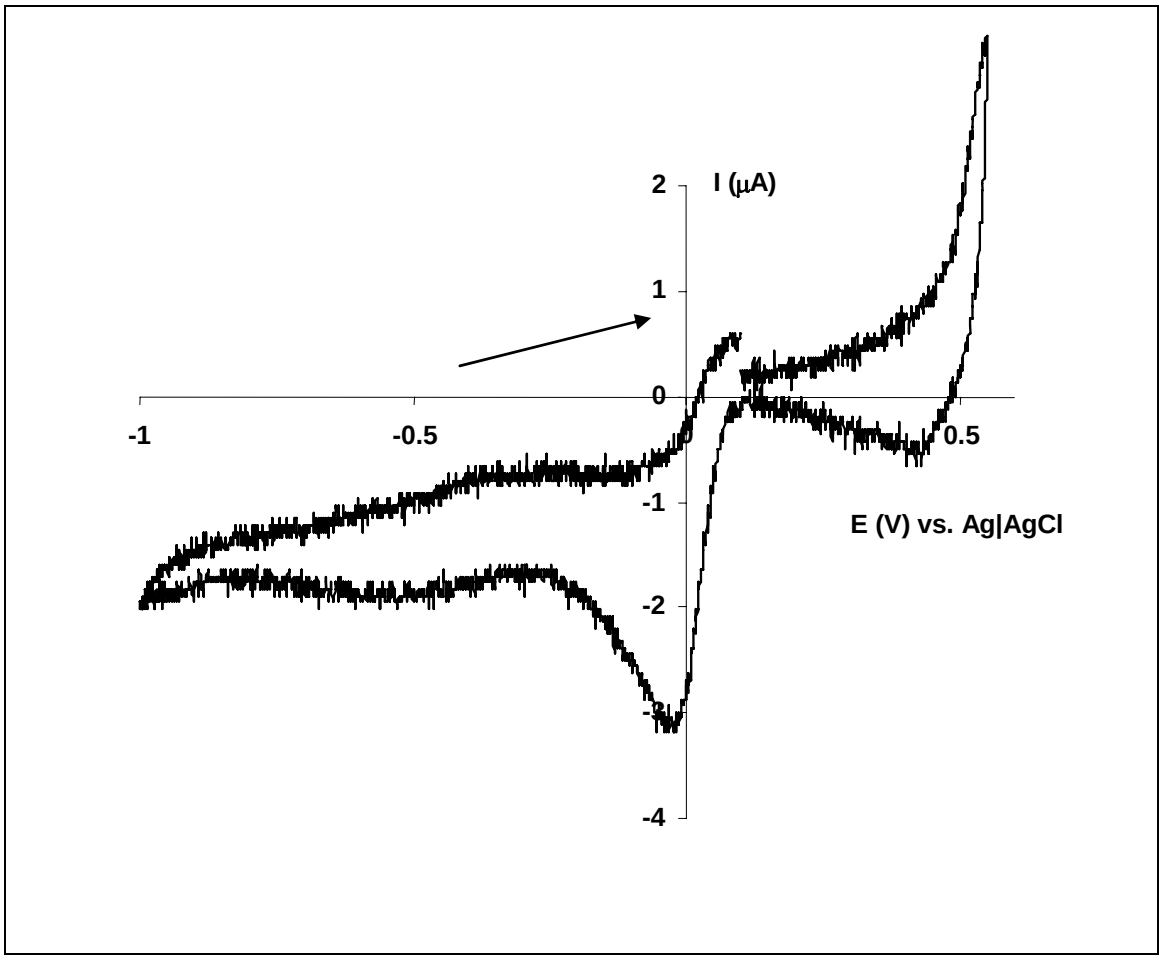

Figure 3.28 Current-potential curve recorded at a bare gold electrode in pH 12 buffer solution in the presence of dissolved oxygen. Scan rate = 50 mV s^{-1}.

Note, from Figure 3.28, that the oxidation of gold and its corresponding regeneration reaction is avoided. A diffusion controlled peak appears around 0 V vs. Ag|AgCl, which is linearly dependent of the dissolved oxygen concentration (not shown). This effect proves that the peak with a maximum around 0 V vs. Ag|AgCl in Figure 3.28 can be attributed to reduction of dissolved oxygen.

3.4.2. Study of Mercaptopropionic acid and DTSP-SAMs

A first set of experiments was performed under nitrogen purging in order to eliminate the dissolved oxygen reduction reaction. The initial idea was to use the gold oxide formation and reduction as a characterization tool. The decrease of peak currents related to those reactions could provide information about surface coverage. However, the oxidative desorption (equation 3.12) of deposited SAMs occurred in the same potential region, thus influencing the gold oxide formation and reduction signal.

$$Au - S - R \quad \leftrightarrows \quad Au + {}^{\bullet}S - R + e^{-} \qquad 3.12$$

Experimental evidence for the SAM formation and its desorption was shown by running a thiol (mercaptopropionic acid or DTSP) modified gold electrode within the limits of –1 to 0.6 V vs. Ag|AgCl in aerated solutions (Figure 3.29).

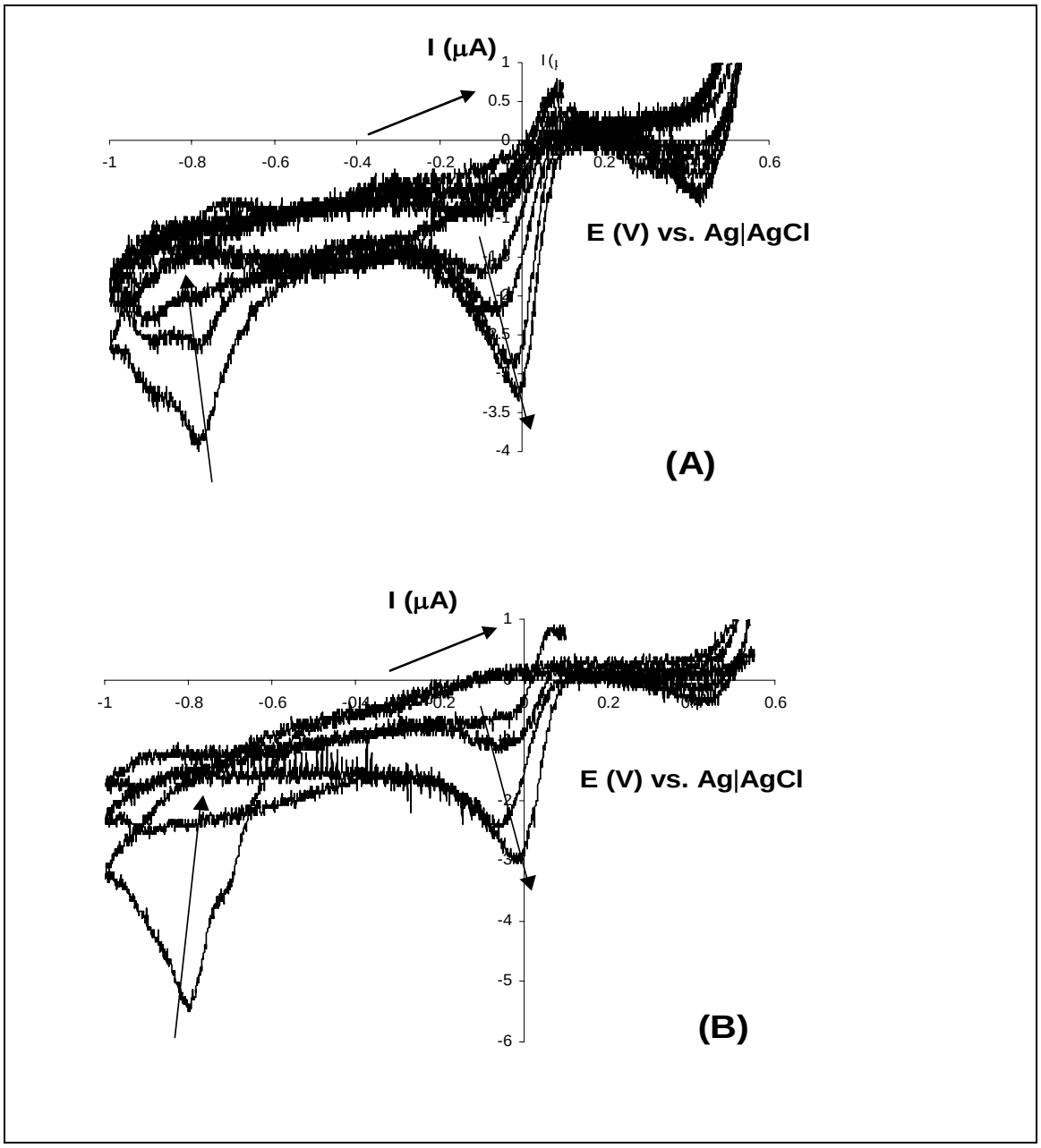

Figure 3.29 Current-potential curves successively recorded at a mercaptopropionic acid (A) and DTSP (B) modified gold electrode in pH 12 buffer in the presence of dissolved oxygen. Scan rate = 50 mV s^{-1}.The arrows represent direction of peak disappearance/growth.

From Figure 3.29 (For both a mercaptopropionic acid and DTSP SAMs), two reduction peaks are observed in the first scan at -0.8 and 0.4 and the reduction reaction of dissolved oxygen (with E_p = 0 V vs. Ag|AgCl) is absent or very weak. Thus the gold surface is covered with a SAM of thiol containing molecules, which inhibit the dissolved oxygen reduction. When the potential is swept to –1 V vs. Ag|AgCl, the SAM is reductively desorbed according to equation 3.13:

$$Au - S - R + e^- \leftrightarrows Au + {}^-S - R \qquad 3.13$$

As a consequence, the gold surface is again exposed to the solution, which is confirmed by the re-appearance of the dissolved oxygen reduction reaction. The peak related to that reaction increases with scan number until a maximum is obtained after about 4 scans, Figure 3.29. The fact that the desorption is not completed in one scan can best be explained as follows: a complete desorption of the SAM is obtained in the first scan but during the time of the return potential sweep (from –0.6 to +0.6 V vs. Ag|AgCl) a certain fraction θ of the thiol molecules re-adsorbs. The other fraction (1-θ) diffuses away from the electrode surface into solution. After about 4 scans the value of θ is so small that no more SAM is detected. This explains the gradual decrease of the SAM-reductive desorption peaks and the related gradual increase of the reduction of dissolved oxygen. For higher scan numbers bare gold behaviour is observed, showing that the SAM is removed completely.

Finally, the potential applied to the mercaptopropionic acid and DTSP SAM modified gold electrodes was swept between –0.5 and +0.6 V vs. Ag|AgCl in order to avoid

oxidative as well as reductive desorption of the SAMs in an aerated solution. Even after 100 scans no oxygen reduction reaction around 0 V vs. Ag|AgCl could be detected showing that the SAM is strongly bonded to the surface, is stable and covers the gold electrode surface completely.

3.4.3. Study of CoTAPc attached on pre-formed SAMs

In this section the gold electrodes modified with the SAMs of mercaptopropionic acid and DTSP were further modified with cobalt tetra-amine phthalocyanine (CoTAPc, **3**) through the procedures described in the Experimental section. As was done in the previous section a cyclic voltammetric experiment was performed by applying a potential sweep between –1 and +0.6 V vs. Ag|AgCl in nitrogen purged and aerated solutions. As an example the current-potential curves are shown for the mercaptopropionic acid SAM – CoTAPc modified gold electrode (Figure 3.30).

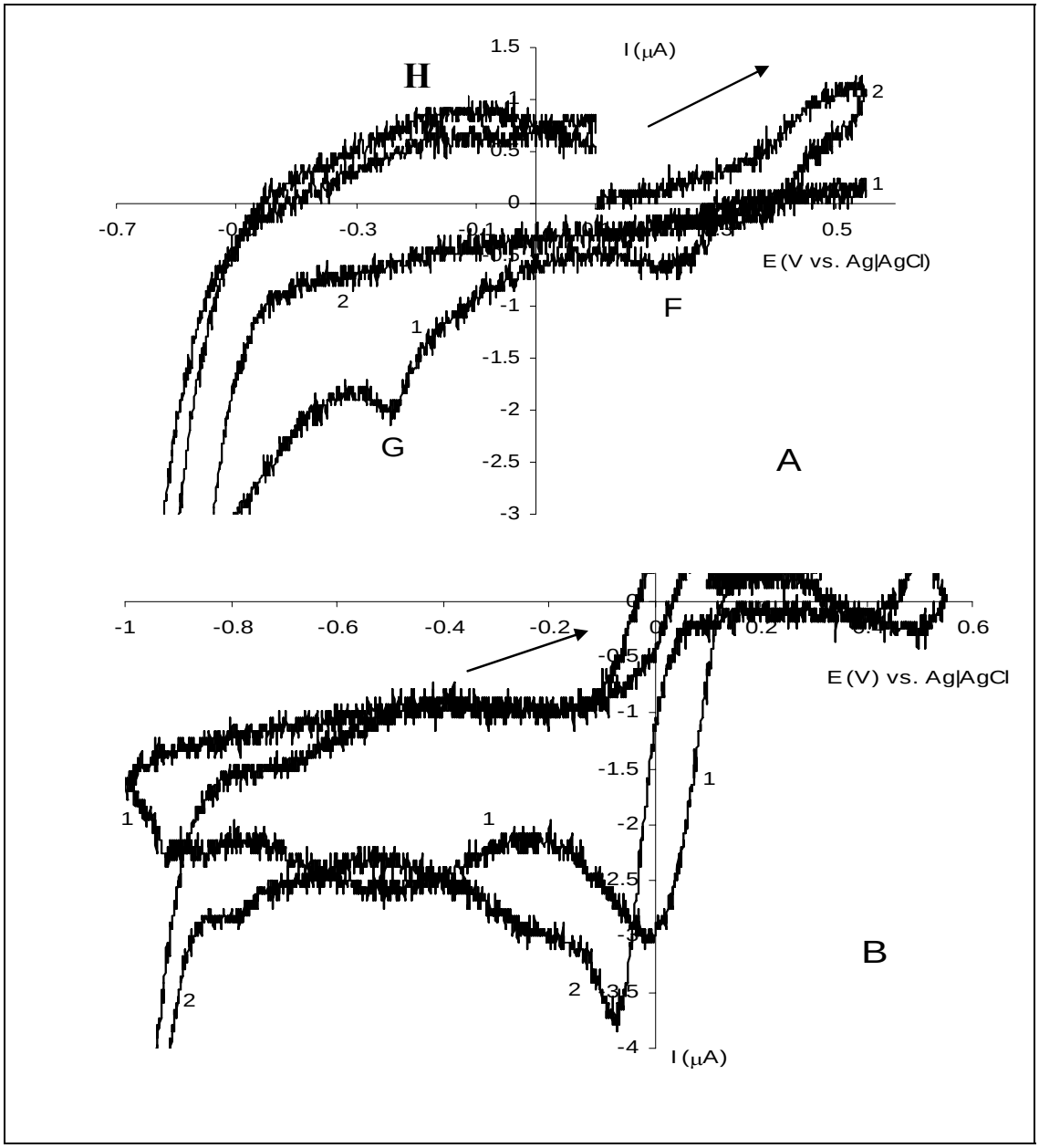

Figure 3.30 Current-potential curves recorded at a mercaptopropionic acid-CoTAPc modified gold electrode in the absence (A) and the presence (B) of dissolved oxygen in pH 12 buffer. Curves 1 and 2 represent a scan at bare gold and at the mercaptopropionic acid -CoTAPc modified gold electrode, respectively. Scan rate = 50 mV s^{-1}.

It can clearly be seen that under nitrogen purging (Figure 3.30A) two reduction peaks and one broad oxidation peak are observed. The two reduction peaks F and G are related to respectively the reduction of Co(III) to Co(II) and Co(II) to Co(I) in CoTAPc. This is confirmed by literature results for peak F[1,96] and G[16,96,97]. The broad oxidation peak can be attributed to the regeneration of Co(II) from Co(I) (peak H, Figure 3.30A). The charge exchanged in peaks F and G are about the same and equal to $7.76\pm0.20\text{x}10^{-7}$ Q. This corresponds to $4.2\pm0.2\text{x}10^{12}$ CoTAPc molecules attached to the surface. The presence of a multi layer is not expected due to the specific coupling reactions that are used in this paper.

In aerated solutions, one can see that from the first scan, the reduction reaction of dissolved oxygen is observed (Figure 3.30B, curve 2) on a thiol-CoTAPc modified electrode. However, its peak maximum is slightly shifted to more negative potentials compared to the oxygen reduction peak at bare gold (Figure 3.30B, curve 1). This is due to the fact that first the active form of the CoTAPc needs to be produced before it can reduce oxygen and this is probably the Co(I) form. The oxygen reduction at SAM-CoTAPc modified gold electrodes starts around –0.1 V, instead of 0 V vs. Ag|AgCl for bare gold (Figure 3.30B, curve 1). The potential where the oxygen reduction at the modified electrode starts to occur is about the same potential at which Co(II) is reduced to Co(I) (Figure 3.30A). Thus, first the Co(I)TAPc form needs to be produced, which is then able to reduce dissolved oxygen.

The comparison of the curve obtained at bare gold and at the SAM-CoTAPc modified gold electrode (Figure 3.30B) clearly shows electrocatalytic effects. First it can be seen that the peak maximum is about 25% higher at the SAM-CoTAPc modified gold

electrode. Second, the peak width is smaller and finally the slope of the inclining part of the peak is higher, revealing faster electron transfer. For electrocatalysis it is also expected that a smaller overpotential needs to be applied to observe the reaction but in this case this is not possible because the electrocatalytic form of CoTAPc is only obtained at potentials more negative than those observed for oxygen reduction at bare gold surfaces.

Finally, long-term stability experiments showed that the SAM and SAM-CoTAPc modified gold electrodes are stable over a long period of scanning (> 100 scans) as long as the potential applied was kept between –0.6 and +0.6 V vs. Ag|AgCl. Outside this potential window the SAM is desorbed reductively (E < -0.6 V vs. Ag|AgCl) or oxidatively (E > 0.6 V vs. Ag|AgCl).

CHAPTER 4: CONCLUSION

Phenylthiol substituted Zn (**10**), Co (**11**) and Fe (**12**) complexes have been synthesized. Phenylthiol substituted Co (**11**) and Fe (**12**) complexes synthesized in this work are easier to reduce than other thiol substituted MPc complexes considering the same solvent/electrolyte system. This is an advantage for future use of thin films of these complexes for catalytic reduction of analytes. Spectroelectrochemistry was employed to characterize the products of oxidation or reduction of the phenylthiol substituted Co (**11**) and Fe (**12**) complexes. The use of this technique is based on the well known fact that the redox process based on the ring drastically affect the Q band while the metal-based redox processes result only in the shift in the Q band, without much change in intensity. The spectra of Fe(I)Pc species is not well known, and this work gives an example of the spectrum of an Fe(I)Pc species which may aid other researchers in identifying it.

The SAMs of novel phenylthiol substituted Co (**11**) and Fe (**12**) complexes on gold electrodes are reported. The densely packed SAM monolayer provided by both of these complexes proved an effective barrier to gold surface oxidation, UPD of copper and the redox chemistry of $Fe(NH_4)(SO_4)_2$ in $HClO_4$. Electrocatalytic oxidation of L-cysteine occurred at relatively low potentials (+0.6 and +0.7 V vs Ag|AgCl for Co (**11**) and Fe (**12**) complexes respectively) demonstrating that the modified electrodes significantly lower the overpotential for cysteine oxidation. These values were however larger than other FePc or CoPc-SAMs. SAM bonding of phenylthiol substituted Co (**11**) and Fe (**12**) complexes to Au provides advantages in that such a procedure is simple, reproducible and offers a high stability through covalent bonding between the SAM and Au surface. However, probable electrochemical application is limited to a narrow potential window (-0.3 to +0.7 V vs Ag|AgCl) in acidic pH. Future study of the SAM electroanalytical

applications may involve the detection and enhancement of redox reactions occurring in acidic biological media.

Amine substituted cobalt phthalocyanine (**3**) was deposited on gold surfaces by using an interconnecting layer of a SAM of mercaptopropionic acid (**6**) or dithiobis(*N*-succinimidyl propionate) (**5**). In both cases the new bond formed is obtained by the creation of an amide. From the experiments performed, the data described and analysed, several conclusions can be drawn. First, a new method is developed for the deposition of metallophthalocyanines at electrode surfaces by using the EDC coupling reaction of carboxyl and amine groups to form an amide. Second, experimental proof is provided that the gold surface is well covered with the discussed SAMs and its CoTAPc coupling. Third, the SAM-CoTAPc modified gold electrodes show electrocatalytic behaviour towards the reduction of dissolved oxygen and proves that the surface is coated with the discussed Co tetra-amine phthalocyanine.

SAM and SAM-CoTAPc modified gold electrodes are stable over a long period of scanning (> 100 scans) within a potential window of -0.6 to +0.6 V vs. Ag|AgCl. Outside this potential window the SAM desorbs reductively (E < -0.6 V vs. Ag|AgCl) or oxidatively (E > 0.6 V vs. Ag|AgCl).

References

1. Leznoff, C. C.; Lever, A. B. P. (eds.) *Phthalocyanines. Properties and Applications*; VCS Publishers, Inc.; Weinheim. **1989**, **1993**, **1996**; vols 1– 4.
2. Wöhrle, D.; Eskes, M.; Shigehara, K.; Yamada, A. *Synthesis* **1993**, 194.
3. Gürek, A.; Ahsen, V.; Gül, A.; Bekaroğlu, Ő. *J. Chem. Soc., Dalton Trans.* **1991**, 3367.
4. Lelievre, D.; Petit, M. A.; Simon, J. *Liquid Cryst.* **1989**, *4*, 707.
5. Wöhrle, D.; Iskandar, N.; Graschew, G.; Sinn, H.; Friedrich, E. A.; Maier-Borst, N.; Stern, J.; Schlag, P. *Photochem. Photobiol.* **1990**, *51*, 351.
6. Mohammed, M. A.; Ottenbreit, P.; Prass, W.; Schnurpfeil, G.; Wöhrle, D. *Thin Solid Films* **1992**, *213*, 285.
7. Braun, A. and Tcherniac, J. *Ber. Deut. Chem. Ges.* **1907**, *40*, 2709.
8. Byrne, G. T.; Linstead, R. P.; Lowe, A. R. *J. Chem. Soc.* **1934**, 1017.
9. Elvidge, J. A.; Linstead, R. P. *J. Chem. Soc.* **1955**, 3536.
10. Brach, P. J.; Grammatica, S. J.; Ossanna, O. A.; Weinberger, L. *J. Heterocyclic. Chem.* **1970**, *7*, 1403.
11. Moser, F. H.; Thomas, A. L. *The Phthalocyanines* C. R. C.: Boca Raton, Florida, **1983**; vols 1 - 2.
12. Cook, M. J.; Dunn, A. J.; Howe, S. D.; Thomson, A. J. *J. Chem. Soc., Perkin Trans.* **1988**, *1*, 2453.
13. Snow, A. W. and Griffith, J. R. *Macromolecules*. **1984**, *17*, 1614.
14. Wöhrle, D.; Schnurpfeil, G.; Knothe, G. *Dyes Pigments* **1992**, *18*, 91.
15. Gürek, A. G.; Bekaroglu, O. J. *J. Chem. Soc. Dalton Trans.* **1994**, 1419.
16. Ozoemena, K.; Westbroek, P.; Nyokong, T. *J. Porphyrins Phthalocyanines* **2002**, *3*, 529.

17. Ozoemena, K.; Nyokong, T. *J. Chem. Soc. Dalton Trans.* **2002**, 1806.
18. Takahashi, K.; Kawashima, M.; Tomita, Y.; Itoh, M. *Inorg. Chim. Acta.* **1995**, *232*, 69.
19. Lux, A.; Rozenberg, G. G.; Petritsch, K.; Moratti, S. C.; Holmes, A. B.; Friend, R. H. *Synthetic Metals* **1999**, 1527.
20. Ban, K.; Nishizawa, K.; Ohta, K.; Shirai, H. *J. Mater. Chem.* **2000**, *10*, 1083.
21. Kaifer, A. E. and Gomes-Kaifer, M. *Supramolecular Electrochemistry* **1999**. Wiley-VCH: Germany.
22. http://www-biol.paisley.ac.uk/marco/Enzyme_Electrode/Chapter1/Cyclic_Voltammetry1.htm
23. Wang, J. *Analytical Electrochemistry* **1994**. VCH Publishers Inc: New York.
24. Brett, M. A. C. and Brett, A. M. O. *Electrochemistry Principles, Methods and Applications* **1993**. Oxford University Press: New York.
25. Hibbert, D. B. *Introduction to Electrochemistry* **1993**. Macmillan: London.
26. Hawkridge, F. M. *Laboratory Techniques in Electroanalytical Chemistry*, 2nd ed. Kissinger, P. T. and Heineman, W. R. (eds) **1996**. Marcel Dekker Inc.: New York.
27. Bard, A. J.; Faulkner, L. R. *Electrochemical Methods: Fundamentals and Applications* **1980**. John Wiley & Sons: New York.
28. http://chem.ch.huji.ac.il/~eugeniik/instruments/electrochemical/square-wave%20polarographs.htm
29. Bard, A. J.; Faulkner, L. R. *Electrochemical Methods: Fundamentals and Applications* **1996**. John Wiley and Sons: New York.

30. Stillman, M. J. In *Phthalocyanines. Properties and Applications* Leznoff, C. C. and Lever, A. B. P. (eds.); VCH Publishers: New York, **1993**, vol 3.
31. Boucher, L. *Coordination chemistry in Macrocyclic compounds* Melson, G. A. (ed.) Plenium Press, **1971**, 461.
32. Stillman, M. J. and Nyokong, T. In *Phthalocyanines. Properties and Applications* Leznoff, C. C. and Lever, A. B. P. (eds.); VCH Publishers: New York, **1989**, vol 1.
33. Lever, A. B. P. *Adv. Inorg. Radiochem.* **1965**, *7*, 28.
34. Gouterman, M.; In *The Porphyrins, Physical Chemistry* Dolphin, D. (ed.); Academic Press: New York, **1978**, vol III, part A.
35. Louati, A.; Meray, M. E. I.; Andre, J. J.; Simon, J.; Kadish, K. M.; Gross, M. and Giraurdeau, A. *Inorg. Chem.* **1985**, *24*, 1175.
36. Hale, P. D.; Pietro, W. J.; Ratner, M. A.; Ellis, D. E. and Marks, T. J. *J. Am. Chem. Soc.* **1987**, *109*, 5943.
37. Myers, J. F.; Canham, R. G. W.; Lever, A. B. P. *Inorg. Chem.* **1975**, *14*, 461.
38. Nyokong, T. *S. Afr. J. Chem.* **1995**, *48*, 23.
39. Matsuda, H.; Okada, S.; Masaki, A.; Nakanishi, H.; Suda, Y.; Shigehara, K.; Yamada, A. *Proc. SPIE-Int. Soc. Opt. Eng.* **1990**, *1337*, 105.
40. Suda, Y.; Shigehara, K.; Yamada, A.; Matsuda, H.; Okada, S.; Masaki, A.; Nakanishi, H. *Proc. SPIE-Int. Soc. Opt. Eng.*, **1991**, *1560*, 75.
41. Finklea, H. O.; In *Electroanalytical Chemistry* Bard, A. J. and Rubenstein, I. (eds.); Marcel Dekker: New York, **1996**, vol 3.
42. Pilloud, D. L.; Chen, X.; Dutton, P. L. and Moser, C. C. *J. Phys. Chem.* **2000**, *104*, 2868.
43. www.chemistry.msu.edu/courses/CEM812/HSAB_Theory.pdf

44. Katz, E.; Schlereth, D. D. and Schmidt, H.-L. *J. Electroanal. Chem.* **1994**, *367*, 59.

45. Biebuyck, H. A.; Bain, C. D.; and Whitesides, G. M. *Langmuir* **1994**, *10*, 1825.

46. Chidsey, C. E. D. *Science* **1991**, *251*, 919.

47. Li, Z. and Lieberman, M. *Supramol. Science* **1998**, *5*, 485.

48. Cook, M. J. *Pure Appl. Chem.* **1999**, *71*, 2145.

49. Yang, W.; Gooding, J. J. and Hibbert, D. B. *J. Electroanal. Chem.* **2001**, *516*, 10.

50. Willner, I.; Blonder, R. and Dagan, A. *J. Am. Chem. Soc.* **1994**, *115*, 4935.

51. Che, G.; Li, Z.; Zhang, H. and Cabrera, C. R. *J. Electroanal. Chem.* **1998**, *453*, 9.

52. Nuzzo, R. G.; Zegarski, B. R. and Dubois, L. H. *J. Am. Chem. Soc.* **1987**, *109*, 733.

53. Nuzzo, R. G.; Fusco, F. A. and Allara, D. L. *J. Am. Chem. Soc.* **1987**, *109*, 2538.

54. Sabatani, E. and Rubinstein, I. *J. Phys. Chem.* **1987**, *91*, 6663.

55. Li, Z. and Lieberman, M. *Fundamental Aspects of Chemically Modified Surfaces* Blitz, J. P. and Little, C. B. (eds.). *Royal Soc. Chem.* Lettchworth: UK, **1999**.

56. Li, Z. and Lieberman, M. *Langmuir* **2001**, *17*, 4887.

57. Ozoemena, K.; Westbroek, P.; Nyokong, T. *Electroanalysis* **2003**, *15*, 1762.

58. Ozoemena, K.; Nyokong, T. *Electrochim. Acta.* **2002**, *47*, 4035.

59. Stryer, L. S. In *Biochemistry*, 3rd ed.; W. H. Freeman and Co.: New York. **1988**.

60. Griveau, S.; Pavez, J.; Zagal, J.; Bedioui, F. *J. Electroanal. Chem.* **2001**, *497*, 75.

61. Zagal, J. H.; Paez, C. *Electrochim. Acta.* **1989**, *34*, 243.

62. Maree, S. and Nyokong, T. *J. Electroanal. Chem.* **2000**, *492*, 120.

63. Halbert, M. K. and Baldwin, R. P. *Anal. Chem.* **1985**, *57*, 591.

64. Tedder, J. M.; Nechvatal, A.; Murray, A. W.; Carnduff, J. In *Basic Organic Chemistry*. John Wiley and Sons: London, **1972**, chapter 6.

65. Katz, E. *J. Electroanal. Chem.* **1990**, *156*, 220.

66. Somashekarappa, M. P.; Keshavayya, J.; Sampath, S. *Pure Appl. Chem.* **2002**, *74(9)*, 1609.

67. http://www.answers.com/topic/hsab-concept?gwp=19

68. Somashekarappa, M. P.; Sampath, S. *Chem. Comm.* **2002**, *12*, 1262.

69. Patolsky, F.; Guoliang, T.; Katz, E.; Willner, I. *J. Electroanal. Chem.* **1998**, *454*, 9.

70. Milusheva, T.; Nikolov, I.; Naidenov, V.; Vitanov, T. *Bulgarian Chemical Communications* **2004**, *36(2)*, 117.

71. Lee, S. H.; Pak, C. H.; Chang, H.; Shin, J. *U.S. Pat. Appl. Publ.* CODEN: USXXCO US 2004161641 A1 20040819, **2004**.

72. Yamamoto, A.; Takada, T.; Nakamura, T.; Sato, A.; Endo, E. *Jpn. Kokai Tokkyo Koho* CODEN: JKXXAF JP 2003200051 A2 20030715, **2003**.

73. Ambert, J.; Gutjahr, M.; Beccu, K. *Patentschrift (Switz.)* CODEN: SWXXAS CH 548115 19740411, **1974**.

74. Kobayashi, N. *J. Am. Chem. Soc.* **1994**, *116*, 879.

75. Simão, D.; Alves, H.; Belo, D.; Rabaça, S.; Lopes, E. B.; Santos, I. C.; Gama, V.; Duarte, T.; Henriques, R. T.; Novais, H. and Almeida, M. *Eur. J. Inorg. Chem.* **2001**, 3119.

76. Kandaz, M.; Yaraşir, M. N. U.; Koca, A. and Bekaroğlu, Ő. *Polyhedron* **2002**, *21*, 255.

77. Golovin, M. N.; Seymour, P.; Jayaraj, K.; Fu, Y. S.; Lever, A. B. P. *Inorg. Chem.* **1990**, *29*, 1719.

78. Nemykin, V. N.; Chernii, Y. V.; Volkov, S. V.; Bundina, N. I.; Kaliya, O. L.; Li, V. D.; Lukyanets, E. A. *J. Porphyrins Phthalocyanines* **1999**, *3*, 87.

79. Lever, A. B. P.; Milaeva, E. L.; Speier, G. *Phthalocyanines: Properties and Applications*, vol. 3. Leznoff, C. C. and Lever A. B. P. (eds.). **1993** VCH Publishers: New York, chapter 1: pp 1.

80. Hickey, S. G. and Riley, D. J. *Electrochem. Commun.* **1999**, *1*, 116.

81. Porter, M. D.; Bright, T. B.; Allara, D. and Chidsey, C. E. D. *J. Am. Chem. Soc.* **1987**, *109*, 3559.

82. Caro, A. C.; Bedioui, F.; Zagal, H. *Electrochim. Acta.* **2002**, *47*, 1489.

83. Hutchison, J. E.; Postlethwaite, T. A. and Murray, R. W. *Langmuir* **1993**, *9*, 3277.

84. Kobayashi, N.; Janda, P. and Lever, A. B. P. *Inorg. Chem.* **1992**, *31*, 5172.

85. Zagal, J. H.; Guilppi, M. A.; Depretz, C. and Lelievre, D. *J. Porphyrins Phthalocyanines* **1999**, *3*, 355.

86. Burke, L. D. and O'Sullivan, J. F. *Electrochim. Acta.* **1992**, *37*, 585.

87. Burke, L. D. and O'Leary, W. A. *J. Appl. Electrochem.* **1989**, *19*, 758.

88. Sirolvi, R. S. and Genshov, M. A. *J. Electrochem. Soc.* **1969**, *116*, 910.

89. Schmid, G. M.; Curley, M. E. In *Encyclopedia of Electrochemistry of the Elements* Bard, A. J. (ed.); Marcel Dekker: New York, **1975**, vol 4.

90. Woods, R. In *Advances in Electroanalytical Chemistry* Bard, A. J. (ed.); Marcel Dekker: New York, **1997**.

91. Montalcuti, F. and Ferrando, R. *Surf. Sci.* **1999**, *435*, 445.

92. Dona, J. M. and Gonzalezvelasco, J. *J. Phys. Chem.* **1993**, *97*, 4714.

93. Burke, L. D. and Lee, B. H. *J. Electroanal. Chem.* **1992**, *330*, 637.

94. Liebermann, H. H. (ed) *Rapidly Solidified Alloys*. Marcel Dekker: New York, **1993**.

95. Suryanarayana, C. *Rapid Solidification*. In *Materials Science and Technology, a Comprehensive Treatment*. VCH Weinheim, **1991**, vol 15.

96. Zagal, J. H.; Sen, R. K.; Yaeger, E. *J. Electroanal. Chem.* **2001**, *512*, 56.

97. Griveau, S.; Gulppi, M.; Pavez, J.; Zagal, J. H.; Bedioui, F. *Electroanal.* **2003**, *15*, 779.